Towards Understanding Reality using Dynamical 3-Space Theory

by

David P. Rothall, BSc Nano (Hons), **BIE (S&T)**

School of Chemical and Physical Sciences
Faculty of Science and Engineering

A thesis submitted in fulfilment of the requirements
for the degree of Doctor of Philosophy

at

The Flinders University of South Australia
June 2016

Contents

List of Figures

List of Tables

Abstract

Towards Understanding Reality using Dynamical 3-Space Theory

by David P. Rothall

This dissertation extends on an alternative model of reality known as Dynamical 3-Space theory. Chapter 1 introduces the incidents in history which lead to the development of Newtonian Gravity and General Relativity models, and explains how these models require additional parameters to explain astrophysical and cosmological phenomena. Chapter 2 introduces Dynamical 3-Space theory, which is a unique generalisation of Newtonian gravity cast into an inflow formalism. This model contains two parameters, namely Newton's gravitational constant G and the fine structure constant $\alpha \approx 1/137$ and where all emerging phenomena such as space and quantum physics are unified. Evidence supporting the Dynamical 3-Space theory is presented later in chapter 2 while the following chapter then discusses known solutions to the model, including the emergence of gravity as a quantum effect, black hole and filament solutions, and also that of the universe's expansion in terms of a Hubble flow.

My original contribution to knowledge begins in Chapter 4, which analyzes data from two experiments by Cahill that suggest that fluctuations in radio-frequency signals and tunneling currents are nonrandom, and can be explained by the presence of a dynamical and fractal space. These works are shown to be new methods of detecting the similar nonrandom effects that Simon Shnoll observed in his experiments throughout his career, especially that of radioactive decay. Chapters 5 - 7 extend on Dynamical 3-Space theory, with chapter 5 discussing a modification to account for the borehole g anomaly while checking that the model still accounts for known astrophysical and cosmological data. Chapter 6 then discusses the discovery of a uniformly expanding universe, i.e. a parameter free Hubble fit to the type 1a supernova data, along with a prediction of cosmic inflation solutions from the newly modified Dynamical 3-Space equation. The final chapter studies black hole solutions embedded in an expanding universe, required by the lack of a free parameter within the Hubble flow, and then discusses a cosmic network of black holes and induced filaments within an expanding universe.

Declaration of Authorship

I, David P. Rothall, declare that this thesis titled, 'Towards Understanding Reality using Dynamical 3-Space Theory' and the work presented in it are my own. I certify that this thesis does not incorporate without acknowledgement any material previously submitted for a degree or diploma in any university; and that to the best of my knowledge and belief it does not contain any material previously published or written by another person except where due reference is made in the text.

Signed: _____

Date: _____

Acknowledgements

When I first walked into Professor Reg Cahill's office to ask him about his research, his first words were literally "Well... This research is awesome." While he was discussing his research I became quite excited to take on a PhD under his supervision, both because of how easily Reg was explaining how his model successfully applied to experimental data, and also because his research field was simply just awesome. I can't thank you enough for giving me the opportunity to do this, and also for providing your guidance and patience for 5 years. I would do this all over again in a heart beat.

I'd also like to thank anyone at uni who stopped to chat about our life as PhD students. We all have our moments, and it was great to talk about where we were at, both with our progress and also our state of mind. It really helped to put things in perspective and realise that all we are doing is not only great research, but it is also just that, research, and not the end of the world if it doesn't go well all the time. Special thanks to Dr. Christopher Gibson who I talked with the most, we should really grab that beer some time!

Thanks to my pool friends and team mates, and also to my good friends on Twitch for putting up with my insanity, as pool and gaming have largely been my outlet from research throughout my PhD. It's definitely helped get me through study.

Finally I'd like to thank my family and also my girlfriend Kristin Cederquist for all their love and support. You have all been extremely supportive and understanding in listening to my rambles, and there were plenty of them! Dad somehow managed to read my first chapter once and proceeded to ask me questions about it. Our conversation then helped mould the introduction to my work. Thank you all for getting me through the last 5 years.

David Rothall
Adelaide, South Australia
June, 2016

Abbreviations

BH	**B**lack **H**oles
CAMB	**C**ode for **A**nisotropies in the **M**icrowave **B**ackground
CMB	**C**osmic **M**icrowave **B**ackground
Dec	**Dec**lination
DSO	**D**igital **S**torage **O**scilloscope
FC	**F**requency **C**utoff
FLRW	**F**riedmann-**L**emaître-**R**obertson-**W**alker
FT	**F**ourier **T**ransform
GaR	**Ga**lilean **R**elativity
GCP	**G**lobal **C**onsciousness **P**roject
GR	**G**eneral **R**elativity
NG	**N**ewtonian **G**ravity
ps	**p**ico**s**econds
RA	**R**ight **A**scension
REG	**R**andom **E**vent **G**enerator
SR	**S**pecial **R**elativity
wrt	**w**ith **r**espect **t**o

Physical Constants

Fine Structure Constant	α	=	$1/137$
Newton's Gravitational Constant	G	=	6.67384×10^{-11} m^3/kg/s^2
Parsec	pc	=	3.086×10^{16} m
Solar Mass	$M_\odot$	=	1.98855×10^{30} kg
Speed of Light	c	=	2.99792458×10^8 m/s

Symbols

v_O	Orbital Velocity
$a(t)$	Scale Factor
$\mathbf{v}(\mathbf{r}, t)$	Velocity Field
$\mathbf{a}(\mathbf{r}, t)$	Acceleration Field
t_0	Present Moment Age of Universe
H_0	Hubble Constant
ρ_c	Critical Density
Ω_b	Baryonic Density Parameter
Ω_{DM}	Dark Matter Density Parameter
Ω_Λ	Dark Energy Density Parameter
$\rho(r, t)$	Matter Density
α	Self Coupling Constant (Long Range)
δ	Self Coupling Constant (Short Range)
$\mathbf{v}_P$	Projected Velocity
$\triangle t$	Travel Time Difference
k	Interferometer Calibration Expression
n	Refractive Index
v_N	Newtonian Speed Prediction
v_P	Absolute Speed Prediction
ρ_{DM}	Dark Matter Density
v_R	Velocity Relative to Absolute Space
β	Black Hole Strength Parameter
μ	Filament Strength Parameter

$H(t)$	Hubble Expression
${}_1F_1(a, b, z)$	Confluent Hypergeometric Function
$\Gamma(z)$	Gamma Function
v_0	3-Space Velocity
κ	Black Hole Structural Parameter
$M(r)$	Effective Mass Function
M_0	Point-like Black Hole Mass
v_{orb}	Orbital Velocity
G_N	Newton's Gravitational Constant
$\triangle g(r)$	Borehole Gravity Residual
g_N	Newtonian Gravity Prediction
M_{DM}	Dark Matter Mass
M_{BH}	Black Hole Mass
σ	Standard Deviation
V_0	Potential Barrier Height
$T(V_0 - E)$	Quantum Tunneling Amplitude
$M_\odot$	Solar Mass
$d_L(z)$	Dimensionless Luminosity Effective Distance
$\mu(z)$	Supernova Magnitude
z	Redshift
Ω_s	Space Density Parameter
Ω_M	Matter Density Parameter
n_s	Scalar Spectral Index
τ	Reionization Optical Depth
$\triangle^2_{\mathbb{R}}$	Curvature Fluctuation Amplitude
$\mathcal{F}_P$	Photon Flux
$\mathcal{L}_P$	Source Photon-Number Density
$\mathcal{F}_E$	Source Energy Flux
$\mathcal{L}_E$	Source Energy Luminosity
$r_L(z)$	Effective Energy-Flux Luminosity Distance
r_c	Critical Radius

Introduction

The Earth travels around the Sun at approximately 30 kilometres every second. Our Solar System travels at a speed of around 230 - 240 km/s within the Milky Way galaxy. The galaxy is also moving universally - towards the Andromeda galaxy, and the Hydra and Virgo clusters at a combined speed of over several hundred kilometres per second. All of this is happening while the universe is expanding, which has been the case for over 13 billion years. Astronomers knew substantially less than this back in 1887, when Michelson and Morley's interferometer experiment was the first to study the absolute motion of Earth through space. At the time it was believed through Kepler's planetary observations and encompassed in the Newtonian theory of gravity, that the universe was an empty unchanging container that objects such as the Earth moved through. Because of this it was believed that the only necessary motion to detect was that of Earth's movement around the Sun, which was assumed to be in a fixed position. We didn't have the knowledge nor the experimental capability to detect other relevant speeds such as solar or galactic motion throughout the universe, nor realise that these speeds might one day need to be taken into account.

If we knew in 1887 before performing the interferometer experiment about the high speeds that we are currently travelling at through the universe, we'd have a much better understanding of how the interferometer works. We would have a more modern relativistic theory of the interferometer as opposed to that based on Newtonian gravity, and Michelson and Morley would not have reported a null result so

quickly. An interesting exercise would be to forget the Newtonian gravity model and the theories of Special and General Relativity for a moment, and ask ourselves what model of reality would ideally suit all of the experimental predictions that we know today. Since the mentioned models are based on only a fraction of the experimental phenomena that are known today, at first glance they are simply inadequate to describe all of what is currently known. We would be immediately taking into account Miller's extensive interferometer observations, NASA spacecraft - Earth flyby Doppler shift data, flat spiral galaxy rotation curves, recession of galaxies, supernova magnitude-redshift data... the list goes on, in order to develop a model without any free parameters.

To this end, instead of following conventional physics my research extends on a model of reality known as Dynamical 3-Space theory, and is a unique generalisation of Newtonian gravity cast into an inflow formalism. The model therefore attempts to explain observable phenomena at least from an absolute motion perspective, i.e. by assuming the presence of a dynamical and fractal space which then influences measurements obtained during experiments. This means for example that Maxwell's equations as well as the Schrödinger and Dirac equations, are required to be generalised to contain absolute motion effects as predicted by Dynamical 3-Space theory. The model is simple yet powerful - it predicts the emergence of gravity as a derivable quantum effect, the equivalence principle, black holes, cosmic filaments and the universe's expansion as determined from type 1a supernova data. Experimentally the model has been able to account for many other phenomena, including the resolution of NASA spacecraft-Earth flyby Doppler shift anomalies, predicting flat spiral galaxy rotation curves and accounting for the Milky Way supermassive black hole data, all without requiring additional parameters. Some of these observations don't implicitly require the Dynamical 3-Space theory for an explanation; any generic model which contains absolute motion effects is able to explain these phenomena, as will be shown in this dissertation in the case for an

expanding universe. Also shown here is a suggested modification to the Dynamical 3-Space theory to further account for the gravitational borehole g anomaly, and also the discovery of new black hole solutions which are embedded in an expanding universe.

Additional to extending on Dynamical 3-Space theory, this thesis also presents the analysis of recent dynamical space detection techniques. The analysis is based from Simon Shnoll's research into nonrandom correlations in seemingly random data sets arising mainly from protein activity, chemical reaction and radioactive decay rates, semiconductor noise and fluctuations in gravitational antennae. Shnoll spent over 50 years studying the similarities between the shapes of histograms generated from 60 - 100 measurement data sets. He found periodic daily, yearly and geographical correlations, gradual evolutions in histogram shape changes and also observed characteristic histogram shapes during solar eclipses. Shnoll later realised that the only way he could explain his results was if he assumed that there were anisotropic fluctuations in the spacetime continuum. My contribution to knowledge here is the analysis of two works by Cahill to show that they also display the overall general nonrandom properties that Shnoll observed, and to explain these properties from a Dynamical 3-Space model viewpoint. These data sets were generated from fluctuations in radio frequency electromagnetic waves travelling through coaxial cables, and also from tunneling current fluctuations in Zener diodes when operated in reverse bias mode. The short term effects Shnoll discovered from histogram shape comparison are also discussed from a Dynamical 3-Space model viewpoint, to show that they also tie in with the growing amount of evidence supporting a dynamical space-type theory.

Chapter 1

From Classical Physics to Big Bang Cosmology

1.1 Introduction

There have been several major incidents in history stemming from the time of Galileo Galilei (1564 - 1642) which have lead to the development of the Big Bang Theory. These incidents arose from assumptions based on the limited knowledge about reality at that particular time, and how these assumptions were then used to guide future experiments. This chapter seeks to illustrate these incidents, and how they then resulted in the introduction of the dark matter and dark energy parameters within conventional physics models which were necessary to explain phenomena that were later discovered.

1.2 Galilean Relativity

Before classical physics was developed, it was believed that a force was required to keep an object moving. Galileo performed an experiment using marbles and 2

inclined planes facing each other, where a marble was rolled down one side and back up to the other side. By smoothing the planes he could get the marble to roll up to the other side closer to the same height the marble started at. He attributed the difference in heights to a frictional force, and hypothesised that rolling a marble down a frictionless surface would then roll back up to the same height it started at. He then supposed that a marble rolling down an inclined plane and onto a frictionless horizontal surface would continue rolling forever, thus forming the first concept of inertia. In his 1632 dialogue Concerning the Two Chief World Systems[1] he related the inability to detect Earth's motion through space by considering a ship moving at constant velocity on a smooth sea, where observers below the deck would not be able to tell whether the ship was moving or not. He then put forth the first concept of relativity, where he assumed at least from a modern point of view[2] that:

1. Absolute space exists, and is modelled as a Euclidean 3-space (E^3) such that the universe is an empty container which objects move through. Here the space is not observable, dynamical nor has any structure,

2. Space and time intervals are recorded by observers using rods and clocks; these intervals are not affected when moving, and

3. Velocities are measured relative to observers O and O' for example, who then relate their time and space coordinates by

$$t' = t, \quad x' = x - Vt, \quad y' = y, \quad z' = z \tag{1.1}$$

where V is the relative velocity of the observers (here when both are moving in the x-direction). The speed w of another object (in the x direction for simplicity) according to each observer, is related by

$$w' = w - V. \tag{1.2}$$

Galilean relativity (GaR) is then defined by the above assumptions, with equations (1.1) and (1.2) forming the GaR Transformation. Isaac Newton used GaR to base his model of relativity on, mainly his theory of gravity, to which General Relativity then reduces to in the limits of low speeds and low matter densities.

1.3 Newtonian Gravity

Galileo is said to have dropped balls of different mass from the Leaning Tower of Pisa to show that they have the same acceleration, although it is unknown as to whether Galileo performed this experiment or not. This is the first mention of the equivalence principle, where the acceleration of a falling object due to gravity is independent of its mass, however the actual cause of gravity at the time was unknown. Meanwhile, Kepler provided laws based on his observations on planetary motions, and Newton later made a heuristic derivation of a theory of universal gravitation based on these observations.[3] This model was based mainly around the assumption that two massive objects mutually and instantly attract each other, and not that there is an underlying phenomenon that causes gravity. Newton's theory, like Galileo's, is also based from a series of assumptions. These include the existence of:

1. A universal, or absolute time referred to as being on a one-dimensional line (Galileo also assumed this). The events are said to occur depending on where they lie on this line.

2. An absolute and infinite space, in which the absolute motion of a body occurs in a way that the inertial motion of an object is uniform and linear, i.e. not accelerating.

3. Infinitely many inertial reference frames which are of infinite size.

4. Inertial reference frames move in all possible relative uniform motion, and two frames are related by a Galilean transformation.

5. The magnitude of a gravitational force is proportional to the inertial mass m_i that it acts on. Here m_i then also acts as a gravitational mass or charge, and so $m_i = m_g$. This equality became known as the weak equivalence principle.

Newton openly declared that his theory was phenomenologically based, and that he was simply axiomatising a set of observations currently known at a solar system level. His model did not explain how gravity emerges, only a definition of what was known about gravity and how it behaves locally. The inverse-square law of gravity is one of Newton's most famous equations, where the gravitational force F between two objects m_1 and m_2 separated by a distance r, is

$$F = \frac{Gm_1m_2}{r^2} \tag{1.3}$$

where G is Newton's gravitational constant and based on Kepler's planetary motion observations in the solar system. Kepler's laws were then explained, with the famous relationship $v^2 \ \alpha \ 1/r$ following from $F = ma = mv^2/r$, i.e. Newton's second law expressed in the form of circular motion, showing how the square of a planet's orbital velocity is inversely proportional to the orbit's radius. The gravitational force was taken to act instantaneously, i.e. the well known 'action-at-a-distance' expression, and could not be explained, only assumed to exist. Central to Newton's law being modelled from observations at a solar system level is the gravitational potential $V(r) = -MG/r$ which has an inverse distance relationship. The potential V depends on the amount of matter M in the gravitational source, and the strength of gravity is universally determined by the value of Newton's fundamental constant G. Newton's theory was then taken to apply universally. Here G is the only 'universal' constant in Newtonian Gravity (NG) and so is a one-parameter theory, but it is always coupled to the product MG, and so it cannot

be measured independently. This is shown by the irreproducibility in determining G experimentally,[4] where G measurements are performed in differing matter distribution environments, some which deviate from spherical symmetry. The $1/r$ dependence on the gravitational potential may not hold in all cases since there are questions as to whether the Newtonian potential is applicable on all distance scales. Newton's equations are also spherically symmetric, and based on such observations (e.g. a planet orbiting the Sun). The universe is known to deviate from such spherical symmetry, and so these two aspects challenge the claim that NG is always applicable. If NG is the fundamental building block of conventional physics models, then concerns can already be raised as to whether these models are most ideal to help describe reality.

1.4 Special and General Relativity

Around 180 years passed before other building blocks of reality were discovered. James Clerk Maxwell discovered how electricity and magnetism were related in his theory published in *A Treatise on Electricity and Magnetism* (1881)[5] and that light behaved as an electromagnetic wave. Maxwell described the interaction via his 4 famous equations, with the result being the derivation of the speed of light c. The existence of waves appeared to demand a medium to propagate through, which was coined the luminiferous aether. At the time, the appearance of a velocity in Maxwell's equations lead to the belief that the equations only expressed the speed of light in the rest frame of the aether, an unknown substance that only the Earth travelled through as the Sun's position remained fixed relative to the aether. Testing of the existence of the luminiferous aether was achieved by Albert Michelson, who conceived and developed an instrument with the intention of detecting the absolute motion of Earth around the Sun. The Michelson interferometer compares the change in the difference between travel times, when

the device is rotated, for two coherent beams of light that travel in orthogonal directions between mirrors; the changing time difference being indicated by the shift of the interference fringes during the rotation. With pointing one arm of the interferometer at the Sun and the other along Earth's orbit Michelson and Edward Morley obtained a result of 8 km/s as the speed of Earth's orbit around the Sun,[6] and hence through the aether, as it was taken that only the Earth was moving through the aether, and not the Sun as well. This was nowhere near the predicted Earth's orbit speed of 30 km/s, and the result was then declared null despite a small effect actually being observed. Galilean invariance - the principle that the fundamental laws of physics are the same in all inertial reference frames, was derived as a result. Michelson and Morley's interferometer results will also be mentioned in more detail in chapter 2. Applying to NG meant that all rods and clocks remain unaffected by a change in velocity. Fitzgerald (1889) and then Lorentz (1892) then offered an explanation for the null result, namely that the failure to get an effect was caused by the actual contraction of the arm moving lengthwise through the absolute space. This became known as the principle of Lorentz invariance, under which rods and clocks *are* affected by a change in velocity as described mathematically by a Lorentz transformation. Michelson and Morley's reported failure to observe the aether drove Einstein's 1905 paper *On the Electrodynamics of Moving Bodies*,[7] where he dismissed the notion of the aether. Absolute motion, i.e. motion relative to space itself had no meaning; it was in principle not detectable in a laboratory setting. Motion of objects was always relative to other objects, according to Einstein, i.e. Galilean invariance overruled Lorentz invariance for every physical observation, and both time and length were forced to be relative quantities. Using these assumptions Einstein went on to construct the Special and then General Theory of Relativity, which uses the notion of four dimensional spacetime to avoid any notion of absolute space. He first proposed via two postulates that:

- The laws of physics have the same form in all inertial reference frames.
- Light propagates through empty space with a definite speed c independent of the speed of the observer (or source).

Einstein dismissed Newton's notion of absolute time (and with it, absolute space), but kept the idea of relative time which is measured with actual clocks associated with local observers, i.e. each observer had their unique frame of reference and their own unique rods and clocks - there now existed no absolute (universal) frame of reference. In this theory, known as the Special Theory of Relativity (SR) time is always connected to the actual clocks of observers, i.e. no universal 'true' time for everybody to base their measurements from - it never flows equably for all observers no matter how they are situated with respect to each other. This however raised compatibility issues between NG and SR. From Newton's first and second laws, the gravitational force is proportional to the inertial mass of an object, and all known experiments point to $m_g = m_i$ to a great degree of accuracy. Einstein's SR was only valid for inertial reference frames, i.e. those without including the effects of gravity. Newton's 'action-at-a-distance' for gravity concept violated SR, as in SR no information can travel faster than the speed of light. Experimentally, NG could also not predict the correct orbit of Mercury due to its precession.

Einstein extended the theory to include the effects of gravity, i.e. reference frames that are accelerating/changing velocity. His 1907 paper *Principle of Equivalence* widened the scope of relativity to include uniformly accelerated motion of reference frames due to connections between such accelerated motion and gravitational fields, i.e. no experiment can locally distinguish between the two. The equivalence principle implied that geometry emerges from any suitable description of gravity, thus the equivalence principle developed to become what is known as the General Theory of Relativity (GR). Here GR is based off of a four dimensional construct

known as *spacetime*, a combination of Galileo's one dimensional time and Newton's absolute space formalisms, where gravitational fields influence the structure of spacetime through affecting light paths and spacetime intervals. Through relating Einstein's field equations to the energy-momentum tensor determined by the energy-matter density, the curvature of spacetime is determined, i.e. gravitational force displays geometrical behaviour instead of that of a force. A 'third' postulate was determined in that, in the limit of low speeds the gravity formalism should agree with Newtonian gravity. At the time, the apparent successful application of GR to (the then) currently observed phenomena such as the perihelion of Mercury and light-bending due to gravity (Sun) lead to rapid recognition and acceptance by the physics community.

1.5 Black Holes and Dark Matter

In 1916 Karl Schwarzschild derived a solution to the Einstein field equations for the case of a single nonrotating massive object, i.e. describing the gravitational field external to a spherical mass.[8] For a 'point-like' mass, the event horizon (i.e. escape speed due to gravity being the speed of light) was defined to be the Schwarzschild radius, i.e. the size of the event horizon as the distance at which no information can escape the point-like mass. Chandrasekhar (1930)[9] and Oppenheimer (1939)[10] predicted conditions in which stars would collapse to form these 'black holes', the term coined by John Wheeler in 1967. Black holes were found to exist at the centre of spiral galaxies in the assumed form of a point-like mass, and the theoretical velocity of a mass in circular orbit around a black hole is simply $v_O = \sqrt{GM/r}$, obtained from equating Newton's gravitational force to that of centripetal acceleration. By knowing how fast objects orbit a central point, its calculated mass can be then compared to the observed amount of luminous matter present by the object. Dutch astronomer Jan Oort in the 1930s

used this technique at least for stellar motions in the local galactic neighbourhood, indicating a mass around 3 times higher than that predicted by luminous matter calculations.[11] He then predicted the existence of a non-luminous matter which accounts for the apparent unseen mass present. In 1933 Fritz Zwicky also used this technique except at a much larger scale, i.e. through studying velocity dispersions in galaxies in the Coma galaxy cluster[12] and found the mass-to-light (ML) ratio (ratio of apparent mass due to velocity dispersion, to luminous mass) to be around 50 (when using the currently known Hubble constant). Zwicky also concluded that a new form of non-luminous matter is present to account for the high velocity dispersions which he coined 'dark matter'. Zwicky's work was largely ignored for decades however Smith (1936)[13] suggested that the Virgo Cluster presented a similar problem, and Babcock (1939),[14] Rubin & Ford (1970)[15] and Roberts & Winehurst (1973)[16] reported that the outer regions of the Andromeda (M31) galaxy rotated with higher velocities than predicted by the Keplerian drop off rate (the rotation curve even appeared 'flat') although Zwicky was rarely cited in articles. Roberts & Winehurst noted that the galaxy mass appeared to increase while the luminous mass did not - it wasn't until the 1970s until the notion of dark matter became accepted when Ostriker, Peebles and Yahil (1973,4)[17, 18] showed that a dark matter halo component could explain the apparent increasing galaxy mass with radius, which is required to explain the flat rotation curve of M31. Since its acceptance forty years ago no physical evidence of dark matter has been found, its discovery now a requirement as a test of GR.

1.6 Universe Expansion and Dark Energy

Einstein preferred the notion of a static universe, which neither contracts nor expands. In 1917 he introduced the cosmological constant into his field equations for GR, a repulsive term equal to the value of the energy density of the vacuum

of space designed to negate the effects of gravity. After GR was accepted however cosmology developed quickly, when in 1929 Hubble observed the recession of galaxies and the discovery of the Universe's expansion, and Einstein removed the cosmological constant from GR saying it was his 'biggest blunder'. A theory for the origin of the Universe was developed by Gamow and dubbed the 'Big Bang' by Hoyle, who rejected Gamow's theory while supporting his (with Bondi and Gold) 'Steady-State' theory that the Universe existed indefinitely.[19] Along with Hubble's discoveries the Big Bang cosmology also predicts the existence and black body nature of the cosmic microwave background (CMB) and its anisotropies, as discussed in section 1.8. Observing the amounts of hydrogen, helium and lithium in stars and gas clouds in galaxies allows us to then predict the light element abundance formed in the first few minutes after the Big Bang. In Big Bang cosmology there are 3 main principles or assumptions,[20] firstly that space is assumed to be homogeneous and isotropic when viewed at sufficiently large scale. This was also known as the Cosmological principle, and can be expressed as a spacetime metric discovered by Friedmann-Robertson-Lemaitre-Walker (FLRW, or FRW) in the form:

$$ds^2 = a(t)^2 \left[\frac{dr^2}{1 - kr^2} + r^2(d\theta^2 + sin^2\theta d\phi^2) \right] \tag{1.4}$$

Here $a = a(t)$ is the scale factor of the universe, i.e. the relative size of the universe at time t, where at current time t_0, $a(t_0) = 1$. k is the curvature of the universe which can be closed ($k = 1$), flat ($k = 0$) or open ($k = -1$), i.e. k describes the geometry of the universe. The FLRW metric then predicts how a straight path through spacetime is affected by the expansion and curvature of the universe. The dynamics of spacetime itself is then described by the Einstein equations which relate the expansion rate of the universe to the energy density ρ and pressure p. The matter present in the universe may also be described as a superposition of two classical perfect fluids i.e. a radiation fluid with a relativistic equation of state (primordial plasma), and an exotic pressure-less matter called 'cold dark matter',

i.e. $p = w\rho$. A relationship between the universe's expansion and the required matter density was derived by Friedmann in 1922 through Einstein's field equations using the FLRW metric and a perfect fluid with mass ρ and density p. Two important results were determined, the first being the 00 (temporal) component of the field equations and relative to chapter 6:

$$\frac{\dot{a}^2 + kc^2}{a^2} = \frac{8\pi G\rho}{3} \tag{1.5}$$

The overdot in a denotes a derivative with respect to time, and so this equation can be used to determine the expansion rate of the universe. For a flat ($k = 0$) universe there would exist a critical density ρ_c which then dictates the evolution of the universe over time. The Perlmutter[21] and Schmidt - Reiss[22] teams studied the universe's evolution through observing type 1a supernovae magnitude-redshift data up to a time where the universe was a third of its current size. These teams realised that equation (1.5) is strongly violated by the data; the observed baryonic density of the universe is 20 - 25 times less than ρ_c. This prompted the introduction of the 'dark energy' parameter, a cosmic repulsion term which then predicts the future expansion of the universe at an exponential rate. It also allowed estimations of the total matter density compositions in the universe, with 73% dark energy, 23% dark matter and only 4% baryonic matter. Perlmutter, Schmitt and Reiss were awarded the 2012 Nobel Prize in Physics for their discovery. This contradicted the previous assumption that the expansion was slowing down due to the presence of gravitational terms only (baryonic matter and dark matter) in the Friedmann equations, resulting in an eventual 'Big Crunch' as the universe's expansion slows, stops and then reverses. So not only does GR require one free parameter to fit one data set (velocity dispersions in stellar and galaxy data) but it then needs a second one to fit a different data set (supernovae magnitude-redshift data), which then demands exotic phenomena such as the accelerating expansion of the universe. The implications of the supernova data will be further studied in chapter 6.

1.7 Black Holes in an Expanding Universe

The motions of stars in galaxies are strongly affected by their central massive black holes, and that of galaxies in clusters are also affected by the expansion of the universe. Then the need arises to analyse black holes in the expanding universe, with the view to checking if that expansion affects black hole characteristics. There is also a long history of attempts to model black holes (BH) while embedded in an expanding universe. Early attempts include the McVittie solution[23] obtained simply by embedding a single BH in the FLRW metric. This BH solution approaches a FLRW universe at infinity however this solution was disqualified as BH in a FLRW universe (see ref 7 of Gibbons and Maeda).[24] There is the Einstein-Strauss model containing a patchwork of Schwarzschild BHs in the background (FLRW) universe[25] and also the Sultana/Dyer solution,[26] which describes the behaviour of BHs in a flat expanding universe (also known as the Einstein-de Sitter universe). The requirement of dark energy in GR then predicts solutions for black holes in an expanding universe starting with the Schwarzschild-de Sitter (uncharged BHs in a DE dominated universe) and Reissner-Nordström de Sitter (charged BHs) solutions.[27, 28] Although these spacetimes are static, they may be transformed into the form of a black hole in an exponentially expanding universe.[29] The effects that an expanding universe has on a point-like object was studied by Nandra *et al.*[30] where it was found that at galaxy cluster level there existed two important radii. The first radius being defined as r_F, is the distance from an object where the forces due to gravity and the expanding universe cancel and thus an object remains a fixed distance away from the centre of a cluster. The second radius r_S relates to the largest possible stable orbit and is typically smaller than r_F. The radius r_F relates to studying galaxy cluster data such as the recessional velocities of galaxies in the M81 group. Peirani and Pacheco[31] use a numerical solution that combines the gravity due to black hole mass with the Hubble constant and dark energy strength to model how galaxies in clusters

recede from each other. A discussion of the effect of embedding black holes in an expanding universe using the Dynamical 3-Space theory model will be presented in chapter 7.

1.8 Cosmic Microwave Background Anisotropies

The accidental discovery of the cosmic microwave background (CMB) and its temperature anisotropies is a major test of cosmological models. The CMB is an isotropic radiation bath that permeates the universe, and is a remnant of the primordial plasma existing at a time when the universe was hotter than 3000 K ($\approx 1/1100$th its current size). The prediction and discovery of the CMB dates back to 1947, with a temperature prediction of 5 K made by George Gamow, Ralph Alpher and Robert Herman, however at the time cosmology was not a widely discussed topic by astronomers. The CMB was again acknowledged in the 1960s independently by Yakov Zel'dovich and Robert Dicke[32] and in 1964 Doroshkevich and Igor Novikov discussed CMB radiation as being a detectable phenomenon.[33] The CMB was accidentally detected by Penzias and Wilson at Bell Telephone Laboratories in 1965, where the instrument they were using for satellite communication experiments had an excess 3.5 K temperature they could not account for. The serendipitous discovery resulted in Penzias and Wilson winning the 1978 Nobel Prize in Physics. Later in 1992, the NASA Cosmic Background Explorer (COBE) detected temperature fluctuations in the CMB to 1 part in a million (2006 Nobel Prize).[34] The Wilkinson Microwave Anisotropy Probe (WMAP, 2001 - 2008)[35] and Planck Mission (2009 - 2013) detected the CMB anisotropies to much greater accuracy.[36] The CMB map provides a sky map of the temperature fluctuations in all directions, and these fluctuations can be plotted in the form of an angular power spectrum which breaks down the data into spherical harmonics. The peaks in the harmonics can then be used to provide information about the Universe.

To obtain a theoretical derivation of the CMB spectrum the FLRW metric is perturbed and combined with the Boltzmann equations, to provide how perturbations in different matter densities (i.e. baryonic, dark matter) evolve over time. This information is then translated into how the temperature fluctuation amplitudes of increasing angle in the sky (related to the spherical harmonics) are affected, and then compared with the power spectra generated by WMAP and Planck data. This theoretical framework has evolved into what is known today as the Λ_{CDM} model, and is the standard model of Big Bang cosmology. The Λ_{CDM} model currently has 6 parameters required to explain the CMB data - these are the baryonic matter Ω_b, dark matter Ω_{DM} and dark energy Ω_Λ densities, scalar spectral index n_s (a measure of the scale invariance of the primordial perturbations), curvature fluctuation amplitude $\triangle^2_{\mathbb{R}}$ (relates to the universe curvature) and reionization optical depth τ (relating to the decoupling period, where the primordial plasma cools to form stable hydrogen over a period of time). Applying the Λ_{CDM} model to CMB data yielded the parameters $\Omega_\Lambda = 0.69$, $\Omega_{DM} = 0.26$, $\Omega_b = 0.05$ and also the Hubble constant $H_0 = 70$ km/s/Mpc.[37]

1.9 Cosmic Inflation

The discovery of the CMB anisotropies generated many problems with the standard model of cosmology. There is no possible causal mechanism to explain the observed large scale isotropy of the CMB, i.e. photons emerging from opposite sides of the sky are not causally connected as information cannot travel faster than the speed of light. This was referred to as the horizon problem. The CMB data predicts the universe to be spatially flat,[38] requiring that the initial energy density ρ must have been incredibly close to that of the critical density ρ_c however $\rho = \rho_c$ is a critical unstable point in standard cosmology. There is also no causal mechanism to generate the required primordial perturbations that later

generate the observed galaxy structure formation, which occurs at a faster rate than is predicted by standard cosmology. An inflationary model of the universe was introduced which predicts a rapid exponential expansion of the universe at early times.[20] This accounts for at least the horizon and flatness problems that the standard Big Bang model produced, as well as containing a mechanism to introduce perturbations into the primordial plasma, and produce the small inhomogeneities that turn into the CMB anisotropies observed today. Evidence for the primordial perturbations was only discovered recently from studying B-mode polarisation modes in the BICEP2 CMB data.[39] This appeared to confirm the existence of an inflationary epoch as required by the standard model of cosmology however the data suggests a much stronger inflationary period than predicted by current models of inflation.[40] The claim of the evidence supporting cosmic inflation was withdrawn by the BICEP team after discovering that the signal was likely to result mainly from dust radiation from the Milky Way galaxy.[41] The discussion here is limited to Big Bang cosmology since it is the accepted model, and also the Dynamical 3-Space theory which is discussed in the following chapter. The CMB spectrum along with cosmic inflation will also be discussed further in chapter 6. There are however other cosmological models such as matter bounce,[42] string gas cosmology[42] and steady state theory.[19] These are not discussed here.

1.10 Concluding Remarks about Chapter 1

The standard Big Bang cosmology framework is based from GR and SR which in turn are based from NG and Galilean observations. These models were based from 'local' observations of planetary motion in the Solar system and then using interferometer experiments and again after the discovery of the Universe's expansion. At each step the newer theory is forced to agree with both observation and the previous theory. Building on the foundations of GR after further discoveries raised

serious questions about its feasibility, and required the introduction of two free parameters, namely 'dark matter' and 'dark energy' to explain such observations. This then produced exotic predictions as to the evolution of the universe, further inconsistencies with experiments, and the creation of cosmic inflation theories to fix these inconsistencies. Chapter 2 uses a different approach to understand these observations via an alternative model of reality which has different fundamental building blocks.

Chapter 2

Justifying An Alternative Model of Reality

2.1 Introduction - Process Physics

Apart from what was mentioned in chapter 1 there were other motivations to find an alternative model of reality.[43] These include:

1. It was not believed that all aspects of time could be completely modelled from a geometrical viewpoint. For example, modelling the present moment required the establishment of a metarule to explain its existence.

2. Elements of a stochastic neural network appeared to be hidden within quantum field theory, suggesting that perhaps all of reality could be modelled to behave in a similar fashion.

3. A syntactical description of reality was considered impossible to describe all of its components, as the emergence of the syntax is taken for granted and cannot be explained.

A theory was developed which acknowledged the limitations of logic discovered by Gödel[44] and extended by Chaitin,[45, 46] by using the notion of self referential noise, and which introduced a radical information-theoretic modelling of reality. In this theory time was modelled as a self organising process, i.e. as the successive ordering of events, as opposed to by modelling geometrically, which has been the case since the time of Galileo over 400 years ago. This self organising process would compete with a stochastic, or random process during each iteration of the model. There was therefore an order/disorder system at the 'start-up' of the modelling but which *a priori* contained no notion of geometry, space or quantum matter. This model can then be considered simply as information which is evolved internally, such that it produces its own relational patterns and modes of behaviour. This theory is known as *Process Physics*[47], and mainly contains components modelling a stochastic neural network as inspired by not only the apparent operation of biological brains, but also through the discovery that conventional quantum field theories appear to display neural network modelling properties. This stochastic neural network then represents information as connection patterns, as opposed to symbols or syntax as found in conventional physics theories. The network was then shown to self organise these patterns in a way that it displays geometrical and fractal properties, along with the emergence and unification of quantum phenomena without any initial assumptions about these phenomena. What also emerged was the development of a Quantum Homotopic Field Theory which was aimed at modelling these properties. This was expected to approximate to a more conventional quantum field theory containing many of the attributes of the current standard model of particle physics.

The idea behind *Process Physics* was originally to derive the emergence of known quantum phenomena, and ideally the syntactical description of reality suggested by General Relativity. What followed instead was a radical deviation from conventional physics, mainly the emergence of a growing fractal geometry which is

dynamic and approximately three dimensional in nature, and the prediction that matter is simply fractal topological defects embedded in the geometry, or quantum foam as it was called. This quantum foam explanation is also emergent from *Process Physics* and provides an explanation for the necessary emergence of gravity, since quantum 'matter' essentially acts as a sink for the quantum foam. By ignoring the non trivial topological aspects of the quantum foam it may then be embedded in the 3 dimensional geometrical manifold used today and referred to classically as a dynamical 3-space, i.e. a real existent fractal network of events and connectivities which rearranges as it flows past an observer. Since the embedding of the space in a geometrical manifold can be arbitrary (i.e. rotated/translated etc.) this then dictates the minimal dynamics for the space at a phenomenological level. While *Process Physics* is currently unable to mathematically transition from a quantum foam theory to a classical theory, a model known as Dynamical 3-Space theory contains a phenomenological derivation based on evidence for an absolute reference frame.

2.2 Dynamical 3-Space Theory

A heuristic derivation of the dynamics of space was developed by firstly assuming that Galileo's observations suggested the existence of a dynamical space, whose acceleration would generate the same acceleration of matter.[48] Its velocity would be shown to match that of observed light speed anisotropy experiments along with the acceleration determining light bending and gravity as refraction effects. As discussed in the introduction, space at a deeper level is probably a fractal quantum foam that can be embedded in a 3 dimensional manifold. However this embedding manifold has no meaningful existence; it is only used to note that space has an approximate dimension of 3 and also to study classical phenomena (i.e. gravity, velocity fields etc.) in the quantum foam using observers with physical rods and

clocks. This is often confused with aether theories, where a substance travels through a real but unobservable space - here both aether and space are viewed as being ontologically real, whereas in Dynamical 3-Space theory there is only the observable quantum foam, and any of its emergent properties are those intrinsic solely to the quantum foam. In this theory[49] space is assumed to have a structure which can be described by a velocity field $\mathbf{v}(\mathbf{r}, t)$ at location $\mathbf{r}$ and time t (Newton instead used a gravitational field, as he took space to be real but unobservable). Since there is now an absolute reference frame, observers in relative uniform motion are required to relate their description of the space velocity field via Galilean and Lorentz Relativity transformations. Lorentz Relativity is also experimentally distinguishable from SR as it is with reference to an absolute reference frame, unlike SR.[2] Part of the minimal dynamics must include the ability to flow, thus introducing an Euler type flow into the space dynamics. This flow is characterised by tracking its change in velocity field over time, i.e.

$$\mathbf{a}(\mathbf{r}, t) = \lim_{\triangle t \to 0} \frac{\mathbf{v}(\mathbf{r} + \mathbf{v}(\mathbf{r}, t)\triangle t, t + \triangle t) - \mathbf{v}(\mathbf{r}, t)}{\triangle t} = \frac{\partial \mathbf{v}}{\partial t} + (\mathbf{v} \cdot \nabla)\mathbf{v}. \tag{2.1}$$

Equation (2.1) describes the acceleration of a constituent element of space by tracking its change in velocity. As the Dynamical 3-Space theory attempts to model a fractal geometry, or 'quantum foam' emerging from *Process Physics*, space then essentially has a quantum structure that permits its velocity to be defined and detected, which experimentally has been achieved and discussed later in this chapter. To simplify (2.1), the flow is assumed to have zero vorticity $\nabla \times \mathbf{v} = \mathbf{0}$, which forces the flow to be determined by a scalar function $\mathbf{v} = \nabla u$. Only one scalar equation is then needed to determine the space dynamics, simply constructed by taking the divergence of $\mathbf{a}$. Equation (2.1) then becomes

$$\nabla \cdot \left(\frac{\partial \mathbf{v}}{\partial t} + (\mathbf{v} \cdot \nabla)\mathbf{v} \right) = -4\pi G \rho(r, t) \tag{2.2}$$

where the inhomogeneous term determines a dissipative flow caused by matter, expressed as a matter density, and where the coefficient turns out to be Newton's gravitational constant G. Note here that even a time independent matter density $\rho(r)$ can still be associated with a time-dependent flow. Also note that this is Newtonian gravity simply cast into an inflow (velocity) formalism, one which Newton didn't consider at the time. This zero vorticity assumption has lead to determination of the speed and direction of space from multiple experiments using the current Dynamical 3-Space equation (see below), which will be discussed in chapter 3. The generalisation of the model to include vorticity effects and its application to gyroscope precession experiments has been reported in [50, 51]. External to a spherically symmetric matter distribution, of total mass M, and a time-independent spherically symmetric flow, equation (2.2) has the solutions

$$\mathbf{v}(\mathbf{r}) = -\sqrt{\frac{2GM}{r}}\hat{\mathbf{r}}, \qquad \mathbf{a}(\mathbf{r}) = -\frac{GM}{r^2}\hat{\mathbf{r}} \tag{2.3}$$

which is an inverse square law emergent from the Euler constituent acceleration, which imposes a space self interaction effect. For the simplest case of the spherical matter density stationary with respect to (wrt) a 3-space the analytic solution is known, however for more complex situations such as matter moving wrt space numerical solutions are required, and which would reveal non trivial wave effects. It is however trivial for two observers in relative motion to relate their description of the space velocity field using Galilean Relativity transformations. While equation (2.2) contains terms describing a space velocity field, there are also additional terms with the same order in speed and spatial derivatives which cannot be *a priori* neglected. Since this derivation would be arising from a deeper theory such as quantum foam theory which *Process Physics* would require, one can also consider a derivative expansion approach. All such terms added are invariant under rotation and translation, and when combined give the current Dynamical

3-Space equation,[52]

$$\nabla\cdot\left(\frac{\partial \mathbf{v}}{\partial t}+(\mathbf{v}\cdot\nabla)\mathbf{v}\right)+\frac{\alpha}{8}\left((trD)^2-tr(D^2)\right)$$
$$+\frac{\delta^2}{8}\nabla^2\left((trD)^2-tr(D^2)\right)+...=-4\pi G\rho\ ,\ \ D_{ij}=\frac{\partial v_i}{\partial x_j}. \tag{2.4}$$

The α and δ (plus additional higher order derivative terms denoted by an ellipsis) terms contain higher order derivatives and derivative terms and describe the self interaction of space at large (α) and small (δ) different scales. The coefficients of the trace terms $(trD)^2$ and $tr(D)^2$ are forced to be equal and opposite, in order to preserve the inverse square law external to a stationary spherical matter density wrt space. Here G is Newton's gravitational constant, which according to Dynamical 3-Space theory now relates the amount of dissipative flow of space (quantum foam) into matter. Equation (2.4) currently isn't derivable from the deeper *Process Physics* theory however it appears to model currently known phenomena quite well, without requiring additional free parameters. It is a heuristic derivation based from generalising Newtonian gravity into an inflow formalism and then adding extra terms which *a priori* cannot be neglected as mentioned above. The value of α, a dimensionless self coupling constant, was determined from laboratory, geophysical[53] and astrophysical[54] data to be the fine structure constant 1/137, demonstrating that space is fundamentally a quantum process and thus unifying space and quantum physics. This data will be discussed in chapter 5. δ has the dimensions of length, most likely at the Planck scale, and has been shown to account for galactic black hole masses and cosmic filament phenomena.[52] The value of δ has yet to be determined from any data so far but is assumed to be very small but non-zero, and is required to study space at very small scales. If $\alpha=\delta=0$, (2.4) reduces to (2.2) and hence Newtonian gravity, i.e. the Dynamical 3-Space equation can be reduced to NG cast into an inflow formalism as opposed to one requiring gravitational fields. As Newton believed matter was gravitationally attracted to each other through a real but unchanging space, he had no need

to rewrite his equation in the form of (2.2) as his observations were only based on examining Kepler's laws of planetary motion. He however makes no mention of what is causing the acceleration of matter although later he did speculate that an aether type substance could account for gravity in 1675, in a letter to Oldenburg, Secretary of the Royal Society, and later to Robert Boyle.[55] Since planetary motion within the solar system is largely spherically symmetric (i.e. low planetary mass wrt the Sun) any α effects observed in the solar system will be negligible, an effect which Newton was unaware of. These α- terms however cannot be *a priori* neglected in the space dynamics due to them having the same order derivatives as the Euler terms. At a galactic scale α effects are quite prominent, where the Milky Way black hole and other galaxy cluster data sets have given evidence for both α and δ terms as will be discussed in chapters 3 and 5. A final note is to observe that equation (2.4) does not involve the speed of light c, is non linear and time dependent, and implies that the universe is more connected than previously thought than using NG. Dynamical 3-Space theory has a number of predictions centering around the phenomenon of gravity along with the time dependent nature of space, which will be discussed in chapter 3 along with testing how matter and EM radiation respond to this dynamical space. The rest of this chapter presents evidence consistent with a dynamical space-type theory.

2.3 Evidence Consistent with a Dynamical Space-Type Theory

2.3.1 Interferometer Experiments

The 1887 interferometer experiment undertaken by Michelson and Morley actually resulted in an absolute light speed anisotropy of 8 km/s **according to their theory of the interferometer**. This was however rejected in favor of a null

result as the result was far less than the expected 30 km/s orbital speed of the Earth, which the experiment was originally designed to study. By the time Dayton Miller realised in the 1920s that the data instead suggested that the theory for the interferometer was incomplete, i.e. that the apparatus moved not only around the Sun, but also at higher speeds through Milky Way galaxy and the universe as we know today, Einstein's theory of SR and GR had already taken hold and absolute motion had become a taboo subject. Further interferometer experiments (and others regarding absolute motion) yielding non null results were scorned, ignored and/or rejected by the physics community.

In 2002 Cahill and Kitto[56] reported a relativistic theory for the operation of the Michelson interferometer in an absolute reference frame, and reanalysed the Michelson-Morley data to obtain a light speed anisotropy of some 360 km/s. This was the first relativistic effects-based theory analysis since the data was published in 1887, mainly due to the large influence Einstein's work held on the physics community. The new interferometer theory contains an expression for the travel time difference between light travelling in the orthogonal arms as (ignoring Fresnel drag effects, which are mentioned later this chapter)

$$\triangle t = k^2 \frac{L|\mathbf{v}_P|^2}{c^3} \cos\left(2(\theta - \psi)\right). \tag{2.5}$$

Here the absolute velocity $\mathbf{v}$ is projected onto the interferometer at angle ψ relative to the local meridian and with velocity $\mathbf{v}_P$, and θ is the angle of one arm with respect to that meridian. L is the interferometer arm length, c is the speed of light and $k^2 = n(n^2 - 1)$ is the new expression which accounts for interferometers travelling in mediums of refractive index n, one which Miller[57] thought existed but had no theory for. The two key effects, namely (i) the path length of the two orthogonal arms changing when the interferometer is in absolute motion, and (ii) that Fitzgerald-Lorentz contraction of the arms along the direction of motion, now a real dynamical effect caused by rods and clocks being affected by the quantum

foam, cancel each other out in vacuum ($n = 1$ and so $k = 0$). This then explains why all interferometers (and resonant cavities for that matter) operated in vacuum mode cannot study light speed anisotropy at all, as indicated by the increasingly accurate null results over the decades[58–60] as they only test for the cancellation of these two effects in vacuum. A null result does agree with Einstein's postulate regarding light speed isotropy however, and hence physicists then misinterpret these results as verifying GR despite the fact that vacuum mode interferometers are insensitive to detecting absolute motion. The two above mentioned effects however are predicted to not cancel when operated in the presence of a gas (k is very small but nonzero) as the speed of light is slowed down as $V = c/n$, thus distinguishing between GR and theories involving absolute motion. Newtonian physics, which the initial studies by Michelson and Miller were based on, contains no Fitzgerald-Lorentz contraction and so $k^2 = n^3$,[61] and so $k \approx 1$ for analyses made in 1887. This is compared to Cahill and Kitto's model predicting $k = 0.0241$ for air, making interferometers around 2000 times less sensitive in air than previously thought. This is certainly shown by interferometer data giving such small fringe shifts. The absolute projected light speed anisotropy v_P compared to speeds using Newtonian physics was then shown to be

$$v_P = \frac{v_N}{\sqrt{n(n^2-1)}} \tag{2.6}$$

where v_N is the speed predicted by Newtonian physics. Projected speeds are therefore dependent on refractive index, as helium has also been used as a medium in interferometers.[62] A summary of the main interferometer results is shown in table 2.1. Michelson and Morley in 1887[6] made observations based in Cleveland (Latitude $41°30'N$) and collected results of 36 full rotations of their air-mode interferometer at 22.5 degree intervals, in 6 separate hours over 3 separate days (1 hour at 12:00 on July 8,9 and 11 and again at 18:00 on July 8,9 and 12). Each rotation took 6 minutes as the interferometer rotated slowly on a tank of mercury

designed to eliminate vibrations. They published and analysed the average of each of the 6 data sets instead of looking at separate rotations, and obtained speeds of 5 - 7.5 km/s. The smaller speeds than that shown in table 2.1 occurred due to this averaging (12:00 data, and separately the 18:00 data), whereas Miller and Cahill report higher speeds between 8 - 8.8 km/s from Michelson & Morley due to studying individual rotations, some of which do not have a sinusoidal form induced by rotating the interferometer. With $k = 0.0241$, the new interferometer theory changes an 8 km/s anisotropy to 331 km/s via equation (2.6), for example. In 1927 Illingworth[62] constructed an interferometer experiment using helium instead which has a refractive index $n = 1.00036$, making $k = 0.00836$, thus checking the n dependence of k. Due to the massive reduction of the sensitivity of the interferometer using helium, Illingworth unsurprisingly reported no "*ether drift to an accuracy of about one kilometer per second*", however Múnera[63] reanalysed the data (along with reanalysing other interferometer data including Michelson-Morley and Miller) and obtained a value of 3.13 ± 1.04 km/s. This yielded a speed of 368 ± 123 km/s, in agreement with the Michelson/Morley data however no direction was able to be obtained as there was insufficient data.

Future interferometer experiments were not repeated immediately after the pioneering work by Michelson and Morley to confirm the results until Dayton Miller's [57] research where, with Morley he developed his interferometer between 1902 and 1906 and took preliminary observations around 1904 - 1905. Miller then went to a great deal of effort to ensure his interferometer was sensitive to only detecting absolute motion, and undertook many rigorous control experiments to study and reduce the effects of vibration and heating, mainly between 1922 and 1924. Over 200,000 measurements were then recorded by Miller, accounts of which are available in Swenson[67], over half of which are in the form of 12,000 rotations performed between April 1925 and February 1926, as compared to Michelson's 36 rotations over 3 days / 6 separate hours. Miller found that that temperature

Table 2.1: Summary of absolute speeds and directions obtained from interferometer experiments.

Person/Group		**Michelson & Morley**[6]	**Miller**[57]	**Illingworth**[62]
Year		1887	1925 - 26	1927
Location		Cleveland, Ohio	Mt. Wilson, California	Pasadena, California
Medium		Atmospheric (n=1.00029)	Atmospheric (n=1.00029)	Helium (n=1.000035)
Original Absolute Velocity	**V (km/s)**	8.4 ± 0.4[6, 57]	10.25 ± 0.95, 209 (Cosmic)	1[62], 3.13 ± 1.04[63]
	RA (^{h})	6.5 (Noon) 12.8 (PM)[57]	4.85 ± 1.15	Unknown
	Dec (°)	Unknown	-69.5 ± 7.5	Unknown
Calibration Factor k[64]		0.0241	0.0241	0.0084
Corrected Velocity[64]	**V (km/s)**	328 ± 50	420 ± 30	368 ± 123
	RA (^{h})	Unknown	5.2	Unknown
	Dec (°)	Unknown	-67	Unknown
Person/Group		**Shamir & Fox**[65]	**Cahill**[66]	
Year		1969	2007-08	
Location		Haifa, Israel	Adelaide, South Australia	
Medium		Perspex ($n = 1.495$)	Optical Fibre ($n = 1.462$)	
Original Absolute Velocity	**V (km/s)**	< 6.64	Unknown	
	RA (^{h})	Unknown	5.9 ± 2.4	
	Dec (°)	Unknown	-72 ± 6	
Calibration Factor k[64]		N/A for solids[61]	N/A	
Corrected Velocity	**V (km/s)**	N/A	N/A	
	RA (^{h})	N/A	N/A	
	Dec (°)	N/A	N/A	

effects could be assumed to be linear provided that each turn was performed sufficiently quickly enough, and a uniform temperature background drift could be removed from the data. Sets of 20 turns (320 measurements over 18 minutes) would be observed in a single sitting however if a single reading was lost due to vibration, miscalculation or other means then that observation was cancelled, thus showing how aware Miller was of the importance of his experiments. Miller in his experiments obtained a speed of (see table 2.1) approximately 10.25 km/s

which corrects to 425 km/s ($k = 0.0241$) using the full theory of the interferometer, which Miller was unaware of (he used the Newtonian theory, where $k = 1$ and which neglects both Fitzgerald/Lorentz contraction and gas presence effects). This speed is consistent with Michelson-Morley's result of 330 km/s as Cleveland has a higher latitude than Mt. Wilson. While Miller didn't know the theory for the interferometer he understood that there was a flaw in the Michelson-Morley analysis. He assumed that the absolute velocity of Earth was split into 2 components - the orbital motion of Earth around the Sun, and the movement of the solar system through the galaxy, and he then introduced the scaling factor k. Here k was only phenomenologically based and Miller had no theory for its value, but he reasoned that since Earth's direction changed he could extract k as well as the solar system velocity component. An effect was potentially missed by Miller, namely the inflow of space into the Sun as predicted by Dynamical 3-Space theory, which will be explained in chapter 3. He undertook interferometer experiments in April, August and September 1925, and February 1926 throughout all hours of the day and determined the velocity of absolute motion (he called this the solar system movement) was 209 km/s in the direction $(4.85^h, -70^\circ)$ and did indeed change slightly throughout the year (see table 2.1 and figure 2.1), and estimated the value of k to be around 0.05, twice that predicted by the full interferometer theory. Reasons for the discrepancy are given in [64]. Miller's results were incredible, and confirmed the validity of the Michelson-Morley observations that absolute motion had been detected. However by then GR had already been established, and Miller's results were refuted, even ignored by the physics community although Miller was regarded highly by the physics community as a careful experimentalist. Fourteen years after Miller's death in 1941 Shankland,[68] a former student of Miller, reported that Miller's results were in fact due to temperature fluctuations and in fact had observed a null result. This was despite the fact that Miller has rebutted several criticisms of his work while he was alive, including that regarding temperature effects. An extensive review of the Shankland analysis and handling

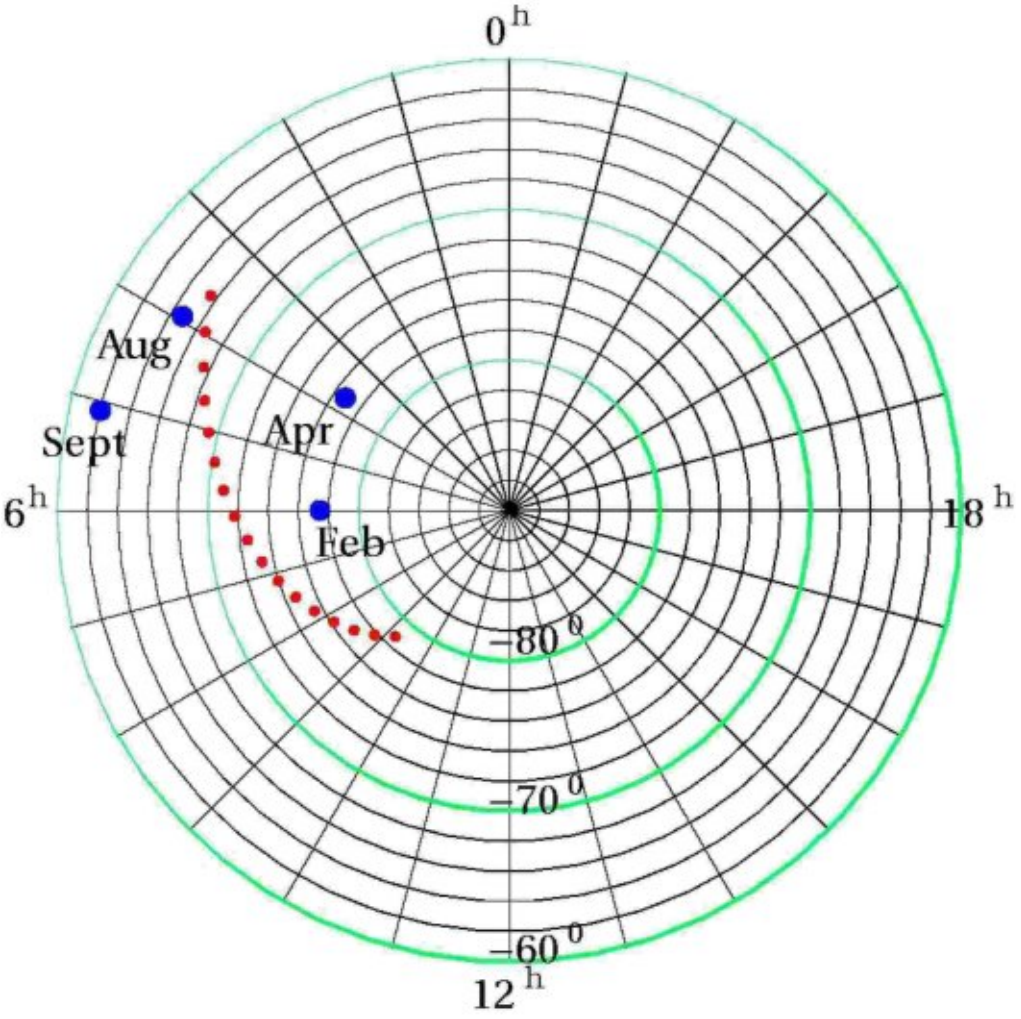

Figure 2.1: Southern celestial sphere, summarising the absolute motion directions found by Miller (Apr 1925 - Feb 1926, blue points) and Cahill (Sep - Dec 2007, red points, trending closer to the south celestial pole over time) using right ascension and declination. Figure source from [66].

of the criticism of Miller can be found at [69].

No other major non-null interferometer experiments had been reported due to the use of vacuum mode (instead of gas mode) interferometers and resonant cavity experiments, until 2007-8 when Cahill reported[70] that optical fibre interferometers detect light speed anisotropy. The results were only preliminary, with photodetector recording voltage readings obtained only and no actual determination of the speed of absolute motion due to the inability to calibrate the apparatus. Cahill however later reported[66] correlated detection of light speed anisotropy by two detectors respectively oriented 6° differently to the local meridian. If apparatuses

are aligned differently they record Earth induced travel time difference minima at different times as they would be aligned with the space flow at different times, which was observed and predicted. The right ascension and declination values reported were also in agreement with that found by Miller.

2.3.2 Non-Interferometer Experiments

One Way Speed of Light Experiments - DeWitte, Torr-Kohlen and Cahill

The gas-mode Michelson interferometer was an extremely difficult and insensitive apparatus to use, as indicated by the arguments in the interpretation of the data. The main problem was that it was a second order device in that the travel time difference between the orthogonal arms was proportional to $(v/c)^2$, which is very small, and without gas the device is rendered useless. A serendipitous discovery in 1991 saw Roland DeWitte, an employee for the Belgacom telecommunications company in Belgium design and use an apparatus to detect absolute motion that was first order in (v/c).[71] The experiment used 1.5 km length coaxial cables buried underground where sets of 3 caesium beam atomic clocks located at either end recorded the travel time difference as radio frequency (RF) signals were sent in opposite directions through the cables. This was undertaken in a research project aimed to synchronise the two sets of atomic clocks. The project included accounting for drifts with temperature, cable length, humidity, pressure, heat capacity of the clocks, magnetic induction and current fluctuation effects and found that any long term drift was linear, reproducible and could not be explained by outside factors affecting the clocks or cables. The drift was analysed over 178 days and the phase signal was found to have a period of 23 h 56 m, i.e. a sidereal day, concluding that absolute motion had indeed been detected as the period of the signal was relative to the stars. What makes this experiment remarkable is that the apparatus was aligned N-S, more in line with the direction of absolute motion

of $-70°$ permitting the study of absolute motion (apparatuses aligned E-W generate a much weaker effect as the direction of absolute motion is perpendicular - see the Torr-Kohlen discussion next). While DeWitte understood that he had discovered absolute motion he expected the direction to coincide with that of the CMB direction ($\approx 11^h$), but he was unaware of Miller's papers and failed to realise that his direction of 5.0^h (17^h is also possible here due to lack of data) agreed almost exactly with that of Miller (5.2^h). DeWitte only released 3 days worth of data and the only mention of his results were through email and website correspondence as he was unable to have his results published, as they contradicted prevailing theories. In his email he writes:

Incredibly, the output of the phase comparator shows a clear and important sinus-like undulation which permits to conclude of the existence of a periodic variation (24 h period) of the speed of light in the coaxial cable around 500 km/s.

In performing the experiment during 178 days, with six cesium beam clocks, the period of the phase signal has been accurately measured and is 23h 56 m +- 25 s. and thus is the sidereal day.

So DeWitte managed to extract the speed and right ascension from his results, which are shown in table 2.2. To this day only 3 days of data out of the 178 are known, making it impossible to determine the Declination. Roland DeWitte died several years later, in 2000 after becoming extremely depressed. He did however, acknowledge two other similar experiments in his email, namely Torr and Kohlen,[72] and Krisher:[73]

This result, like the one of D.G. Torr and P. Kolen (Natl. Bur. Stand. (U.S.), Spec. Publ. 617, 1984) is well understood with a new space-time theory based on a new electron theory.

Table 2.2: Summary of absolute speeds and directions obtained from non-interferometer experiments.

Experiment	Author	Year	V (km/s)	RA (^{h})	Dec (°)
Coaxial Cable	DeWitte	1991	500	5.0[71]	N/A
	Torr/Cohlen [72]	1981	N/A	5.0[71]	-70[71]
	Cahill[74]	2012	499	2.75	-77
Optical Fibre One Way Speed of Light	Krisher[73]	1990	N/A	6.09[64]	N/A
Spacecraft-Earth Flyby Doppler Shift Data[75]	Cahill [76]	Dec 1990/92	491 (Galileo)	5.23	-80
		Jan 1998	497 (NEAR)	3.44	-80
		Aug 1999	478 (Cassini)	5.18	-70
		Mar 2005	499 (Rosetta)	2.75	-77
Zener Diode Quantum Detector	Cahill[77]	1 Jan 2013	512	4.8	-83
Random Event Generator (GCP)	Cahill[77]	1 Jan 2013	528	5.3	-81
	Cahill[77]	1 Aug 2012	471	5.4	-82
Brownian Motion	Dai[78]	2014	N/A	5.0[79]	-60[79]
Fine Structure Constant Anisotropy	Webb *et al.* [80]	2011	N/A	**17.3 ± 1.0**	-61 ± 10
Moving Mirror / Earth Lorentz Contraction	Courvoisier [81]	1921 - 1955	600	5.0	**+40**

It is also the case for the nearly negative result of the experiment of Krisher et al, with a fiber optics instead of a coaxial cable (Physical review D, Vol 42, number 2, 1990, pp. 731-734).

The Torr and Kohlen experiment was performed in Utah ten years prior to DeWitte's experiment and had the same principle i.e. 2 rubidium atomic clocks separated by 500 metres of coaxial cable, however their apparatus was oriented E-W meaning that the space velocity projection onto the apparatus was substantially lower than observed by Miller and DeWitte. Nevertheless they observed a

positive result, and was in agreement with the theoretical prediction of 433 km/s in the direction $(\alpha, \delta) = (5.2^h, -67^\circ)$. Torr and Kohlen also reported fluctuations in both the magnitude and time of the maximum variations in travel time as observed by both DeWitte and Miller. The experiment performed by Krisher *et al.* for 5 days in November 1988 used optical fibres instead of coaxial cables but at the much larger scale of 29 km where Krisher noted that the phase variations corresponded to a right ascension of 4.96^h (corrected to 6.09^h to account for the orientation of the cable wrt the local meridian) but compared this to the CMB direction of $(\alpha, \delta) = (11.20^h, -7.22^\circ)$ some 6 hrs difference.[76] The CMB direction is determined by removing the dipole component of the CMB anisotropy as to make the preferred frame of the thermal 3° K radiation bath isotropic, relative to the movement of the solar system. Krisher didn't notice that his results in fact coincided with that of Miller. In 2012 Cahill reported both that one way speed of light measurements could be achieved without clock synchronisation along with reporting such an experiment using shorter coaxial cables and a single atomic clock.[82] The experiment was also shown to work due to the absence of Fresnel drag, an effect that slows down the speed of light in dielectric materials to speed $v(n) = c/n + v(1 - 1/n^2)$ as the dielectric itself passes through space, and which induces second order refractive index effects. Without the Fresnel drag effect a detector which is first order in (v/c) can detect/characterise dynamical space while requiring only one clock (if Fresnel drag is present then 2 synchronised clocks are required). Cahill found that his apparatus displayed the Earth rotation effect, i.e. daily periodic fluctuations of the travel time difference while the effect disappeared when aligning the coaxial cables with the space flow, and allowed the permission to study gravitational turbulence effects more accurately. Using the Earth rotation effect the space flow was found to be 499.2 km/s in the direction (2.75^h, -76.6°), a theoretical prediction from the data suggested in the spacecraft-Earth flyby Doppler shift data.[74, 76]

Doppler Shift - NASA Spacecraft-Earth Flyby Data

Planetary probe spacecraft are sent into outer space by completing close flybys of Earth or other planets, and in the heliocentric frame of reference their speeds are increased upon this happening. In the Earth frame of reference however there should be essentially no change of asymptotic speed, only in the direction. Doppler shift observations of spacecraft-Earth flybys of Galileo, NEAR, Cassini and Rosetta have all yielded unexplained asymptotic speed anomalies. These anomalies were shown[76] to be artificial, and a product of using the incorrect theory for the relationship between Doppler shift of RF transmissions and the speed of the spacecraft, i.e. assuming that the speed of light is isotropic in all frames. Using a model which is more similar to that of the anisotropic speed of sound these anomalies vanished completely, and in conjunction with the Krisher data[73] yielded 3-space velocities given in table 2.2. These velocities were also in excellent agreement with the Miller interferometer data (see figure 2.2), and also fluctuate during the year in a predictable manner. The flyby data also permitted the first ever prediction of the inflow speed into the Earth, an effect predicted by Dynamical 3-Space theory, which was reported to be 12.4 ± 5 km/s, in agreement with the theoretical prediction of 11.2 km/s as reported by Cahill.[76]

Quantum Detectors

Shortly after the coaxial cable experiment in 2012 a correlation study between Adelaide and London was performed, in order to determine the speed of space as it passed two different points on Earth. Originally the dual RF coaxial cable apparatus was set up at both locations however later it was noticed that the 'clock jitter' within the instruments, i.e. the Digital Storage Oscilloscope (DSO) internal noise was actually correlated between the 2 locations, even without joining the coaxial cable apparatus to the DSO. The Adelaide 'clock jitter' signal was found to be 13 - 20 seconds ahead of the London signal. This fluctuated depending

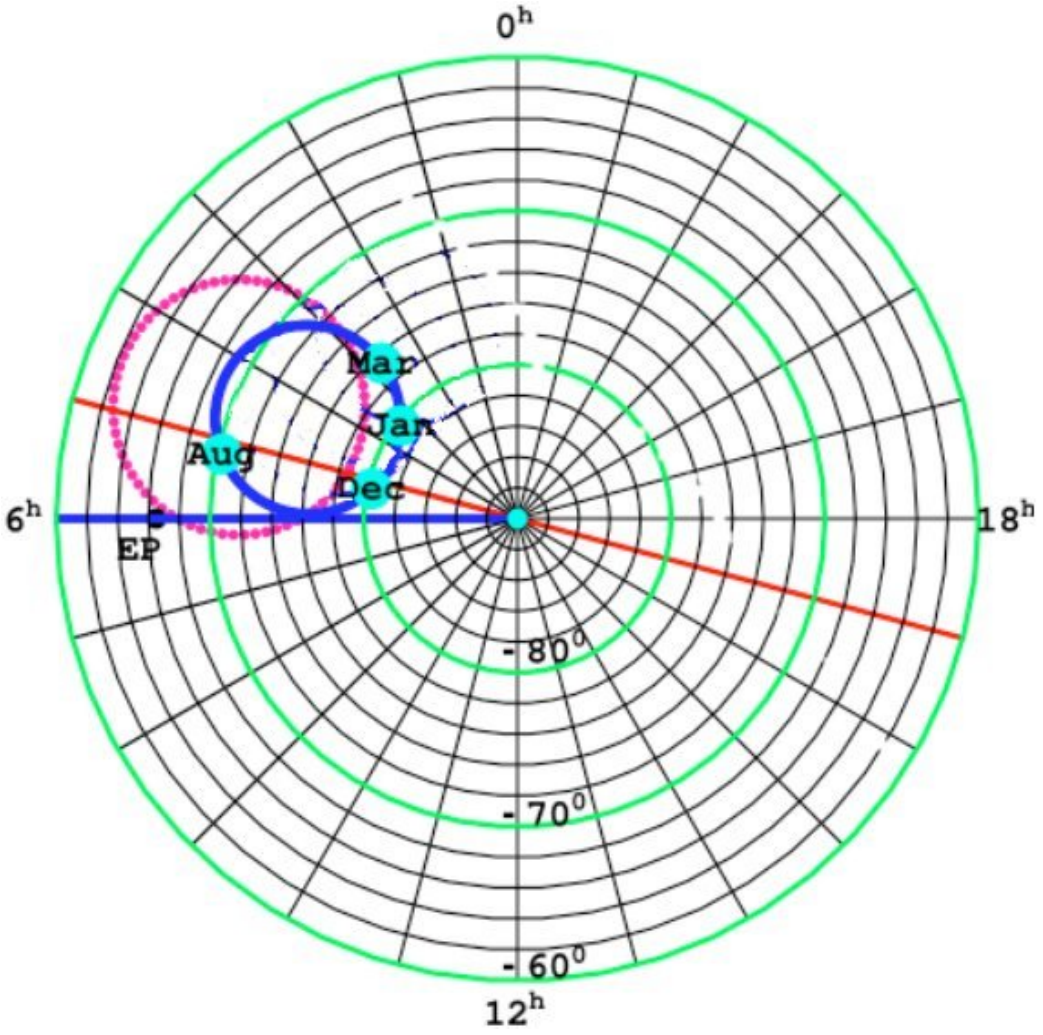

Figure 2.2: Southern celestial sphere, summarising the absolute motion directions found by Miller (pink circle) and that from the NASA Spacecraft Earth Flyby Doppler shift data (blue circle) using right ascension and declination. Figure source from [76].

on sidereal time, and also from gravitational turbulence effects along with differences due to London not being exactly 'downstream' from Adelaide in terms of space flow direction, where the fractal and evolving nature of space affects the DSO signals slightly differently. The analysis suggested that not all of the internal noise was caused by a random process intrinsic to the DSO, but by some other process which affected both instruments. Efforts were then taken to study Zener diodes, which were suggested to be found within the time difference measurement hardware inside DSOs but also used in some of the Random Event Generators (REGs) in the Global Consciousness Project (GCP).[83] Zener diodes have the

property that they display quantum tunneling effects when operated in reverse current mode. The tunneling events are recorded classically by REGs as the electron wavefunction collapses on either side of a barrier inside the diode, in which the REGs used in the GCP count the number of quantum tunneling events every second (averaging around 100/second). Correlations in REGs located around the world are then obtained by the GCP, in an effort to predict global events and attribute them to the collective emotional responses of people affecting the REGs in some way. The REGs in Perth - London were studied by Cahill and found to be correlated with a time delay that also fluctuated with sidereal time corresponding to some 470 - 520 km/s in the direction $(5.3^h, -81^\circ)$, also agreeing with the previously mentioned experiments. The correlation of the REGs and that found in Zener diode current fluctuations[84] suggested that the interpretation of quantum theory was incorrect in that electron wavefunction collapse on either side of a barrier is not a random event intrinsic to a quantum system. Instead, the collapse was suggested to be due to fluctuating space affecting the relative barrier quantum tunneling amplitude that the electron has to pass through, an effect which would be sensitive to any change in $\mathbf{v}$. Current fluctuations would then be completely determined by the fluctuations in the passing space - any similar fluctuations in space flowing past instruments would generate similar current fluctuations.[84] An extended discussion of this will also be shown in chapter 4 as the work presented here requires the same explanation. In [85] it was shown that Zener diodes generated the same signal as resonant gravitational wave antennae operated in Rome and Frascati in 1980. The power spectrum of both data sets display the same Earth vibration frequencies, although the Zener diodes wouldn't physically detect them in the same way as the gravitational wave antennae. This suggested that the same phenomenon affected both apparatuses namely the existence of a fluctuating dynamical space travelling past Earth. The other potential correlations noted are that the GCP data from 2000 - 2012 tracks Solar Cycle 23 reasonably well and that the Zener diode data precedes solar flare activity by a few days,[86] however

this has only been discovered recently and not studied in depth.

Anisotropic Brownian Motion

Potential evidence for anisotropic Brownian motion was reported in 2014 by Jiapei Dai[78] along with Felix Scholkmann reporting a sidereal time dependence of Dai's data in 2015.[87] This indicated the possible driving of Brownian motion to an absolute preferred direction. The data consisted of 24 measurements made in a day of studying Brownian motion of a toluidine blue solution dropped into a container of water, with 15 such experiments performed from December 2011 to March 2013. It was suggested[79] that this direction of approximately 5^h is in agreement with other experiments. The right ascension according to the data does appear to vary throughout the year, as observed in the Miller and NASA flyby Doppler shift data. It would be interesting to study whether multiple Brownian motion experiments performed within days of each other produced similar right ascensions.

Study of Quasars - Fine Structure Constant Variation

Webb *et al.*[80] reported a variation of the fine structure constant when studying distant quasars. They found that the value of α is larger to one part in $\approx 100\,000$ in the direction $(17.3^h, -61°)$, from using two independent data sets, namely the Very Large Telescope and Keck samples. While this direction is different from the other experiments listed here it does observe very distant phenomena as opposed to the 'local 3-space', perhaps arising from flows into the galaxy, local cluster or great attractor.

Leopold Courvoisier's Experiments

Leopold Courvoisier (1873 - 1955)[81] was a Swiss observer at the Berlin / Babelsberg astronomical observatory from 1905 - 1938. His earlier work was based around publishing several star catalogues but later moved to detecting the motion of the solar system through the aether, as he disagreed with the SR and GR

models. During a routine measurement published in 1905 (earlier than the development of GR by Einstein) Courvoisier noticed that the RA and Dec of fixed stars changed slightly when observed close to the Sun. He called this 'annual refraction', due to the influence having a period of one year, and the effect was interpreted as being due to the refraction of light by a denser medium around the Sun as opposed to being a consequence of relativity, i.e. the gravitational deflection of light rays. Courvoisier's opposition to Einstein grew steadily from this point. Courvoisier also preferred the idea of a static aether, but also that movement through the aether caused real contraction of moving bodies although not exactly for the same reasons as what Lorentz proposed. He directly denied the principle of Relativity and invented two novel techniques which independently measured the motion of the Solar System through the aether. His first technique involved determining star positions through reflecting light emitted by a star from a mercury mirror and recording the reflection angle, which deviated slightly from the incident angle relative to the proper reference frame of the mirror. Courvoisier reasoned that any observable effect was second order effect in (v/c). He then either performed different experiments using either a single or double mirror involving rigorous control experiments, or took previously published data from star catalogues published from reputable sources (such as the Leyden Observatory) over an 80 year time span. This makes it difficult to explain away his results as instrumental or other systematic effects. Courvoisier's second method was based on the Lorentz contraction of the Earth as it moved through the aether, as only the local vertical would undergo contraction effects as the Earth rotated. He then assumed that there would be a periodic effect noticeable. Courvoisier also performed many other smaller and different experiments, all of which amount to a speed of the solar system through the aether of some 600 km/s in the direction $(5.0^h, +40°)$. This speed is higher than the other experimental methods discussed, and the declination differs greatly from the other velocities shown in table 2.2. No checks of Courvoisier's theoretical derivations are known and it is assumed that he was

unaware of potential inflows into the Sun, for example. Courvoisier's work was largely ignored by the scientific community, for many reasons both scientific and historical, as the bulk of his research was undertaken after World War 1 and after the acceptance of Einstein's Relativity models. Most of Courvoisier's research was also published in a anti-relativistic journal called the *Astonomishe Nachrichten* which the general science community ignored. His theories were also phenomenologically based, i.e. he had no real model to base his research and results from. The large fluctuations in the results he published meant that they could easily be thought of to have contained systematic or random errors. He however made sure to mainly use data published by other observers as to ensure that his results could be checked by other astronomers if they so wished, something which was apparently not performed. Apart from publishing his work, Courvoisier did not attempt to join other astronomers to produce a stronger anti-relativistic front.

2.3.3 Simon Shnoll - Histogram Fine Structure and Correlations

Professor Simon Shnoll is a Russian scientist who along with his team conducted many unique experiments at the Institute of Biophysics in Pushino, Russia.[88] He originally started with attempting to reduce the uncertainty in the activity of ATPase in his reactions of radioactive amino acids with proteins. He was very careful in the manner of preparing these reactions, but found that the activity rates varied too much for the way he was preparing them. Shnoll mentions being extremely careful in his youth to ensure that scientific processes are kept when performing these reactions. He later started to study the ATPase activity of muscle proteins over time in parallel, and found that they appeared to not only take on preferred or discrete values, but the individual reaction rates of the solutions also correlated with each other at the same time. He began to explain the scattering of these

measurements in terms of wave patterns in the restructuring of water originating from how the hydrophilic and hydrophobic parts of the proteins interacted with the water. Shnoll however later found that reaction rate changes were also found in many other processes including but not limited to all proteins, chemical reaction and radioactivity rates, gravitational wave antennae and semiconductor noise,[89] all of which have different mechanisms and fluctuation amplitudes.[90, 91] All of the experiments Shnoll performed, whether it be studying a single experiment such as protein activity, or comparing 2 completely different phenomena in parallel yielded that the changes in the activity correlated in some way, and that the Gaussian distributions of these processes had a fine structure which did not smooth out after taking more measurements. This fine structure was then broken down into 60 - 100 measurement histograms and Shnoll realised that the histograms had daily (both solar and sidereal) and annual cycles. Histograms from experiments separated by distance also correlated with each other, both instantly and also by a time difference corresponding to the Earth's rotation between the experiments. Shnoll collected results for over half a century, and found that:

- The measurement scatter appeared to be intrinsic to all processes studied (over 20 different processes were investigated).
- The amplitude of fluctuations (i.e. the scattering of measurements) relative to a measured value varied depending on the process studied.
- The shape of a histogram, i.e. the distribution of results evolved over time, where the current histogram shape was most similar to the one preceding it. The histogram shape obtained at the same time and place is also independent of the process.
- Histogram similarity and fine structure depended on the direction of study.[92]

The only factor that Shnoll could conclude that would cause the behaviour observed in all of his experiments was that they must be affected by *"fluctuations in the space-time continuum caused by the movement of an object in the inhomogeneous gravitational field."*[88] He suggests that the initial structure to spacetime itself must cause the scattering of measurements found in his experiments, and that the inhomogeneity results from the existence of massive objects, namely the Sun, Moon etc. disrupting these fluctuations. In chapter 4, a discussion on Shnoll's work from a Dynamical-3 Space theory viewpoint along with its implications will be presented along with two new methods of studying the effects Schnoll observed.

2.4 Concluding Remarks about Chapter 2

There exists an incredible amount of evidence supporting a theory involving absolute motion. The data alone suggests that the absolute motion of Earth is in the order of ≈ 400 km/s in the direction $\approx (5^h, -70°)$. Dynamical 3-Space theory is one candidate to explain this data and while phenomenologically derived it arises from a deeper, pregeometric model of reality. Chapter 3 will discuss what is currently known about Dynamical 3-Space theory.

Chapter 3

Dynamical 3-Space Theory - Emerging Phenomena

3.1 Introduction

The dynamics of space can be characterised by solving equation (2.4) in terms of either $\mathbf{v}(\mathbf{r},t)$ or $\mathbf{a}(\mathbf{r},t)$. Just to reiterate, equation (2.4) is

$$\nabla\cdot\left(\frac{\partial\mathbf{v}}{\partial t}+(\mathbf{v}\cdot\nabla)\mathbf{v}\right)+\frac{\alpha}{8}\left((trD)^2-tr(D^2)\right)$$
$$+\frac{\delta^2}{8}\nabla^2\left((trD)^2-tr(D^2)\right)+...=-4\pi G\rho,\quad D_{ij}=\frac{\partial v_i}{\partial x_j} \tag{3.1}$$

and will be referred to as equation (3.1) for the remainder of this thesis. As it turns out, there are both simple and complex solutions depending on the absence or presence of matter, or when considering either long ($\alpha\neq 0,\delta=0$) or short ($\alpha\neq 0,\delta\neq 0$) range effects. To clarify further, from the known available experimental data α appears to be the fine structure constant while δ appears to be a small but nonzero Planck-type length. The consideration of long range effects means to search for solutions which hold for sufficiently large r such that any δ effects are

negligible, and so δ may be set to zero. When these solutions are found to not agree with data, the full solutions requiring both nonzero α and δ are then required. The only solutions to the full Dynamical 3-space theory (with $\delta \neq 0$) that are currently known are those for time independent and radially symmetric flows into black holes and filaments, and without the presence of matter; these will be discussed in this chapter. The presence of a dynamical space also required alterations to other well known equations by Schrödinger, Dirac and Maxwell. This chapter summarises these alterations and solutions to the Dynamical 3-Space theory to further justify its use.

3.2 The 'Dark Matter' Effect

While the Dynamical 3-Space theory is essentially Newtonian Gravity cast into an inflow formalism it contains additional α and δ terms (as stated in chapter 2) which cannot be *a priori* neglected. Rearranging these terms, through combining the expression for $\mathbf{a}(\mathbf{r}, t)$ (equation (2.1)) and (3.1) the theory can be written in the form

$$\nabla \cdot \mathbf{a} = -4\pi G\rho - 4\pi G\rho_{DM}, \tag{3.2}$$

where

$$\begin{aligned}\rho_{DM}(\mathbf{r}, t) \equiv & \frac{\alpha}{32\pi G}\left((trD)^2 - tr(D^2)\right) \\ & + \frac{\delta^2}{32\pi G}\nabla^2\left((trD)^2 - tr(D^2)\right)\end{aligned} \tag{3.3}$$

which introduces an effective 'dark matter' density term ρ_{DM} which is observed in systems such as spiral galaxies, for example.[64] This suggested that the unexplained velocities found in spiral galaxy rotation curves were explained by space self interaction effects, and not by the presence of extra unobservable matter. These effects manifest at both large (α) and small (δ) scales and is completely

emergent from the theory. For $\delta = 0$, this effect has been shown to account for spiral galaxy rotation at least asymptotically, lensing effects in galaxies, systematics of black hole masses, the borehole g anomaly and anomalies in measurements of the fundamental constant G.[49, 64]

3.3 Action at a Distance

The spatial dynamics is non-local and instantaneous, which points to the universe being highly connected, consistent with the deeper pre-space *Process Physics* paradigm. Historically this was first noticed by Newton who called it action-at-a-distance. To see this (3.1) can be written as an non-linear integro-differential equation[54]

$$\frac{\partial \boldsymbol{v}}{\partial t} = -\nabla\left(\frac{v^2}{2}\right) - G\int d^3r' \frac{\rho_{DM}(\boldsymbol{r}', t) + \rho(\boldsymbol{r}', t)}{|\boldsymbol{r} - \boldsymbol{r}'|^3}(\boldsymbol{r} - \boldsymbol{r}'). \tag{3.4}$$

This shows a high degree of non-locality and non-linearity, and in particular that the behaviour of both ρ_{DM} and ρ manifest at a distance irrespective of the dynamics of the intervening space. This non-local behaviour is analogous to that in quantum systems and may offer a resolution to the horizon problem arising from CMB observations.

3.4 Emergence of Gravity and the Equivalence Principle

A very important result arises from using the Schrödinger equation to determine the acceleration of test masses in the presence of a dynamical space, namely the emergence of gravity as a derivable quantum effect. A generalisation to the

Schrödinger equation was required to include additional terms to describe the evolution of wavefunctions with respect to a dynamical space, and not to an embedding space, the equation shown below,[51]

$$i\hbar\frac{\partial\psi(\mathbf{r},t)}{\partial t} = -\frac{\hbar^2}{2m}\nabla^2\psi(\mathbf{r},t) - i\hbar\left(\mathbf{v}.\nabla + \frac{1}{2}\nabla.\mathbf{v}\right)\psi(\mathbf{r},t). \tag{3.5}$$

Here the space and time coordinates x, y, z, t ensure that the separation of the dynamical 3-space and quantum matter systems from a deeper and unified process, are properly tracked and connected by an observer using these same coordinates, i.e. unifying both systems from one theory. The additional terms on the RHS of the modified Schrödinger equation model a quantum system in the presence of the space velocity field. The extra $\frac{1}{2}\nabla\cdot\mathbf{v}$ term is required to maintain the Hermitian properties of the operator, where the $\left(\frac{\partial}{\partial t} + \mathbf{v}\cdot\nabla + \frac{1}{2}\nabla\cdot\mathbf{v}\right)$ operator remains invariant under an observer's rotation and/or translation, and that the wavefunction norm is also time invariant.

The Lorentzian interpretation of relativistic effects suggests that the speed of light is c with respect to the quantum foam system predicted from *Process Physics*. Any time dilation and length contraction effects are thus predicted to be real phenomena, caused by the motion of rods and clocks relative to the quantum foam. From a Dynamical 3-Space model point of view this suggests that objects travel at speed $\mathbf{v}_R$ with respect to the space flow. This is in contrast to the SR formalism, in which time dilation effects exist for two observers in relative motion wrt each other, and arise by the choice of coordinate system used in the mapping. This was shown by the discovery of an exact linear mapping between Galilean Relativity and Special Relativity as discussed in [2, 93], differing only by definitions of space and time coordinates. These relativistic effects are currently not emergent from Dynamical 3-Space model but are expected to be derived directly from the Quantum Homotopic Field Theory that describes the quantum foam system.[47] The elapsed proper (time dilated) time of an object travelling through a time

dependent and inhomogeneous space flow is defined by

$$\tau[\mathbf{r}_0] = \int \left(1 - \frac{\mathbf{v}_R^2}{c^2}\right)^{\frac{1}{2}} dt. \tag{3.6}$$

Here $\mathbf{v}_R(\mathbf{r}_o(t), t) = \mathbf{v}_o(t) - \mathbf{v}(\mathbf{r}_o(t), t)$ is the absolute velocity of a wave packet, i.e. matter travelling relative to the local dynamical space, and $\mathbf{v}_o$ and $\mathbf{r}_o$ are the velocity and position of a wave packet relative to an observer. The 'gravitational' acceleration of quantum matter is then found to be an effect induced by wave refraction and by maximising the elapsed proper time wrt space. From using (3.5) and (3.6) this is then found to be[51, 94]

$$\mathbf{g} = \frac{\partial \mathbf{v}}{\partial t} + (\mathbf{v}.\nabla)\mathbf{v} + (\nabla \times \mathbf{v}) \times \mathbf{v}_R - \frac{\mathbf{v}_R}{1 - \frac{\mathbf{v}_R^2}{c^2}} \frac{1}{2} \frac{d}{dt} \left(\frac{\mathbf{v}_R^2}{c^2}\right). \tag{3.7}$$

The third term is an effect known as the Lense-Thirring effect and is a vorticity driven effect, and results in planets' orbits to become slightly perturbed when orbiting a rotating star, for example. The last relativistic term generates the planetary precession effect, and arises from maximising the elapsed proper time with respect to the quantum matter wavepacket trajectory. This entails that matter undergoes a local time dilation effect, and has a maximum speed c with respect to the 3-space, and not wrt an observer as in SR. Matter is predicted to be able to travel faster than c with respect to other observers in the Dynamical 3-Space model provided they are at rest inside a bubble of space, for example, as their v_R will be zero in this case. Clocks taking different trajectories through space will thus predict different times upon meeting again. In the case of zero vorticity and in the non relativistic limit $v_R/c \to 0$, equation (3.7) reduces to $\mathbf{g} = \mathbf{a}$, i.e. that the matter acceleration is exactly that of the 3-space acceleration, and independent of the mass of an accelerating object, in agreement with Galileo's observations and a derivation of the weak equivalence principle. The Global Positioning System (GPS) also allows for an excellent test of the Dynamical 3-Space model. It has

been shown[94] that for the case of spherical symmetry (see the following sections regarding spatial inflow solutions) and then considering a constant cosmic flow of space past the Earth, that the timing of the satellite clocks are affected in the same way as that when applying the General Relativity model. The Dynamical 3-Space and GR models for the GPS are thus mathematically equivalent in this case however their interpretations are quite different. In conventional physics the relativistic effects involve the time dilation induced by Special Relativity effects along with the gravitational potential energy effects predicted by GR. In the Dynamical 3-Space model the only effects present are that of time dilation produced by the motion of clocks through space, where the velocities $\mathbf{v}_R$ of the clocks depend on the vector sum of their orbital velocity around earth and also the space inflow speed into the earth. Once allowing for the non-sphericity of the earth and considering gravitational inflow turbulence, then minor timing effects at higher orders of (v_R/c) would become noticeable in the GPS satellites as the space flow becomes time dependent, affecting time dilation properties. The GPS system therefore would provide an excellent method of characterising the 3-space.

An analogous generalisation of the Dirac relativistic wave equation was also required, [54] giving the coupling of the spinor to a dynamical 3-space, and not wrt to observers/an embedding space as

$$i\hbar\frac{\partial\psi(\mathbf{r},t)}{\partial t} = -i\hbar\left(c\vec{\alpha}.\nabla + \mathbf{v}.\nabla + \frac{1}{2}\nabla.\mathbf{v}\right)\psi + \beta mc^2\psi \tag{3.8}$$

where $\vec{\alpha}$ and β are the usual Dirac matrices. The generalised Dirac equation can also be used to obtain (3.7) through performing the same wavepacket acceleration anaylsis as for the generalised Schrödinger equation, and thus predicts the trajectory of a spinor wave packet in the dynamical 3-space.

3.5 Maxwell's Equations

Maxwell created these equations but without respect to any absolute reference frame. Generalising these equations for the electric and magnetic fields as excitations of dynamical space gives, in the absence of charges, currents and matter,[93]

$$\begin{aligned} \nabla \times \mathbf{E} &= -\mu_0 \left(\frac{\partial \mathbf{H}}{\partial t} + \mathbf{v} \cdot \nabla \mathbf{H} \right) \quad , \quad \nabla \cdot \mathbf{E} = 0, \\ \nabla \times \mathbf{H} &= \epsilon_0 \left(\frac{\partial \mathbf{E}}{\partial t} + \mathbf{v} \cdot \nabla \mathbf{E} \right) \quad , \quad \nabla \cdot \mathbf{H} = 0. \end{aligned} \tag{3.9}$$

This was originally suggested by Hertz in 1890, but with $\mathbf{v}$ being a constant vector field to account for an aether model of reality.[95] The speed of EM radiation is still $c = 1/\sqrt{\mu_0 \epsilon_0}$ but now with respect to the Dynamical 3-Space, and not wrt an observer moving through the space. A time dependent / inhomogeneous velocity field (as expected in reality as objects in the universe aren't static) causes the refraction of EM radiation, which can be calculated in an opposite fashion to quantum matter by using the Fermat least-time approximation and ensures that neighbouring paths are in phase. The EM ray paths $\mathbf{r}(t)$ are hence calculated by minimising the elapsed travel time

$$T = \int_{s_i}^{s_f} \frac{ds |\frac{d\mathbf{r}}{ds}|}{|c\hat{\mathbf{v}}_R(s) + \mathbf{v}\left(\mathbf{r}(s), t(s)\right)|}, \mathbf{v}_R = \frac{d\mathbf{r}}{dt} - \mathbf{v}\left(\mathbf{r}(t), t\right) \tag{3.10}$$

by varying both $\mathbf{r}(s)$ and $t(s)$, where s is a path parameter and $c\hat{\mathbf{v}}_R$ is the velocity of EM radiation with respect to the Dynamical 3-Space. The denominator in the first term is the speed of the EM radiation wrt an observer's Euclidean spatial coordinates. Equation (3.10) can then be used to determine the amount of gravitational lensing by matter (the Sun, for example), and by black holes and cosmic filaments, the solutions which will be discussed shortly.

3.6 Spatial Flow ($\alpha \neq 0, \delta = 0, \rho = 0$) Effects

Equation (3.1) with $\rho = \delta = 0$ has solutions where space flows into a singular point. These are also referred to as black holes as they have an event horizon where the speed of the space inflow equals the speed of light. Their gravitational acceleration is however not inverse square dependent and so differ from that predicted by GR. The other major difference is that they are emergent from Dynamical 3-Space theory, whereas they are required to exist in GR but their existence unexplained. There are two categories of black holes:

- Minimal - Large inflow speeds induced by the presence of a large amount of matter, such as a spherical galaxy or globular cluster. The effective black hole mass of these systems is minimal. The minimal black hole mass and total baryonic mass of these systems appears to be related by the fine structure constant - see section 3.8.2 and chapter 5 for a further insight.
- Non-Minimal - Primordial black holes, i.e. those left over at the beginning of the universe, which matter is then attracted to. These typically result in spiral galaxies, and their effective mass is much larger than required by a minimal black hole induced by matter. These contain an inflow singularity at $r = 0$, and have a much more powerful gravitational influence than what is predicted by GR, and do not require the presence of matter to function.

3.6.1 Primordial (Non Minimal) Black Holes

In the absence of matter, the Dynamical 3-Space theory, equation (3.1) has a simple yet elegant spherically symmetric and time independent solution for a primordial black hole, namely

$$v(r) = -\frac{\beta}{r^{\alpha/4}} \quad , \quad g(r) = \nabla\frac{v^2}{2} = -\frac{\alpha\beta^2}{4r^{1+\alpha/2}} \tag{3.11}$$

where β is a parameter which characterises the strength of a black hole, and the minus sign denotes an inflow. The inflow speed at large distances is effectively constant. The gravitational acceleration of these black holes has the stronger and longer range $1/r$ gravitational acceleration as opposed to the black holes predicted by GR ($1/r^2$). The dark matter density obtained from equation (3.3) is thus

$$\rho_{DM}(r) = -\frac{\alpha\beta^2(2-\alpha)}{256\pi G r^{2+\alpha/2}} \tag{3.12}$$

which has an inverse square relationship as determined by 'dark matter' interpretations of the flat rotation curves of spiral galaxies, however here it is purely a space self interaction effect. Spiral galaxies are formed by matter infalling on primordial black holes, i.e. space inflow singularities remaining from the Big Bang, leading to rotation of the matter as the infall will never be symmetric. Matter orbiting such black holes would have approximate circular orbital velocities given by

$$v_O(r) = \sqrt{rg(r)} = \frac{\alpha^{1/2}\beta}{2r^{\alpha/4}} \tag{3.13}$$

in which the velocity drops off extremely slowly with distance, which is observed for spiral galaxies, at least for at large distances. An explanation of the rotation curve at shorter distances is currently unavailable but would perhaps have to do with finding solutions to the orbital velocity for when δ is also nonzero. This is one class of solutions found in the Dynamical 3-Space theory, and the simplest, since $\rho = 0$. For a spiral galaxy with a non-spherical matter distribution, numerical solutions are required to determine the inflow velocity. Sufficiently far away from a black hole however, the inflow will have spherical symmetry. Equation (3.1) then has an exact non-perturbative two parameter analytic solution,

$$v(r) = K\left(\frac{1}{r} + \frac{1}{R_s}\left(\frac{R_s}{r}\right)^{\alpha/2}\right)^{1/2} \tag{3.14}$$

where the 1/r term arises only if matter is present, and the second term is responsible for the primordial black hole effect (at far distances, where $\rho = 0$). If no matter is present, the presence of the $1/r$ term does not satisfy (3.1) for $\rho = 0$, and so (3.14) then reduces to (3.11).[96] Here R_s characterises the length scale of the non-perturbative part of this expression, and K depends on α, G and the matter distribution itself. It was argued that the constants K and R_s are found by matching the matter and non-matter regions from spiral galaxy data together. The exact analytic solution then yields for the orbital velocity,

$$v_O(r) = \frac{K}{2}\left(\frac{1}{r} + \frac{\alpha}{2R_s}\left(\frac{R_s}{r}\right)^{\alpha/2}\right)^{1/2} . \tag{3.15}$$

The asymptotic part of the rotation curve decreases very slowly with distance, which is observed for spiral galaxies. In the absence of the α dynamics, this expression then reduces to the Keplerian form, thus providing an alternative explanation to the galaxy rotation anomalies.

3.6.2 Cosmic Filaments

Straight-line cosmic filament solutions were obtained by writing equation (3.1) in cylindrical coordinates (r, z, ϕ). These solutions are:[97]

$$v(r) = -\frac{\mu}{r^{\alpha/8}} \ , \ g(r) = -\frac{\alpha\mu^2}{8r^{1+\alpha/4}} \ , \ \rho_{DM}(r) = -\frac{\alpha\mu^2}{1024\pi G r^{2+\alpha/4}} \tag{3.16}$$

for arbitrary filament strength μ. These are time independent (i.e. static) solutions for a single infinitely long and straight filament, and similar to black holes, have a long range gravitational acceleration that is directed perpendicularly towards the centre of the filament. As these solutions are using $\delta = 0$ they only apply at sufficiently large distances from the centre of a filament. Closer to the filament the δ effects would become noticeable, which is mentioned later. The existence of

both black hole and cosmic filament solution classes brought the conjecture that reality consists of a network of black holes connected by cosmic filaments emergent from Dynamical 3-Space theory.

3.6.3 Expanding Universe

The Dynamical 3-Space theory has spatial 'outflow' solutions which are time dependent. This is referred to as the centreless expansion of the universe as the solutions have a Hubble form $\mathbf{v}(\mathbf{r},t) = H(t)\mathbf{r}$. In the absence of matter this solution is[49]

$$H(t) = \frac{1}{(1+\frac{\alpha}{4})t}, \qquad a(t) = \left(\frac{t}{t_0}\right)^{\frac{1}{(1+\frac{\alpha}{4})}}. \tag{3.17}$$

Here $a(t)$ is the scale factor indicating the relative size of the universe, and where $a(t_0) = 1$ for the present moment t_0. The solution for the scale factor indicates essentially a uniform expansion rate (due to the small value of α), and gives a parameter free account of the type 1a supernova magnitude-redshift data, i.e. without requiring the dark matter or dark energy parameters which the Friedmann equations require in order to predict the universe's expansion. More on the expanding universe solutions will be mentioned in chapter 6. Solution (3.17) contains a singularity at $t = 0$, i.e. that at very early times the universe would have expanded at an exponential rate, as α- dynamics become prominent at early times and the universe's expansion becomes nonuniform. This is brought on by the small value of α which produces a nonuniform expansion rate at early t, and gives rise to an inflationary epoch, also discussed in chapter 6.

3.7 Spatial Flow $(\alpha \neq 0, \delta \neq 0, \rho = 0)$ Effects

In 2011 the Dynamical 3-Space equation was altered via a semi-classical derivative expansion approach to include higher derivative δ terms which model much shorter

length-scale dynamics of space.[52] Solutions to equation (3.1) with $\delta \neq 0$ were found, and for $\rho = 0$ there exist two parameter, v_0 , $\kappa \geq 1$ black hole solutions

$$v(r)^2 = v_0^2(\kappa - 1)\frac{\delta}{r}\left(1 - {}_1F_1\left[\frac{-2+\alpha}{4}, -\frac{1}{2}, -\frac{r^2}{\delta^2}\right]\right) \\ -v_0^2\kappa\left(\frac{4-2\alpha}{3}\right)\frac{r^2}{\delta^2}\frac{\Gamma(\frac{2-\alpha}{4})}{\Gamma(\frac{-\alpha}{4})}{}_1F_1\left[1+\frac{\alpha}{4}, \frac{5}{2}, -\frac{r^2}{\delta^2}\right] \tag{3.18}$$

where ${}_1F_1[a, b, w]$ is the confluent hypergeometric function, which are used to model both small and very large flows simultaneously, like blood flow[98] for example. Here v_0 sets the strength of the black hole and κ sets its structure by altering the relative strength of the two ${}_1F_1$ terms above. Equation (3.18) is a generalisation of (3.11), and for $r \gg \delta$ gives an asymptotic description of the inflow velocity as

$$v(r)^2 \approx A\frac{\delta}{r} + B\left(\frac{\delta}{r}\right)^{\alpha/2}. \tag{3.19}$$

From equation (3.7) i.e. the gravitational acceleration of matter this then gives $g(r) = GM(r)/r^2$, where $M(r)$ defines an 'effective mass', using a two parameter description,

$$M(r) = M_0 + M_0\left(\frac{r}{r_s}\right)^{1-\alpha/2} \tag{3.20}$$

This 'effective mass' mimics the amount of matter enclosed within radius r outside a black hole, however this is now completely induced by the space interaction effects, and does not contain any actual matter. Here r_s is the distance where $M(r_s) = 2M_0$, and $r < r_s$ is the region where $M(r)$ is essentially constant, and increases outside this region. Equation (3.20) was used to fit the Milky Way SgrA* black hole mass data remarkably well, and showed how space dynamics can be used to mimic the increasing matter density outside a primordial black hole.[52] In chapter 5 it will be shown how to use the Dynamical 3-Space theory to mimic the effective mass parameter to fit the SgrA* data using BH solutions to a modified version of equation (3.1). The parameters κ and δ relate to each other

in the way that if one is altered, the other automatically rescales to compensate. The value of δ cannot be set to zero however. This suggested the existence of a very small but nonzero structure to space which has a Planck-like length. At large r, the inflow speed decreases very slowly, predicting essentially flat rotation curves given by [52]:

$$v_{orb}(r)^2 = GM_0 \left(\frac{r_s}{r}\right)^{\alpha/2} \frac{1}{r_s}. \tag{3.21}$$

The rotation curves would also require additional contributions from present matter density however the primordial black hole would be the major contributor to the inflow speed. For the Milky Way, for example, the black hole contribution at a distance $r = 8$ kpc i.e. at the location of our solar system, was predicted to be $v_{orb} = 117$ km/s, and determined by M_0 and r_s. Various correlations such as that between supermassive black hole mass and stellar speed dispersion in their spiral galaxy bulges may be explained by the black hole being an extended structure as given by this theory.

Exact filament solutions for (3.1) also exist when $\delta \neq 0$, as a generalisation of (3.16):

$$v(r)^2 = v_0^2 \frac{r^2}{\delta^2} {}_1F_1 \left[1 + \frac{\alpha}{2}, 2, -\frac{r^2}{2\delta^2}\right]. \tag{3.22}$$

Here r is the distance perpendicular to the axis of the filament and $v(r)$ is the inflow in that direction. The only known filament solution is still for one that is infinitely long and straight. Both (3.18) and (3.22) are well behaved functions which converge to zero as $r \to 0$, i.e. the in-flow singularities are removed, and the δ dynamics self-regulate the interior structure of the filament which again has a Planck length scale. At long range, i.e. $r \gg \delta$, $v(r) \propto 1/r^{\alpha/8}$ and $g(r) \propto 1/r^{1+\alpha/4}$, i.e. reduces to the $\delta = 0$ case as per equation (3.16), thus still producing a long range gravitational attraction. Cosmic filaments have been detected using techniques that combine weak gravitational lensing with statistical tomography.[99]

3.8 $\rho \neq 0$ Effects

3.8.1 Gravity Inside Matter - Borehole g Anomaly

The borehole g anomaly is a deviation from Newtonian gravity when studying gravitational effects upon digging deeper into the Earth's core via the Airy method,[100] which compares gravity gradients above and below the Earth's surface. These gravitational anomalies were never resolved in literature. The Dynamical 3-Space theory gives an exact analytical solution (for $\delta = 0$ at least) for the gravity inside a uniform and spherically symmetric object, and is compared to that of NG in table 3.1. As seen, external to a spherically symmetric uniform matter density the Dynamical 3-Space theory matches NG, and explains why the α dynamics aren't prominent in Kepler and Newton's study of planetary orbits. Inside an object however the theories give different results, as stated by the gravity residual being to first order $\triangle g(r) = 2\pi\alpha G_N \rho(r - R)$. The Dynamical 3-Space theory then predicts the borehole g anomalies in the Greenland Ice shelf[101] and Nevada[102] data to require a two parameter fit, namely Newton's gravitational constant G_N (defined as $G_N \equiv \left(1 + \frac{\alpha}{2}\right) G$), and also α which is approximately the fine structure constant, 1/137.

3.8.2 Minimal Black Holes

Based off of evidence from black holes in 19 spherical galaxies, the black hole mass is proportional to the observable mass of the galaxy, to a factor of $\alpha/2$.[54] Dynamical 3-Space theory predicts a relationship between the dark matter mass M_{DM} of a black hole and its observable mass to be

$$M_{DM} = 4\pi \int_0^\infty r^2 \rho_{DM}(r) dr = \frac{\alpha}{2} M + O(\alpha^2) \tag{3.23}$$

Table 3.1: Summary of the gravity profiles internal and external to an object of uniform and spherical matter density.

Theory	Solution
Dynamical 3-Space	$g(r) = \begin{cases} \frac{\left(1+\frac{\alpha}{2}\right)GM}{r^2} \ , \ r \geq R, \\ \frac{4\pi G}{r^2}\int_0^r \left(\int_s^R s'\rho(s')ds'\right) ds \ , \ r < R \end{cases}$
	$g(r) = \begin{cases} \frac{G_N M}{R^2} - \frac{2G_N M}{R^3}(r-R) \ , \ r \geq R \\ \frac{G_N M}{R^2} - \left(\frac{2G_N M}{R^3} - 4\pi(1-\frac{\alpha}{2})G_N\rho\right)(r-R) \ , \ r < R \end{cases}$
Newtonian Gravity	$g_N(r) = \begin{cases} \frac{G_N M}{R^2} - \frac{2G_N M}{R^3}(r-R) \ , \ r \geq R \\ \frac{G_N M}{R^2} - \left(\frac{2G_N M}{R^3} - 4\pi G_N\rho\right)(r-R) \ , \ r < R \end{cases}$
Gravity Residual	$\triangle g(r) \equiv g_N(r) - g(r) = \begin{cases} 0 \ , \ r \geq R \\ 2\pi\alpha G_N\rho(r-R) \ , \ r < R \end{cases}$

for a spherical galaxy. Dynamical 3-Space theory currently defines $M_{DM} = M_{BH}$ although there is no derivation of this; it is only conjecture. This result is applicable to any spherical matter distribution however, meaning that planets and other massive objects also have an inflow singularity at their centre, and contributes to the effective mass of planets and hence their gravity profiles, as was touched on in the previous section. In star systems however the minimal black hole effect becomes more prominent as was backed up by the spherical galaxy data.

3.8.3 Reverberation Effects

Perturbing the spatial inflow into matter (i.e. simulating gravitational waves) was shown recently to produce reverberations in which the wave generates trailing copies of itself.[103] This reverberation effect is caused by the non-linear nature of the flow dynamics evident in equation (3.1), and was detected in Zener diode data, where the data signal contains approximate 20 second periodic fluctuations.[77] The scale of the reverberations was predicted to change depending on the matter

in the local environment, e.g. Moon, Earth, Sun, galaxy etc. These reverberations were predicted to be detectable in many experimental processes.

3.9 Concluding Remarks about Chapter 3

The Dynamical 3-Space theory predicts the emergence of many observable phenomena such as gravity, black holes, cosmic filaments and an expanding universe with an inflation epoch. While these predictions are only found in the most simplest cases such as requiring time independence or spherical symmetry, they have all been so far backed up by experiment and also without requiring the dark matter or dark energy parameters predicted by GR.

Objectives of this Thesis

The new work presented in this dissertation covers two areas. Chapter 4 furthers the understanding the effects a dynamical and fractal space has on macroscopic processes. This is achieved through analysing the data obtained from the apparatuses in two works reported by Cahill, one showing fluctuations in RF electromagnetic (EM) waves propagating through coaxial cables, and the other studying tunneling current fluctuations in Zener diodes. These are shown to be two new methods of studying the effects Shnoll observed when studying nonrandon measurement scattering in data sets. The final part of this work offers an explanation of the effects Shnoll observed from a Dynamical 3-Space theory viewpoint.

The remainder of the thesis extends on the Dynamical 3-Space theory, starting in chapter 5 with revisiting the borehole g anomaly data in order to show that the α terms in the model (equation (3.1)) must be altered in order to fit this data set. Other data that the Dynamical 3-Space theory has been applied to, such as the SgrA* black hole, spiral galaxy rotation and the type 1a supernova magnitude-redshift data will be revisited to check that the theory still predicts these phenomenon. This will then lead to showing in chapter 6 that the supernova data predicts a uniformly expanding universe from a model independent viewpoint, and then discussing how the NG/GR and Dynamical 3-Space models predict the universe's expansion and potential inflation epochs. New black hole solutions embedded in a uniformly expanding universe that are emergent from the Dynamical 3-Space theory are discussed in chapter 7 along with their implications.

Chapter 4

Measurement Scatter in Coaxial Cables and Zener Diodes, and the Shnoll Effect

4.1 Introduction

There is significant evidence suggesting that fluctuations in macroscopic processes aren't randomly generated.[88, 90] There are over 20 different processes studied over a 5 decade period by Simon Shnoll which suggest this, and include protein activity and chemical reactions,[88] radioactive decay,[92], dark current fluctuations in photomultipliers,[104] and germanium semiconductor noise.[89] Shnoll studied the rates of change of these processes by breaking the data signal into 1 - 1.5 minute segments and then taking the respective histograms of these segments. These segments typically contain 60 - 100 measurements - a measurement is usually taken every second in the case for radioactive α decay rates which Shnoll studied in depth. He then compared the similarity in histogram shapes both over time and also between different experiments as they were run in parallel. Not only

did these shapes repeat periodically over time but they did so regardless of the process studied. Amongst others, he found that histogram shapes:[105]

- from a single apparatus were most likely to correlate with that of the following histogram in time,
- repeat periodically, over both solar and sidereal days and years, moon cycles and during solar eclipses,
- from apparatuses (regardless of whether they studied the same process or different) located next to each other correlated at the same time,
- from apparatuses separated geographically correlated either instantly and/or with a time delay corresponding to the Earth's rotation, depending on the direction of detection, and
- contained characteristic features during solar eclipses.

The study of histogram similarities using 60 - 100 measurements, and the results reported by Shnoll has been coined as the Shnoll effect. All of his correlation studies were performed via double blind experiments over tens of thousands of measurements, and also by several different human experts, which dramatically reduces the probability of findings being randomly generated and/or biased. Shnoll mainly studied radioactivity, as it was the most reliable process to study, and he has performed many control experiments which rule out common factors such as varying temperature, pH, humidity, concentration, container/apparatus shape and fluctuations in the electric mains. He ended up attributing the effects observed to cosmophysical factors,[91] i.e. inhomogeneities in the spacetime continuum. These inhomogeneities are *"caused by the movement of an object in the inhomogeneous gravitational field"*,[88] e.g. as the Earth rotates/orbits the Sun, for example. While these inhomogeneities were not characterised by Shnoll there is a remarkable amount of evidence supporting this conclusion. No explanation of these effects has

yet been provided by anyone nor have the experiments been successfully repeated outside of Russia. A major concern appears to be that the correlations were made by human experts and not via pattern recognition algorithms. A 20 year history of the attempts made by Shnoll to automate the histogram similarity process is found in chapter 2 of [88]. In the history for example he mentions a graduate from Moscow who trained a neural network algorithm to learn histogram similarities over a 2 month period based on previous similarities. When presented with new data however the algorithm failed to detect the correlations at all, whereas a human expert would find obvious histogram similarities. This appeared to be the case for all attempted pattern recognition and correlation algorithms at the time. The human brain appears to be a much more suitable device for pattern recognition, and so the work performed by Shnoll and his colleagues was tedious but necessary.

Shnoll also reports longer term studies of radioactive decay rates over time. These studies are achieved by taking a layered histogram, essentially stacked histograms of the series of measurements as an experiment progresses. An example of this is shown in figure 4.1, which shows a layered histogram of 352,980 successive measurements of the α decay rate of a ^{239}Pu source. The layers show a fine structure which builds up over time instead of cancelling out as in the case of a typical random, or Poisson distribution. This suggests that the radioactivity of ^{239}Pu takes on discrete (preferred) values, and is not completely random. This is usually ignored in favour of a random distribution after either smoothing the data or taking into account statistical probabilities. This chapter firstly discusses the new analysis of two works published by Cahill in an effort to further understand at least the long term effects Shnoll observed.[106, 107] The dual radio frequency coaxial cable EM speed anisotropy experiment[74] allowed a preliminary analysis of understanding the long term measurement scattering effect, and is shown here to be a potential new technique for observing the short term Shnoll effects. The resolution of this

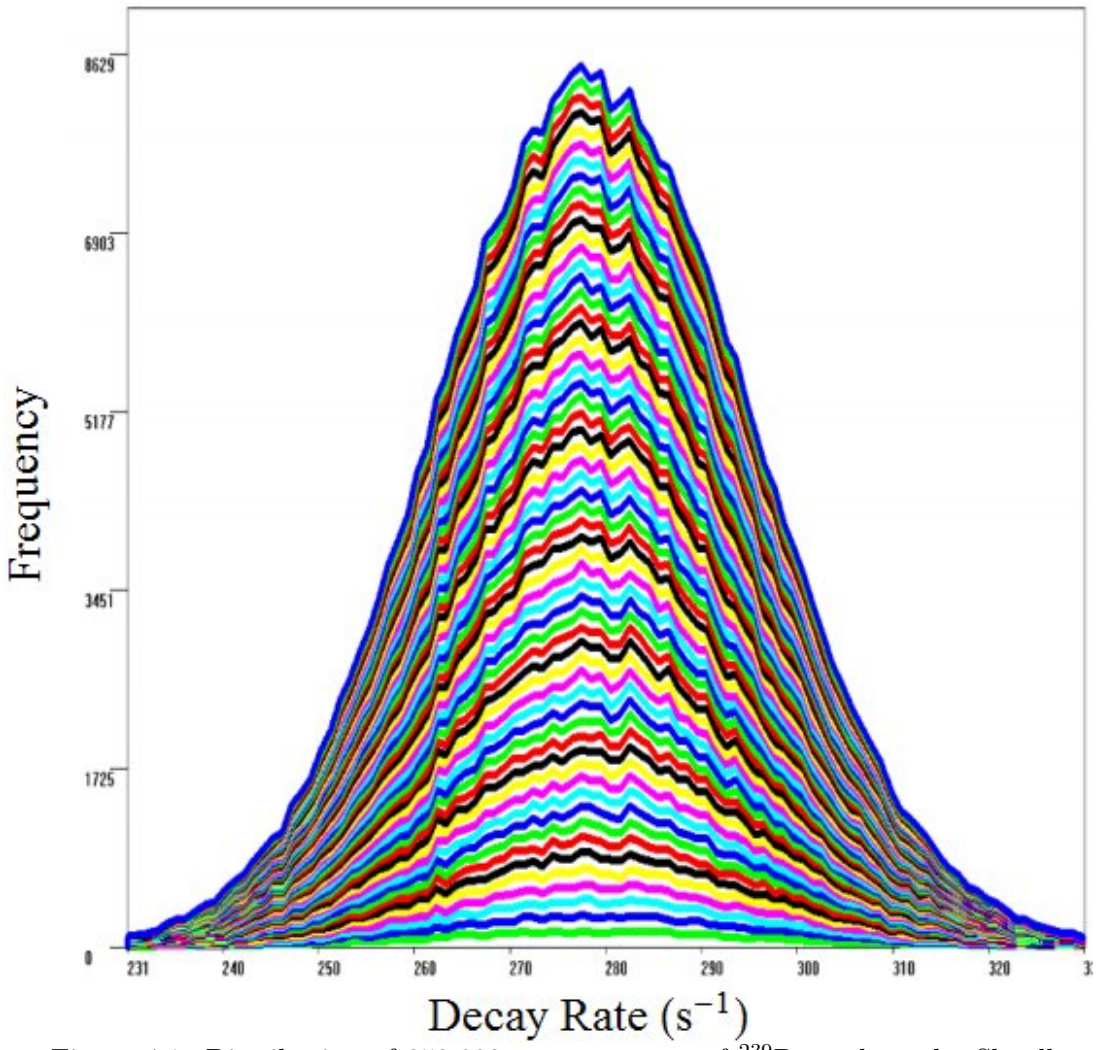

Figure 4.1: Distribution of 352,980 measurements of ^{239}Pu α decay by Shnoll performed in May 2004 (Figure 2-2 of [88]). The layered histograms are taken every 6000 measurements. The x-axis denotes the number of decay events per second and the y-axis is the frequency of measurements.

data was however insufficient to further study changes in histogram shapes containing only 60 - 100 measurements. The second experiment however used a newer technique with current fluctuations in Zener diodes[77] produced data which had a much higher timing resolution, and could in the future be used to study the Shnoll effect. A discussion of how the presence of a dynamical space could affect the apparatuses used by Cahill to generate the resultant data sets is presented.[106, 107] The rest of the chapter discusses the short term Shnoll effects from a Dynamical 3-Space model viewpoint, which will suggest that Shnoll's work also indicates the existence of a richer reality than predicted by conventional physics models.

4.2 Materials and Methods

4.2.1 Dual RF Coaxial Cable Experiment

Figure 4.2a shows the dual RF coaxial cable apparatus used by Cahill[74] for collecting data. The apparatus relied on soldering two phase stabilised Andrew coaxial cables with differing refractive indices (HJ4-50, $n = 1.11$, FSJ1-50 A, $n = 1.19$) together into 2 circuits, in a way where the EM waves in one circuit would travel in one direction through one type of coaxial cable, and then back through the other, and vice versa with the other circuit. This is better represented in figure 4.2b. All 16 of the HJ4-50 cables were tightly bound into a 4x4 array such that they all locally have the same temperature, and similarly with the FSJ1-50 cables (see the gray conduit boxes at the bottom of figure 4.2a). The cables in one of the circuits were embedded into the cables in the second circuit, which then allows the cancellation of any temperature effects present in both circuits. The apparatus was also aligned N-S and horizontally, 35° with respect to Earth's spin axis as to allow Earth to naturally change the angle of the apparatus wrt the space flow, which is predicted to have a declination of approximately $-70°$. Aligning the apparatus with respect to the Earth's spin axis removed any Earth rotation induced effects which would then allow the characterisation of the 3-space wave effects, however for the data analysed here the apparatus was oriented at the angle mentioned above. The travel time difference of two 10MHz RF signals from a Rubidium (Rb) frequency standard clock was detected using a LeCroy Waverunner 6000A Digital Storage Oscilloscope (DSO) as the signals travel one way in one type of coaxial cable and return via the other type of coaxial cable. Any temperature effects that affect one circuit also affect the other circuit in the same manner (as they are bound together), and so the travel time difference is only affected by the overall temperature of the cables, Rb clock and DSO. The effects on travel time due to temperature were removed from the data by

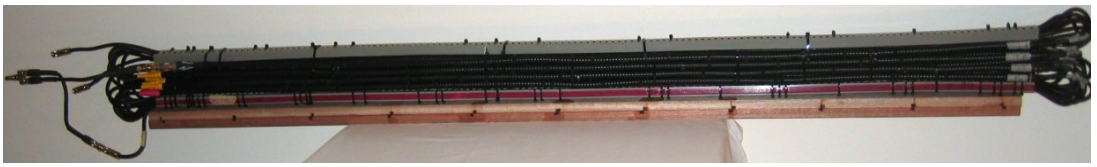

(a)

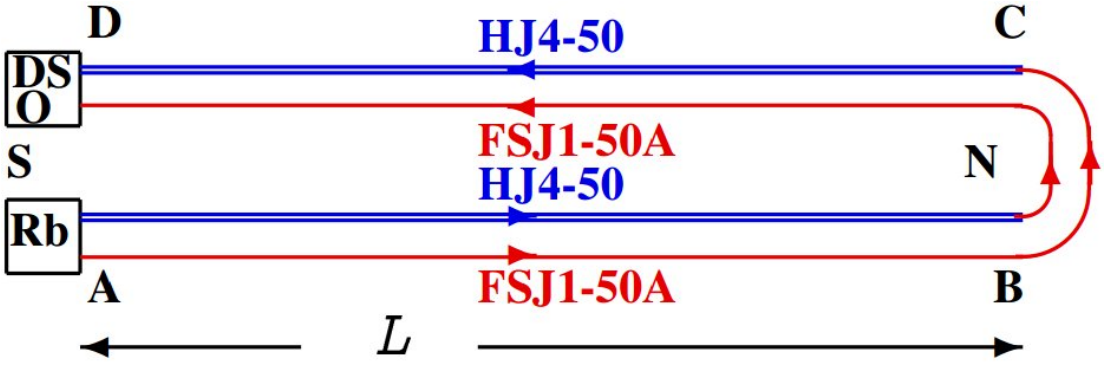

(b)

Figure 4.2: (a) Dual RF coaxial cable apparatus, see figure 5 of [74], with 2 circuits of alternating lengths of HJ4-50 coaxial cable soldered to FSJ1-50A cable. Each circuit was 1.85 x 16 = 14.8 m long. (b) Schematic of the coaxial cable apparatus, see figure 6 of [74]. In each circuit the 10 MHz RF signal travels one-way in one type of coaxial cable and returns via a different kind of coaxial cable, and the travel time difference is measured via a DSO.

positioning the detector in a closed room, while allowing the room temperature to fluctuate slowly over a period of time. The timing errors were assumed to be proportional to changes in temperature, and were found to have a distinct time signature approximately 4 times that of the true 8 ps signal. The circuit phase data was obtained by subtracting the temperature induced $\triangle t = a + b\triangle T$ from the data, after determining coefficients a and b. Data was collected every 5 seconds, from 12:00 am March 4, 2012 to 12:00 am March 2012 (9 days), and contains 155,520 data points over this period. The data has a resolution of 1 ps, i.e. the travel time difference was recorded in integer picosecond values. The data obtained and used was that after taking into account temperature fluctuations, i.e. the raw data was not obtained nor required for analysis.

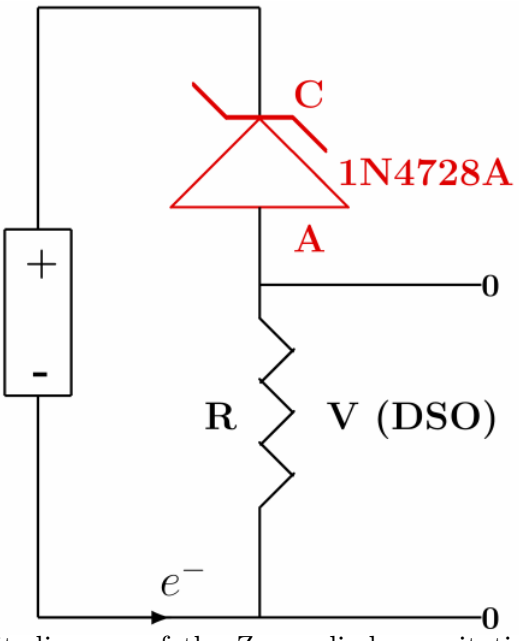

Figure 4.3: Circuit diagram of the Zener diode gravitational wave detector, showing 1.5 V AA battery, 1N4725A Zener diode operating in reverse bias mode, and having a Zener diode of 3.3 V, and resistor $R = 10$ kΩ.[107]

4.2.2 Zener Diode Experiment

The Zener diode gravitational wave detector experiment performed in August 2013 was set up as shown in the circuit diagram in figure 4.3.[77] The setup is quite simple and only uses a 1.5 V AA battery, a 1N4728A Zener diode operating in reverse bias mode, having a Zener voltage of 3.3 V, and a resistor $R = 10$ kΩ. The voltage V across the resistor is measured and used to determine the fluctuating tunnelling current through the Zener diode. The apparatus was attached to a LeCroy Waverunner 6051A DSO and data was collected at 1 second intervals, from 5:06:55 am August 20th, 2013 to 3:12:42 am August 27th 2013 (8 days), and contains 376,101 data points over this period. The current fluctuation amplitude data has a much higher resolution than that of the coaxial cable data (μA, to multiple decimal places as opposed to ps, and is the limitation of the DSO for the coaxial cable experiment). Due to power issues the recording of the data was intermittent, which is discussed in the results section.

4.2.3 Data Analysis and Layered Histogram Generation

The coaxial cable and Zener diode data was analysed in the work presented here using Mathematica 9.0. The code used contains a mechanism to reduce or eliminate unwanted low frequency effects such as the Earth rotation effect, temperature drift and tunneling current drift from decreasing battery power (in the Zener diode experiment), for example. The code works in the following manner:

1. Import the required data set (either coaxial cable or Zener diode data) and plot in a signal form.

2. A Fourier Transform (FT) of the data set is performed.

3. A low frequency cutoff (FC) is set which then eliminates the lowest frequencies observed in the raw data, like Earth rotation effects and any potential residual temperature effects for example. An inverse of this FT then leaves the remaining data without the unwanted lower frequencies. This data set is then plotted in a signal form.

4. The data is split into segments each containing 3350 (coaxial) or 6100 (Zener) measurements, starting from the first measurement - the remainder of the measurements not divisible by the above numbers (155520 - coaxial cable, 376101 - Zener diode data sets) are discarded.

5. To ensure that numerical artifacts are minimised, the first and last segments of the coaxial cable data set, and the first/last 5 segments from the Zener diode data set are discarded - see the results section on this for a further justification on numerical artifact removal.

6. The data points from the first remaining segment are placed into a histogram of width $\pm 3\sigma$, where σ is the standard deviation of the data set generated. The histograms are divided into 70 bins of fixed width.

7. The second histogram was taken in a similar manner except it uses both the 1st and 2nd data segments, the third containing 1st to 3rd segments, and so on, to achieve a series of layered histograms that build up over time. These layered histograms don't necessarily contain all the data points, just those that fall within $\pm 3\sigma$ of the mean value of all data points collected over the duration of the experiment.

8. All histograms are plotted together to show how the data builds up over time. Layered histograms of width 1σ and 2σ were also generated to show how the data is affected by scaling effects.

In both the coaxial cable and Zener diode data cases a background of the data was also taken in which the above FT process was also used. This background was obtained by:

1. Taking a moving average of a data set, using 250 points.

2. Repeating the above once, to further smooth the data. This gives a smooth background as will be shown in the results section.

3. Using the mentioned FT process to remove low frequencies from the background data set.

4.3 Results

4.3.1 Coaxial Cable Experiment: Code Robustness

Figure 4.4 shows the data from the dual RF coaxial cable experiment performed in 2012 - see [74]. There are periodic peaks and troughs which are caused by the rotation of the Earth changing the orientation of the apparatus wrt to the space

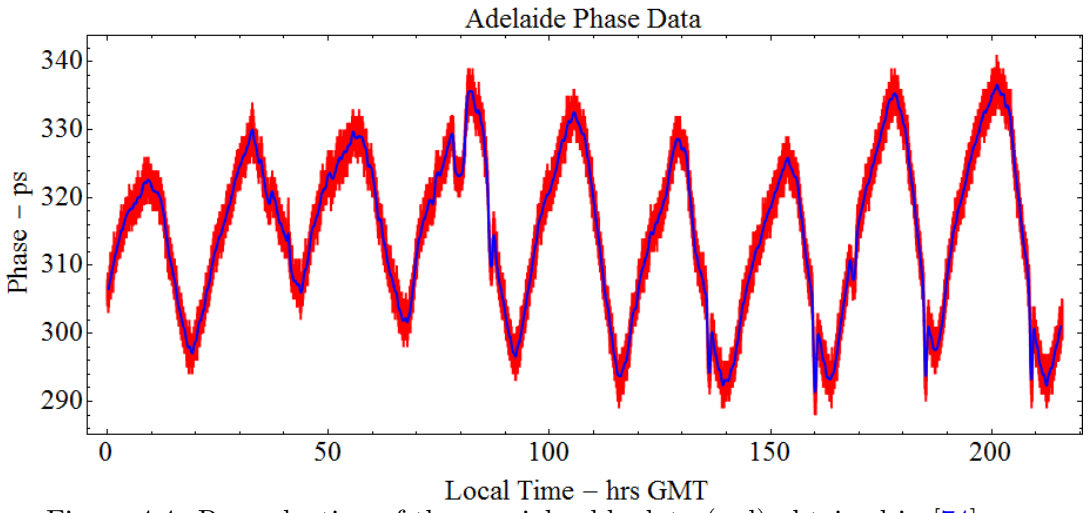

Figure 4.4: Reproduction of the coaxial cable data (red) obtained in [74], over the duration Mar 4 - 12, 2012. The blue plot represents a moving average of the raw data. The y axis represents the travel time difference between the two coaxial cables, in ps, to integer precision.

flow, hence changing the travel time. The travel time difference between the circuits at the DSO is independent of temperature, and is

$$\triangle t = \frac{2v\cos\theta L(n_1^2 - n_2^2)}{c^2} + ... \tag{4.1}$$

where $L = 14.8$ m is the length of each circuit, n_1 and n_2 are the refractive indices of the two coaxial cable materials used and $v\cos\theta$ is the 3-space velocity projected onto the apparatus, which changes as the Earth rotates. The apparatus relies on exploiting the Fresnel drag anomaly, i.e. that there is no apparent Fresnel drag in coaxial cables. The Fresnel drag effect is an additional slowing effect which EM waves experience when moving through a dielectric that is itself moving through space. A clarification of the Fresnel drag formalism in the presence of a dynamical space can be found in section 3 of [108]. A key point is that if Fresnel drag was present in coaxial cables then the $n_1^2 - n_2^2$ term in 4.1 is replaced by 0, and no first order term in v is present.[74, 108] This is clearly violated by the actual data recorded by the coaxial cable experiment, as the Earth rotation effect is apparent. These results are in remarkable agreement with the velocity of absolute

motion of Earth determined from both the Miller data[57] and that from NASA spacecraft Earth-flyby Doppler shift data,[109] which revealed a light/EM speed anisotropy of 486 km/s in the direction $(4.3^h, -75.0°)$. This anisotropy, or 3-space velocity varies throughout the year in a predictable fashion because of the orbital motion of the Earth - the aberration effect discovered by Miller, see figure 2.1 but also shows fluctuations with fractal characteristics. The flyby data provides an excellent comparison with coaxial cable 3-space velocity predictions; if Fresnel drag is present then the space velocity for DeWitte's coaxial cable data was predicted to be 1125 km/s, which also disagrees with the flyby data.[74] The regular dipping spikes in the data at 135, 160, 183 and 208 (and likely also at 86) hours occur at around 3 - 4 am on those days and are likely caused by power grid fluctuations. The data also only contains measurements at integer values of picoseconds, as this is the extent that the DSO can measure. This is the one major limitation of the DSO in that it cannot physically record a higher timing resolution than this.

The Fourier Transform process used is designed to remove any low frequency effects observed in the coaxial cable data, including daily Earth rotation, residual temperature anomalies arising from the linear fitting process and the effects due to power grid fluctuations. This results in a signal which is caused solely by fluctuations in space flowing past the apparatus, and ideally allows the characterisation of these fluctuations. Figures 4.5a - 4.5c show the data after the described FT process after using different low FC strengths ranging from 20 to 1000. The strength values are only meaningful in that they reflect the strength of the frequencies removed from the 155520 data points used. It is noticed that having an insufficient (too low) FC introduces sinusoidal numerical artifacts into the data along with insufficient removal of the data spikes, as is shown by having low FCs of 20 and 100. The sinusoidal effects and data spikes were observed to decrease with increasing low FC. The presence of the mentioned power spikes in the coaxial cable data in figures 4.5a (20) and 4.5b (100) demand a higher low FC, such as 1000 which

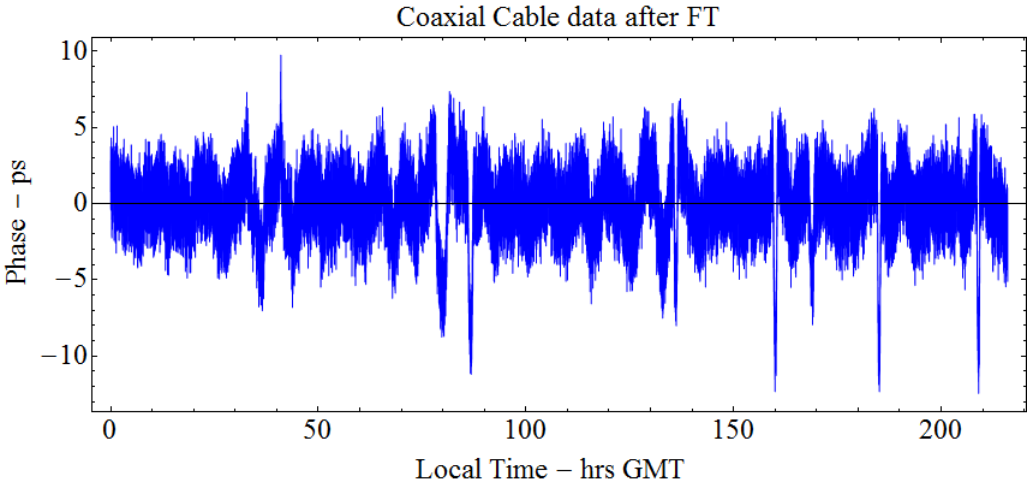

(a) Low FC = 20

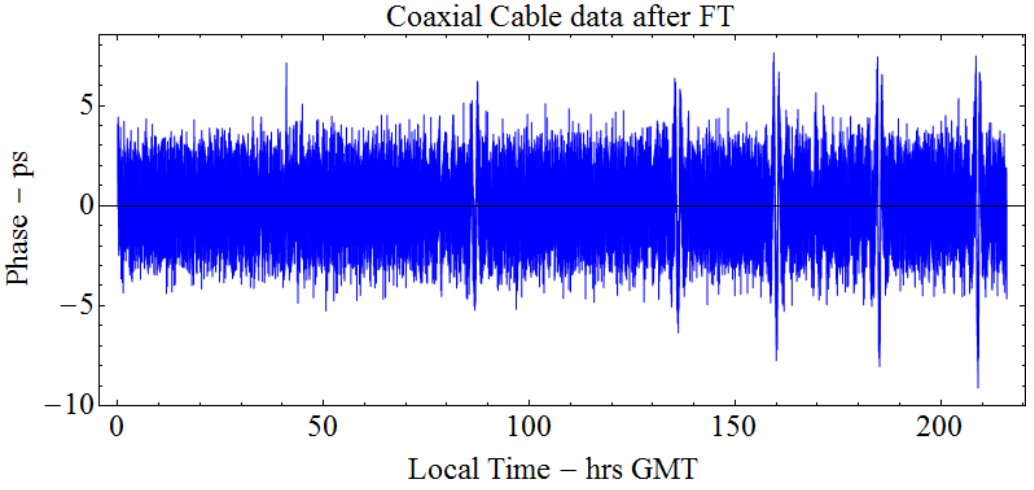

(b) Low FC =100

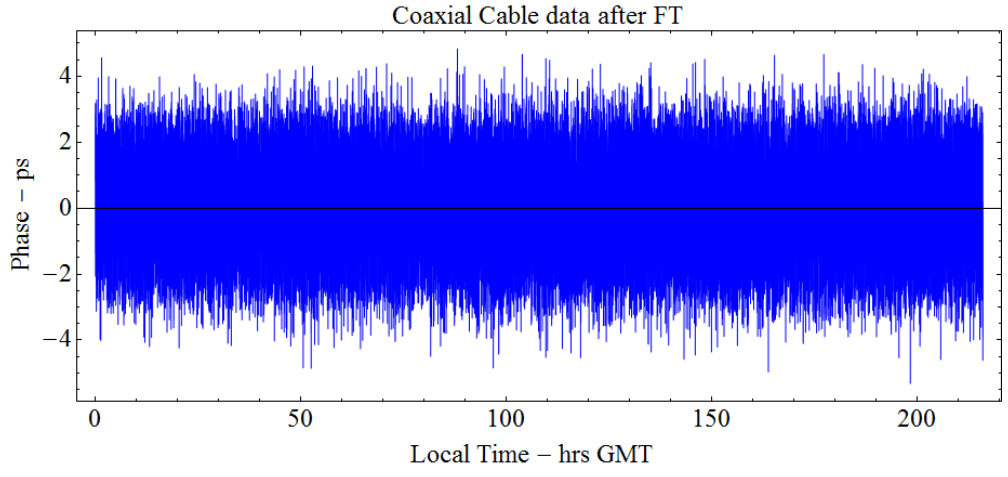

(c) Low FC =1000

Figure 4.5: Coaxial Cable data after FT using increasing low frequency cutoffs from 20 to 1000 (from 155520 measurements).

appear to remove this completely.

To be certain that all unwanted artifacts from a signal were removed, the extent to which numerical artifacts in the data set after background removal were quantified. There are different ways to do this, the easiest of which is to simply subtract the background from the data. It was decided however to determine a smoothed background of the coaxial cable data, while then using the FT process to reduce the background to zero by varying the low FC strength. One then gains the added benefit of being able to remove not only the background but also the lower frequencies in the true signal, allowing the study of various frequency bands observed in the data if desired. This is the role of the low FC, to set all sufficiently low frequencies observed in a data set to zero; a high FC may also be used to remove higher frequencies. This will then guarantee a clean data set after the FT process while demonstrating the robustness of the Mathematica code used. The blue plot in figure 4.4 shows the background of the coaxial cable data, while figures 4.6 and 4.7 show how the background reduces when the low FC increases from 200 to 2000. The inserts of these two figures are zoomed in sections after removing the first and last 3350 measurements (since the ends contain higher numerical artifacts induced by the FT process, these data points are discarded when compiling the layered histograms), and further show the reduction in the background signal. For a low FC of 200, figure 4.6a, the numerical artifacts due to power grid fluctuations are clearly evident. These are virtually eliminated at higher strengths such as from 500 - 2000.

For a low FC value to sufficiently reduce the background signal to a point where it will not affect the resultant layered histograms, the numerical artifacts observed in figures 4.6 and 4.7 must be at least lower than the bin width of the histograms. If the background noise is too high, a data point could be shifted to the bin next to it, thus a layered histogram will become unreliable if there are too many numerical errors present in the data. Table 4.1 shows the bin widths of the resultant layered

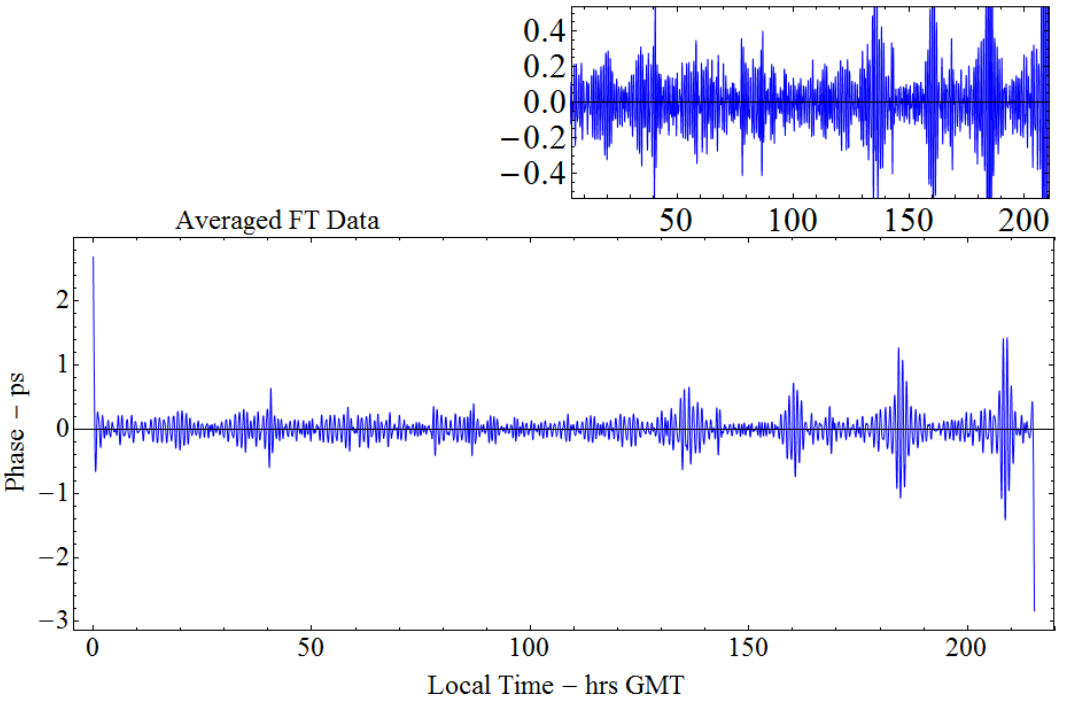

(a) Low FC = 200

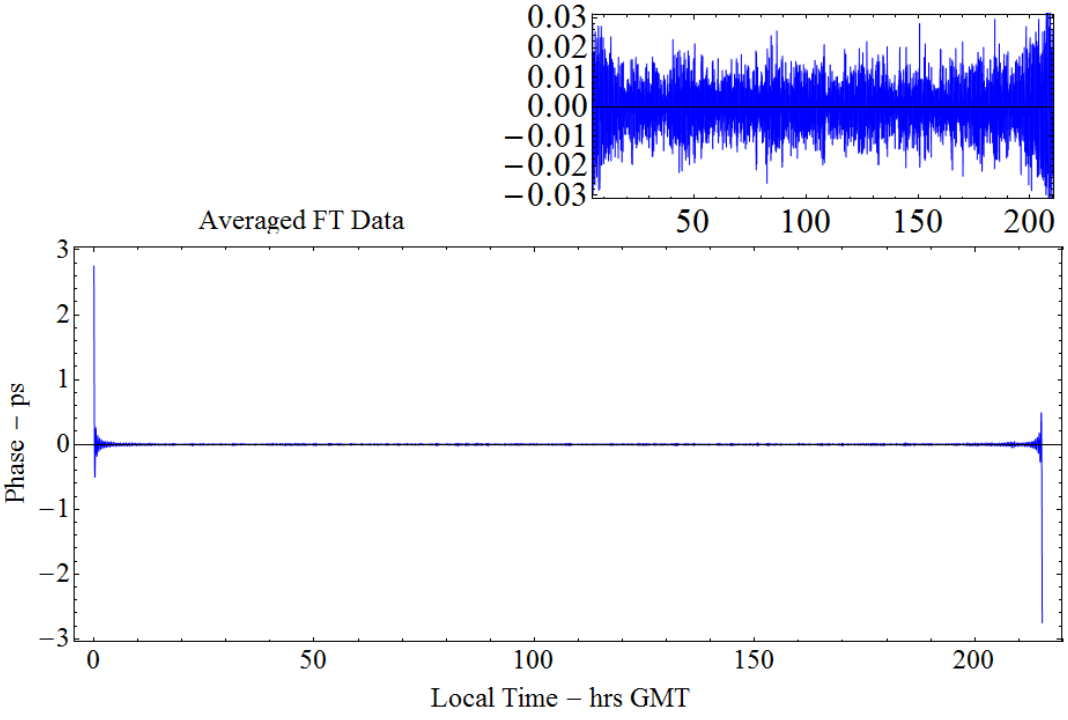

(b) Low FC = 500

Figure 4.6: Residual noise of smoothed coaxial cable data after FT using increasing low FCs of 200 and 500 (from 155520 measurements).

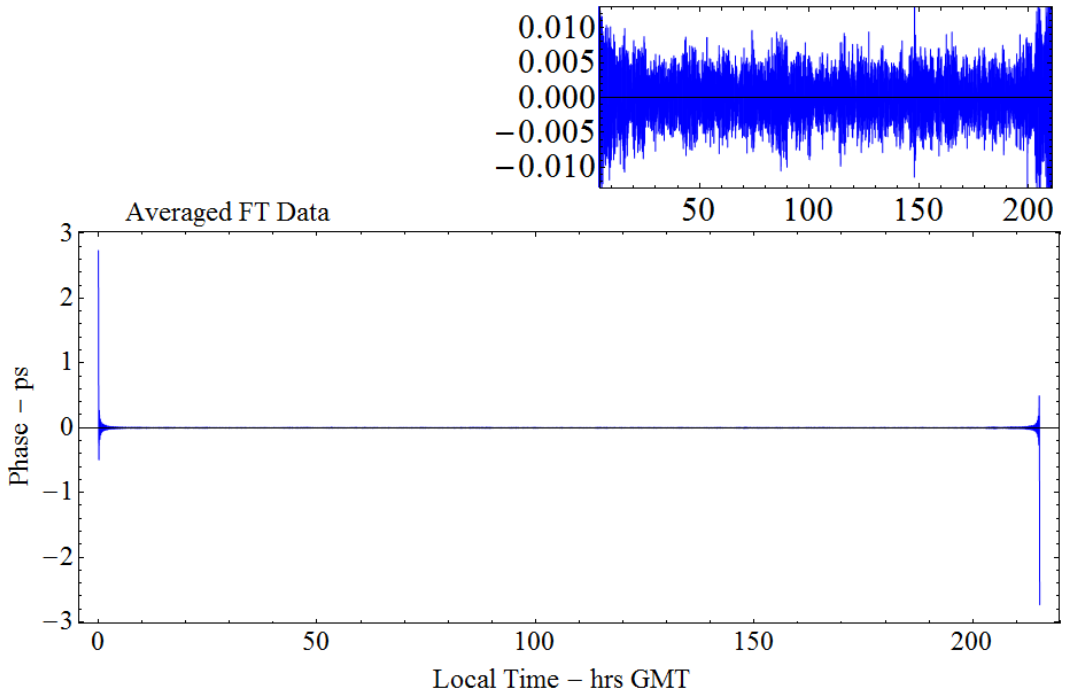

(a) Low FC = 1000

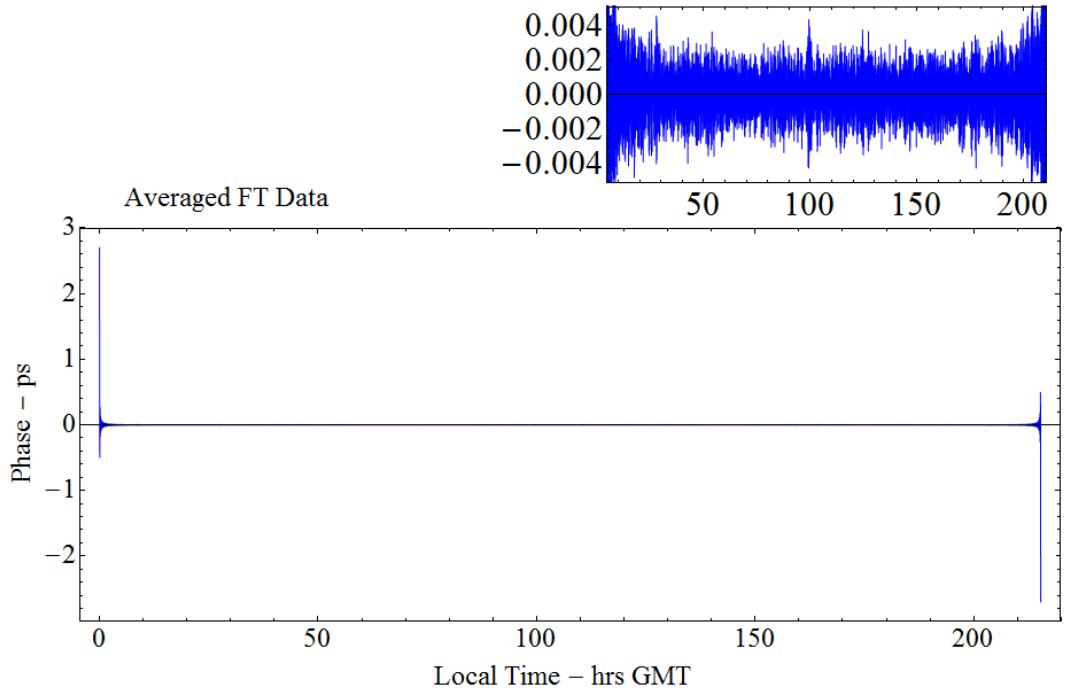

(b) Low FC = 2000

Figure 4.7: Residual noise of smoothed coaxial cable data after FT using increasing low FCs of 1000 and 2000 (from 155520 measurements).

Table 4.1: Background coaxial cable data after the FT process, for low FCs from 200 to 2000. The resulting layered histogram bin width is shown along with the estimated noise from the background signal.

Low FC	σ	Bin Interval	Estimated Smoothed FT Noise
200	1.2288	0.0529	> 0.4
500	1.1707	0.0500	0.030
1000	1.1511	0.0500	0.010
2000	1.1300	0.0486	0.004

histograms for a given low FC, along with the estimated background noise for the coaxial cable data. A FC of 200 for example (figure 4.6a) shows clear numerical noise mainly from the daily spikes in the raw data resulting from the FT process, while the estimated background noise is almost 8 times higher than the resultant layered histogram bin width. It could be argued that using a low FC of 500 (figure 4.6b) shows this as well, or at the very least at the end points since the FT noise is 0.03 and comparable to the bin interval of 0.05, meaning that the first and last histograms would likely contain a lot of numerical errors which then persist throughout a layered histogram. As table 4.1 shows, a FC of at least 1000 is required for background numerical effects to be reduced enough to generate meaningful layered histograms.

Figure 4.8 shows the layered histogram generated for a low FC of 1000. The structure observed in the layered histogram appears to build up over time instead of cancelling out. This suggests that the coaxial cable data is affected by a non-random process as the data is taking on discrete, or preferred values. Layered histograms with different low FCs also display this property though, such as those still containing some numerical effects as shown in figure 4.9a for a low FC of 500, or when more of the true signal is removed from the histogram (figure 4.9b uses a low FC of 2000, for example). These histograms appear noisier than the ones Shnoll produced (see figure 4.1 earlier in this chapter) but this may be due to the fewer data points obtained than Shnoll (352,980 measurements), or due to the timing resolution of the DSO used in the experiment. What is noticeable is that there

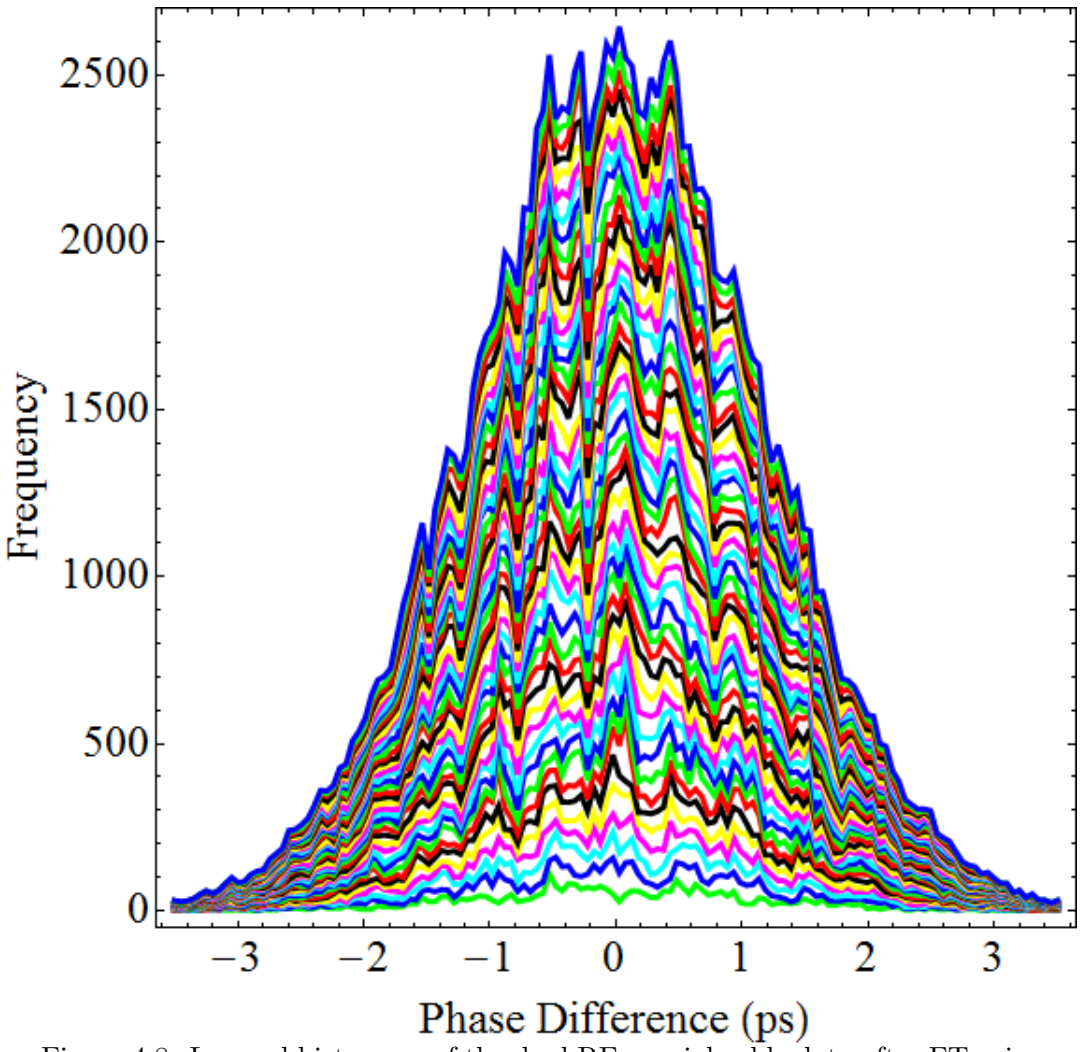

Figure 4.8: Layered histogram of the dual RF coaxial cable data after FT using increasing a low FC of 1000.

are peaks at non integer values, which contradicts the coaxial cable data initially, as this contained only integer picosecond values. This is likely caused by the FT process interpolating the data after removing the low frequency effects, leading to non integer data points being generated. Since all 3 layered histograms show similar properties, it can be said that the Mathematica code used is sufficiently robust enough to study the Zener diode data, which has much better timing resolution as discussed next.

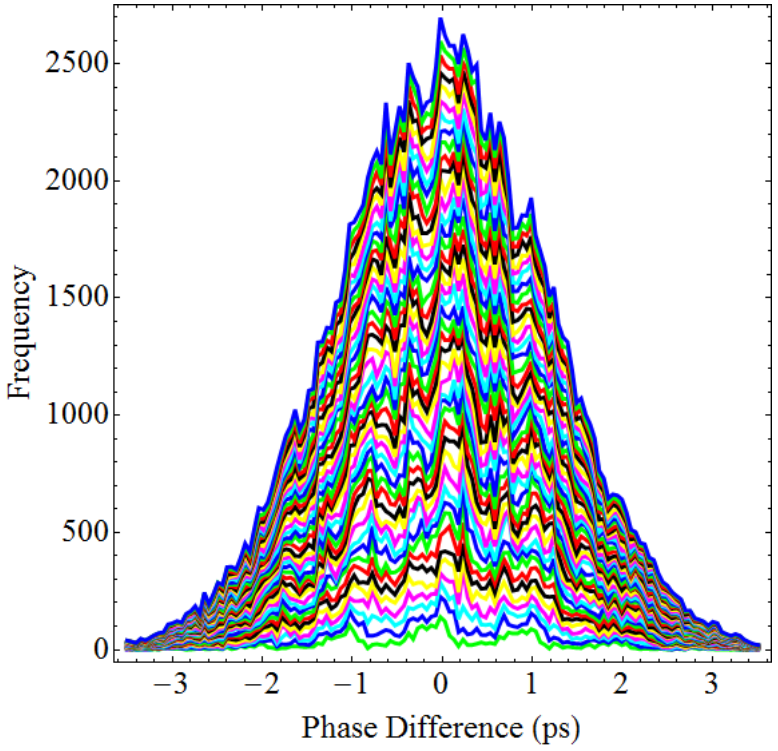

(a) Low FC = 500

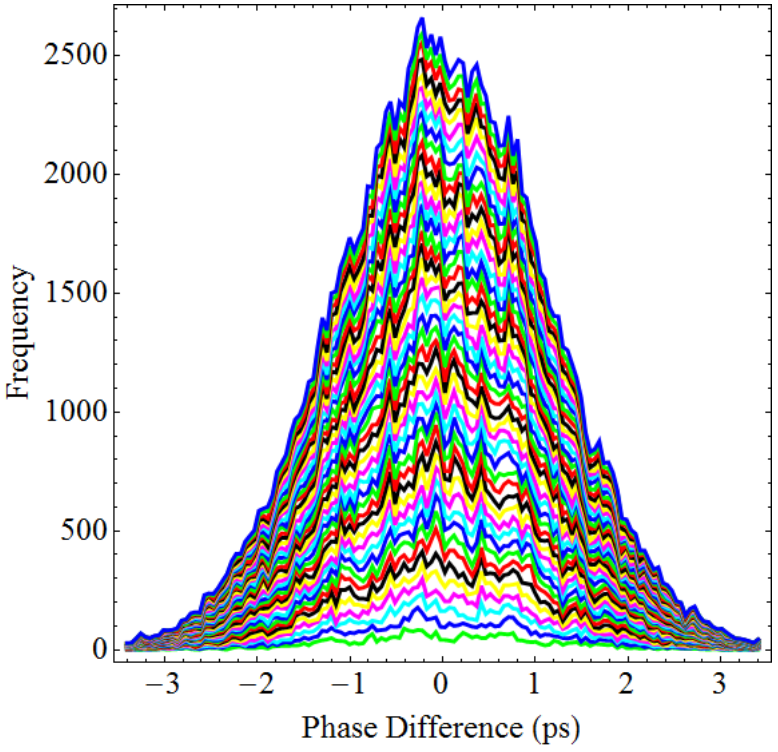

(b) Low FC = 2000

Figure 4.9: Layered histograms of the dual RF coaxial cable data after FT using increasing low FCs of 500 and 2000.

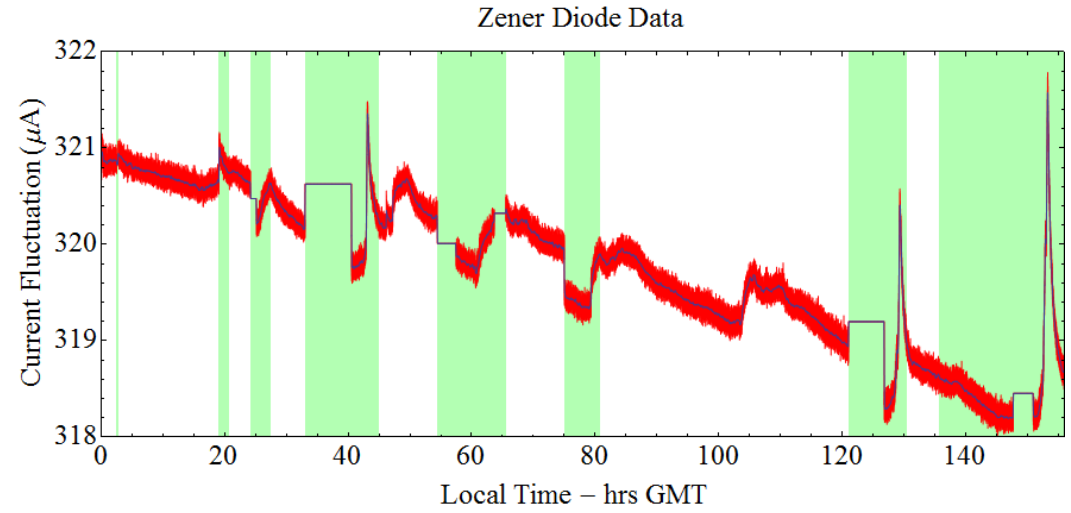

(a) Collected data

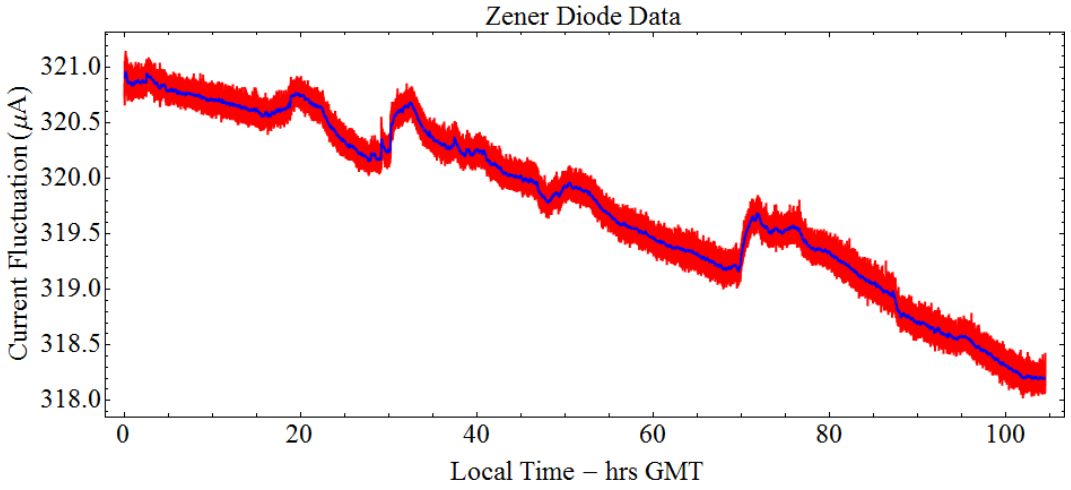

(b) Used data

Figure 4.10: Zener diode data obtained from 20 - 27 August, 2013, in Adelaide. Part (a) is the entire data showing periods of intermittance and data spikes and part (b) shows the data after removal of unwanted periods.

4.3.2 Zener Diode Experiment

Figure 4.10a shows all the raw data obtained from the reverse biased Zener diode experiment performed in Adelaide, from 5:06:55 am August 20 - 3:12:42 am August 27, 2013, along with a smoothed fit performed in a similar way to that of the coaxial cable data (see figure 4.4). The data contains periods of intermittance (flat lines caused by the DSO stopping recording data or power issues), dips (e.g. at 75 hours - the cause of this is unknown) and spikes (43, 127 and 151 hours likely caused by

power grid fluctuations at midnight) which make it difficult to generate layered histograms of this data without introducing numerical errors at these periods. The gradual current decay is attributed to the batteries in the circuit draining over time. It was decided to remove these undesired periods and obtain a data set with no current spikes, thus allowing the general study of tunneling current fluctuations over time.

Figure 4.10b shows this data with periods removed to obtain a data set with no major spikes or dips. The resulting data set was smoothed (see blue plot of 4.10b) and the FT process was performed. Table 4.2 summarises the standard deviation and bin intervals of the Zener diode data as a function of low FC as well as the corresponding estimated smoothed noise. It was required to remove the first and last 3 segments of data (18300 data points on either side) as the numerical artifacts at either end of the resulting data sets were too large to include. From table 4.2 it is apparent that a low FC of at least 2000 is required to study the Zener diode data (the estimated smoothed noise of 0.001 is less than half of the bin interval of 0.00214) although using a FC of 5000 would produce a more reliable layered histogram as well. Figures 4.11a and 4.11b show the layered histograms generated for low FCs of 2000 and 5000. The histogram shape is very similar to that of what Shnoll detected, see figure 4.1, i.e. smoother than the coaxial cable layered histograms but still containing features which persist over time instead of washing out as in the case for a typical random distribution. This suggests that the long term effects Shnoll observed will also be evident in both the coaxial cable and the Zener diode data. Figures 4.12a and 4.12b show layered histograms for a low

Table 4.2: Summary of FT of unsmoothed and smoothed Zener Diode data, used in order to determine the low FC used for further study.

Low FC	σ	Bin Interval	Estimated Smoothed FT Noise
500	0.0565	0.0024	0.0060
1000	0.0529	0.00223	0.0015
2000	0.0509	0.00214	0.0010
5000	0.0491	0.00214	0.0004

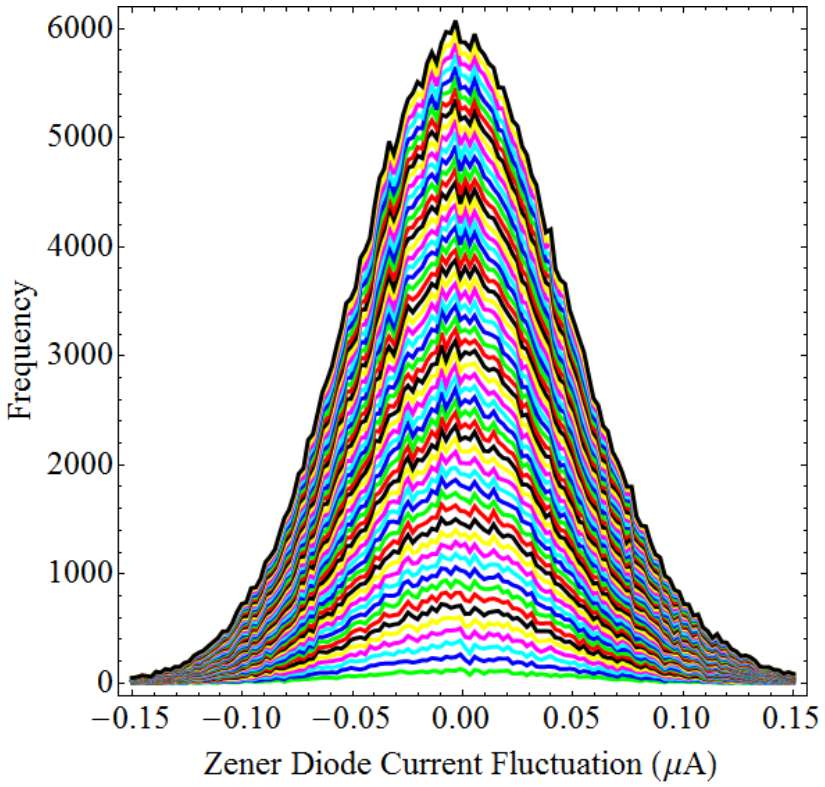

(a) FC = 2000, 3σ scale

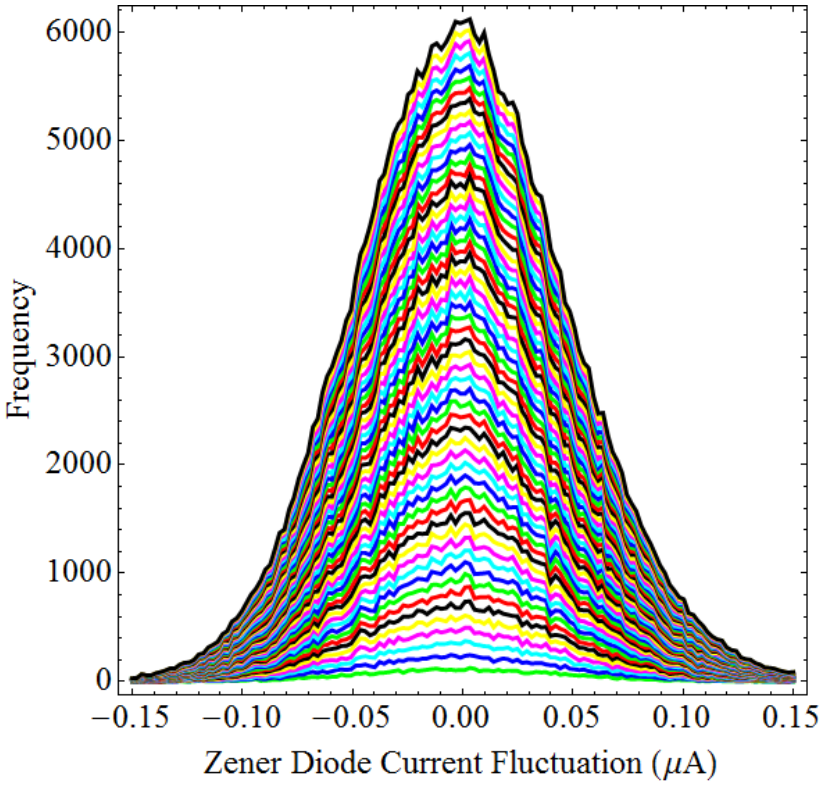

(b) FC = 5000, 3σ scale

Figure 4.11: Layered histograms of the Zener diode data after FT using increasing low FCs of 2000 and 5000.

FC of 5000, but at increased time scales, effectively 'zooming in' on the layered histogram. These layered histograms show even more structure that builds over time. This buildup appears to occur regardless of the time scale used, suggesting that the phenomenon causing this has a fractal nature.

4.4 Interpretation of Data

There are properties which arise in the layered histograms for both the dual RF coaxial cable and Zener diode data sets. These are:

1. The data consists of preferred or discrete values instead of random values. This is shown through figures 4.8 and 4.12 having nonrandom distributions.

2. The distributions have persistent structure regardless of the cutoff frequency used to produce them, i.e. the structure exists for differing frequencies used in the histogram.

3. The structure also persists when observed at different scales, see figure 4.12.

Point 1 suggests a nonrandom phenomenon causing the observed distributions while points 2 and 3 suggest a fractal nature of the phenomenon. If this is indeed caused by a dynamical and fractal 3-space then the persisting structure observed in the layered histograms correspond to regions of space passing the Earth that have preferred/discrete velocities, and not random ones, as randomly distributed velocities would result in a Poisson distribution, i.e. no features. This is better illustrated using a bubble diagram shown by figure 4.13. Here the bubbles can be thought of as the regions of space with differing speeds and directions and which evolve over time. A likely explanation for this is that the gravitational waves propagating in the 3-space inflow of the Earth or Sun could become phase locked due to the relative locations of massive objects. This would cause reverberation effects,

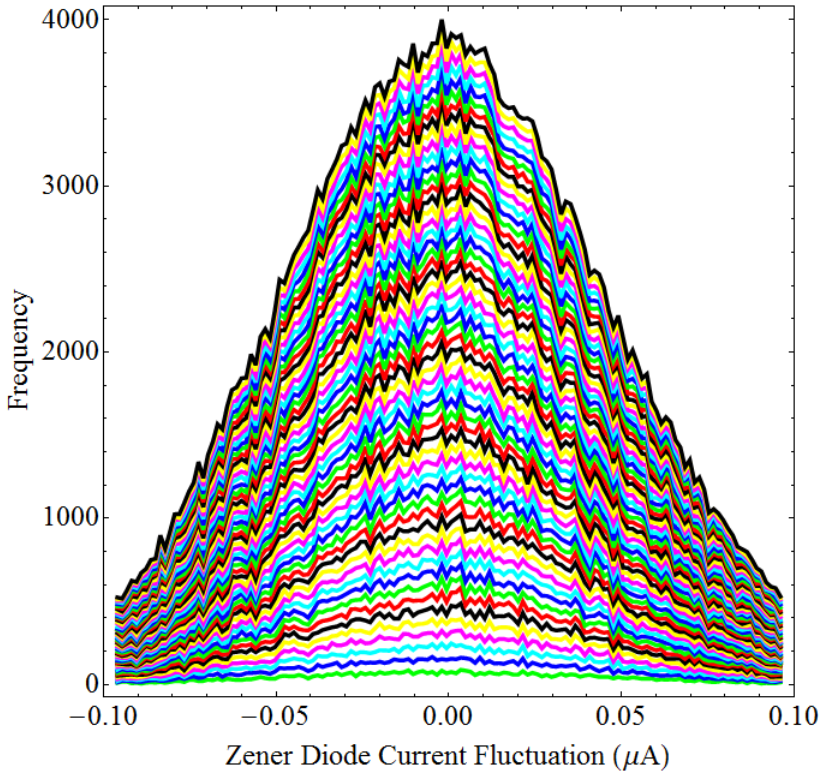

(a) FC = 5000, 2σ scale

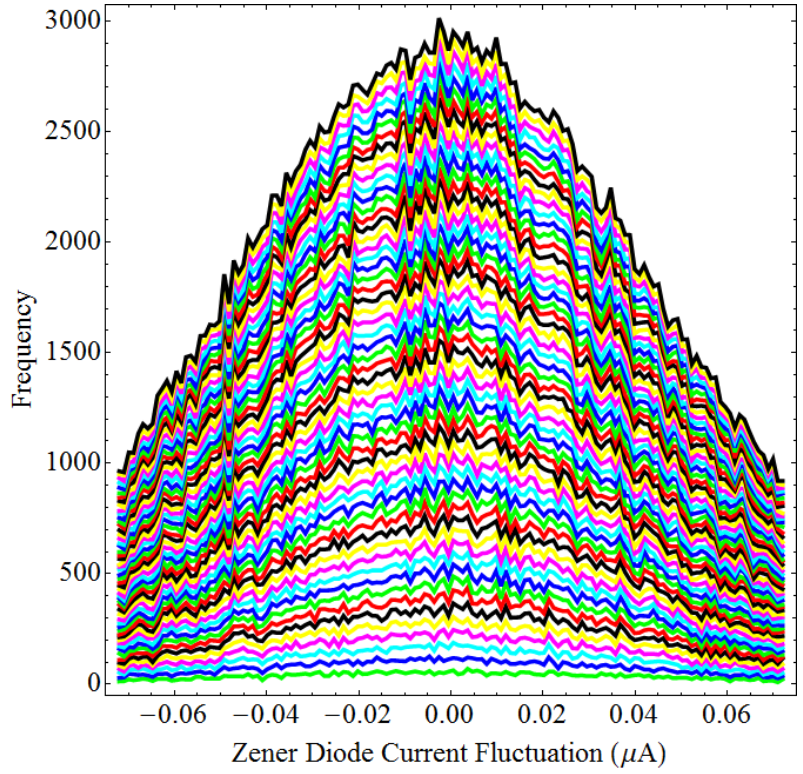

(b) FC= 5000, 1.5σ scale

Figure 4.12: Layered histograms of the Zener diode data with 2 σ and 1.5 σ scale for a low FC of 5000.

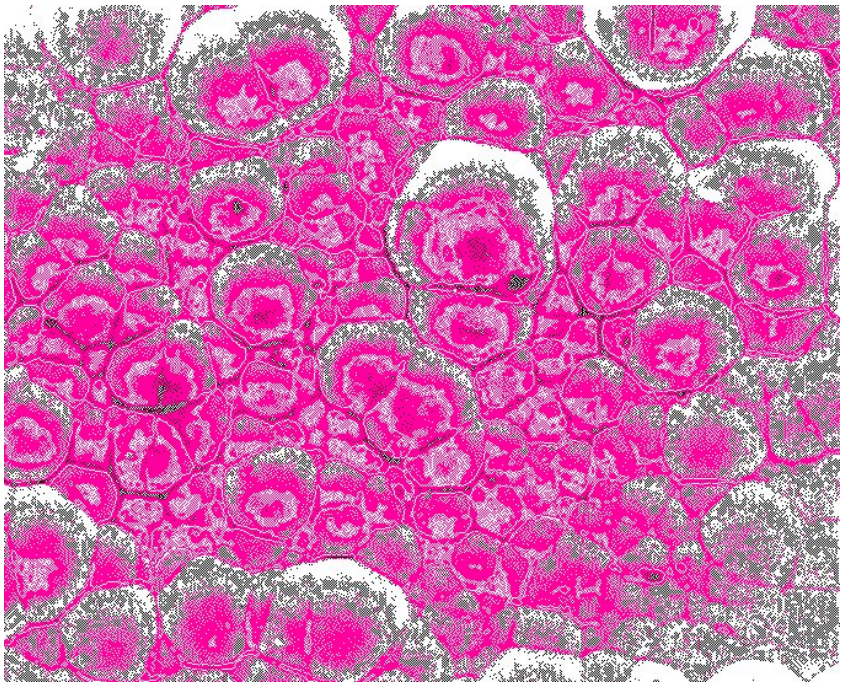

Figure 4.13: Bubble representation of the fractal wave data as revealing the fractal and dynamical structure of the 3-space. The cells of space would contain slightly different velocities which evolve over time, and move wrt the Earth with a speed of $\approx$ 500 km/s.

i.e. regions of space which have similar speeds and directions, which then repeat over time. The reverberations would be detectable in many other experiments such as EM anisotropy, radiation decay, semiconductor noise generation etc. and could in the future be used to further characterise the dynamics of space. Characterising these reverberation effects however would be quite difficult, at least using this study since the reverberations would change shape while the Earth rotates and orbits the Sun, and also as the Moon orbits the Earth, at least from a local point of view. It could be possible, if one had enough instruments to perform multiple experiments in parallel while the relative positions and orientation of Earth, Sun and Moon are fixed, but this however was not possible in the work presented here.

For the above claim to be true, a mechanism is required which describes the interaction of space with these devices to produce the mentioned effects. Certainly the coaxial cable data set contains light speed anisotropy effects arising from the apparatus changing angle wrt the space flow as the Earth rotates, which explains

the periodic change in the travel time observed. To explain the scatter of measurements in the data signals one must turn to clock jitter effects within a DSO and tunneling current fluctuations within Zener diodes, which were suggested to exist within the time difference measurement hardware within DSOs.[77] It was mentioned briefly in chapter 2 regarding clock jitter, the effect which appears to be correlated when the DSOs are separated geographically. The discovery was later followed by correlations observed in Zener diode devices in the Global Consciousness Project between Perth and London, i.e. at a much larger scale. The work presented here was later followed by a study by Cahill[84] where the signals from Zener diodes separated by distance were also found to correlate, with a time delay corresponding to a 3-space speed of 476 km/s when the diodes were oriented N-S. This then provided further justification for space fluctuations being responsible for causing Zener diode fluctuations. Why fluctuations in space also drive current fluctuations in Zener diodes was then understood. Consider the generalised Schrödinger equation in the presence of a potential $V(\mathbf{r},t)$,[51]

$$\begin{aligned} i\hbar\frac{\partial\psi(\mathbf{r},t)}{\partial t} &= -\frac{\hbar^2}{2m}\nabla^2\psi(\mathbf{r},t) + V(\mathbf{r},t)\psi(\mathbf{r},t) \\ &\quad -i\hbar\left(\mathbf{v}(\mathbf{r},t).\nabla + \frac{1}{2}\nabla.\mathbf{v}(\mathbf{r},t)\right)\psi(\mathbf{r},t) \end{aligned} \tag{4.2}$$

which is (3.5), and models quantum matter as a purely wave phenomenon, as mentioned in chapter 3. It is possible to use the generalised Schrödinger equation to understand current fluctuations in reverse biased Zener diodes that are driven by fluctuations in space. Figure 4.14 shows the operating voltage and energy levels for electrons at the *pn* junction of a Zener diode. The current when operated in reverse biased mode only occurs due to quantum tunneling, and is very small. One can consider wave packet solutions to (4.2) applicable to the situation shown in figure 4.14, using a complete set of plane waves,

$$\psi(\mathbf{r},t) = \int \psi(\mathbf{k},\omega)e^{i(\mathbf{k}\cdot\mathbf{r}-\omega t)}d^3\mathbf{k}d\omega. \tag{4.3}$$

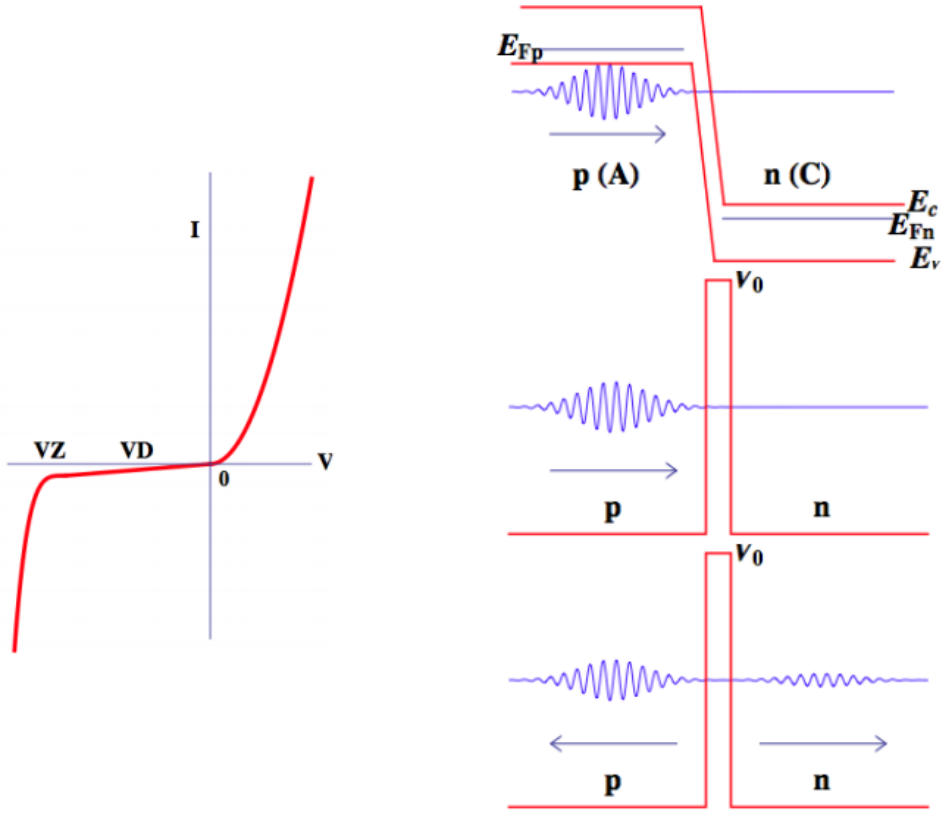

Figure 4.14: (Left) Current-Voltage (VI) characteristic plot for a Zener diode. In this study $VZ = -3.3$ V is the Zener diode, and $VD = -1.5$ V is the operating voltage used (AA Battery). The reverse bias region is when $V < 0$, and produces a small tunneling current when operated near voltage VD. (Right) Top: Schematic of an electron incident on a *pn* junction of a Zener diode in reverse bias mode. The electron travels from the anode (A) to the cathode (C) as labelled in figure 4.3, E_c is the bottom of the conduction band, E_ν is the top of the valence band, and E_{F_p} and E_{F_n} are the respective Fermi levels. No states are available in the depletion region. Middle/Bottom: Schematic of electron wavepacket incident on a Zener diode *pn* junction in reverse bias mode. Note the reflected and transmitted components after electron tunneling through the potential barrier with height V_0. Image source from figures 2 and 3 of [84].

These solutions would be applicable to not only the electrons in the current but also for the Zener diode as an individual quantum system itself, with resultant wavenumbers $\mathbf{k}$ for the diode being much larger than that of electrons. Provided we can approximate the 3-space velocity $\mathbf{v}(\mathbf{r}, t)$ as a constant over a short distance and time, the space driven term added to the generalised Schrödinger equation then mainly contributes the term $\hbar\mathbf{v} \cdot \mathbf{k}$ to the equations for $\psi(\mathbf{k}, \omega)$. This effectively results in space fluctuations driving the change in the potential barrier height of the Zener diode, $V_0 \to V_0 + \hbar\mathbf{v} \cdot \mathbf{k}$. The barrier height change then alters the

quantum tunneling amplitude, $T(V_0 - E) \rightarrow T(V_0 + \hbar \mathbf{v} \cdot \mathbf{k} - E)$ where E is the electron's energy, and which changes the Zener diode current. Notice that the current fluctuations would then be very sensitive to fluctuations in space.

The correlations in Zener diode data found by Cahill marked a major discovery regarding the current interpretations of quantum theory, and implied a need for its reinterpretation in terms of a fractal and dynamical space, and not the Euclidean embedding space solely used for position labelling. Quantum theory can predict the transition amplitude $T(V_0 - E)$, with $|T|^2 i$ giving the average Zener diode current (i is the current at the *pn* junction). Quantum theory however contains no randomness nor probabilities, i.e. the Schrödinger equation is purely deterministic and does not describe the localisation of quantum matter when measured. For example, in figure 4.14, the middle and bottom schematics depict an electron wavefunction $\psi(\mathbf{r}, t)$ becoming delocalised around a potential barrier, and has now evolved to the superposition $\psi_r(\mathbf{r}, t) + \psi_t(\mathbf{r}, t)$, the reflected and transmitted electron components respectively. Such an electron in a delocalised state when interacting with a detector, i.e. a system in a metastable state, would put the combined system in a delocalised state which is then observed to localise. The detector records an event at one location, but for which quantum theory can only provide the expected average distribution, i.e. in this case $||\psi_r(\mathbf{r}, t)||^2$ and $||\psi_t(\mathbf{r}, t)||^2$ for reflected and transmitted photons respectively. The theory is however unable to make predictions as to the fluctuations that lead to these observed averages. Interpretations of the Schrödinger equation from an *ad hoc* probability viewpoint such as the Born metarule and Copenhagen interpretation ultimately demand that measurements are completely random. This is because the probability of detection events are intrinsic to individual quantum systems, but this is false from the reported correlations in Zener diode data sets. *Process Physics* suggests that delocalised states become localised through interaction with the dynamical space, and that the variations in detections are produced by fluctuations in space

itself, which would be observed in quantum processes. This is achieved simply by the addition of a dynamical space component to the Schrödinger equation, as discussed here.

4.5 Interpretation of the Shnoll Effect

The nonrandom processes and correlations discovered by Shnoll are similar examples of the effect explained above. Alpha decay for example, involves the Coulomb repulsion between an α particle and its nucleus generating a potential energy barrier that the α wavepacket then tunnels through.[110] The distinction here is that the fluctuations in space would affect the potential barrier height of the nucleus more than that of the α particle, thus allowing fluctuations in the radioactive decay rate. Shnoll also reports many correlations and properties of α decay studies, mainly through studying correlations in histogram shapes of 60 - 100 measurements taken in sequence. This was referred to as the Shnoll effect, and is different to studying real time fluctuations in experimental data by instead looking at the collective behaviour of a phenomenon over a small time period (usually a minute).

Absolute time correlation of histogram shapes measured at different geographical locations was observed by Shnoll. Because his results were typically collected over a 60 second period this limits the time resolution of his results. Histograms of α decay rates taken over a 1 second time interval for example should detect the space driven time delay effects observed by Cahill, if the studies were well separated geographically N-S. Histogram shapes of studies separated geographically were also found to correlate with a time delay corresponding to that caused by the rotation of the Earth, i.e. the time taken for Earth to rotate one apparatus to the same longitude that the other apparatus was previously at. These studies are taken using a collimator to allow directional studies. This suggests that radioactive decay is affected by the characteristic space fluctuations flowing in a particular

direction. For example, using no collimator or aiming one E-W will yield local time correlations as it picks up wavefronts travelling past Earth which align in an E-W direction. Aiming a collimator towards the south celestial pole (to detect cosmic flows) or at the Sun (as space flows into massive objects) allows for absolute time histogram correlations instead, as space flows in this approximate direction.

The Shnoll effect manifests itself periodically with respect to both sidereal and solar days and years as well with more subtle periods such as the Sun's synod period and the lunar month. The alignment of the massive objects in the sky is then likely to affect the space fluctuation patterns flowing past Earth in a predictable fashion. For specific cases such as during solar eclipses and to a lesser extent with new moons there exist characteristic histogram shapes which are repeatable and observed mainly in the Global Consciousness Project, which studies the change in XOR gate altered various diode setups in one second intervals. This is likely caused by the existence of filaments forming between the Sun-Earth, Earth-Moon and Sun-Moon combinations, with the filaments aligning during these events, causing space to behave in the Earth's vicinity in a predictable manner. Filaments are predicted in Dynamical 3-Space theory however only single, infinitely straight filaments are predicted in the absence of matter, with numerical solutions required for more complex cases. Modelling the velocity field for a Sun-Earth-Moon environment, and then perturbing the inflow into these massive objects is predicted here to produce both filaments as well as complex reverberations that would evolve as they pass Earth.

For a single radioactive decay study, histogram shapes were found to correlate with those closest in time, i.e. with that of the following histogram generated. This also occurs over a wide range of time scales ranging from 6 hour histograms down to 0.13 ms when studied using germanium semiconductors.[89] Since there is currently no time scale at which the mentioned effect is unobserved it suggests that space is both fractal and evolves over time. This effect was referred to as the

'near zone effect', and is most strongly observed when aiming collimators at the Sun, or without a collimator, suggesting that the evolution of space flowing into the Sun can be detected and characterised. Over 20 different processes display the effects Shnoll observed, including the previously mentioned phenomena but also in photomultiplier dark noise fluctuations, electrophoretic mobility in latex particles, proton relaxation times and neutrino emission fluctuations in the Earth's crust. These processes have energies and fluctuation amplitudes differing in many orders and suggests the ability of space turbulence to affect processes universally. This then allows the study of how space interacts with these phenomena.

4.6 Concluding Remarks about Chapter 4

The data from coaxial cable and Zener diode - gravitational wave experiments display the nonrandom characteristics Shnoll observed previously in radioactivity experiments. It is suggested that these two experiments (along with other work by Shnoll) are caused by the fractal nature of space, together with the reverberation effect from gravitational waves, as predicted by the Dynamical 3-Space theory. Quantum tunneling current fluctuations and alpha decay rates are also suggested to be nonrandom and completely caused by the fractal and dynamical nature of space as it passes by an instrument. Through generalising the Schrödinger equation to contain dynamical space effects one can explain how space can cause the localisation of wavefunctions on either side of a potential energy barrier, thus requiring a reinterpretation of quantum theory. The short term Shnoll effects were also able to be explained in terms of the presence of a dynamical space. Shnoll's extensive research therefore opens up many opportunities to study space dynamics. This work was performed more recently; further studies of the Shnoll effect was limited as it is quite time consuming. The following work is more theory based and is aimed at further developing the Dynamical 3-Space theory.

Chapter 5

Dynamical 3-Space Theory Modification

5.1 Introduction - the Borehole g Anomaly

The Dynamical 3-Space theory, equation (3.1) is phenomenologically based i.e. not derived from theory but instead from experimental data. The only theoretical foundations the model contains is from that suggested by *Process Physics*, and also through generalising Newtonian gravity into an inflow formalism which contains the α and δ space self interaction effects that cannot *a priori* be ignored. As discussed in chapter 2 it has links to the fine structure constant, which is the value $\alpha \approx 1/137$ found from geophysical and astrophysical data which will be discussed throughout this chapter.

Upon checking the application of Dynamical 3-Space theory to the Greenland Ice Shelf borehole data[111] an error was found in the analysis of the results in which the value of α was off by a factor of ten, i.e. $\alpha = 1/13.7$ was required to fit the data using (3.1) and the predictions in table 3.1. It is therefore proposed here that the Dynamical 3-Space theory be modified to include an extra factor of π^2, which

allows α to remain $\approx 1/137$ as in the equation below:

$$\nabla\cdot\left(\frac{\partial \boldsymbol{v}}{\partial t}+(\boldsymbol{v}\cdot\nabla)\boldsymbol{v}\right)+\frac{\pi^2\alpha}{8}\left((trD)^2-tr(D^2)\right)$$
$$+\frac{\delta^2}{8}\nabla^2\left((trD)^2-tr(D^2)\right)+...=-4\pi G\rho,\quad D_{ij}=\frac{\partial v_i}{\partial x_j}. \tag{5.1}$$

This is allowed as the model is phenomenologically based - all that has been modified here is the coefficient of α has been altered from $1/8$ to $\pi^2/8$. The value $\pi^2 = 9.870 \approx 10$ has instead been suggested since the final form of (5.1) is still unknown, and is largely dependent on whether future studies of the *Process Physics* paradigm can derive the Dynamical 3-Space theory in this form. It is also believed that this model is likelier to contain a factor of π^2 than a factor of 10. An alternative for example would be to drop the division of α by 8 instead however this changes α; experimentally α appears to be the fine structure constant $\approx 1/137$, and so historically this model has accommodated for this fact.

The new solutions for the expected gravitational acceleration inside matter are shown in table 5.1. As observed, the gravity residual i.e. the difference between NG and Dynamical 3-Space model predictions for the gravity inside a spherical matter distribution now includes the additional π^2 factor when compared to that in table 3.1. This is required to explain the borehole g anomaly for the Greenland Ice

Table 5.1: New gravitational acceleration solutions inside a spherical matter density (see table 3.1)

Type	**New Solution**
Gravity Inside & Outside Matter	$g(r)=\begin{cases}\frac{\left(1+\frac{\pi^2\alpha}{2}\right)GM}{r^2}\ ,\ r\geq R,\\ \frac{4\pi G}{r^2}\int_0^r\left(\int_s^R s'\rho(s')ds'\right)ds\ ,\ r<R\end{cases}$
	$g(r)=\begin{cases}\frac{G_NM}{R^2}-\frac{2G_NM}{R^3}(r-R)\ ,\ r\geq R\\ \frac{G_NM}{R^2}-\left(\frac{2G_NM}{R^3}-4\pi(1-\frac{\pi^2\alpha}{2})G_N\rho\right)(r-R)\ ,\ r<R\end{cases}$
Gravity Residual	$\triangle g(r)\equiv g_N(r)-g(r)=\begin{cases}0\ ,\ r\geq R\\ 2\pi^3\alpha G_N\rho(r-R)\ ,\ r<R\end{cases}$

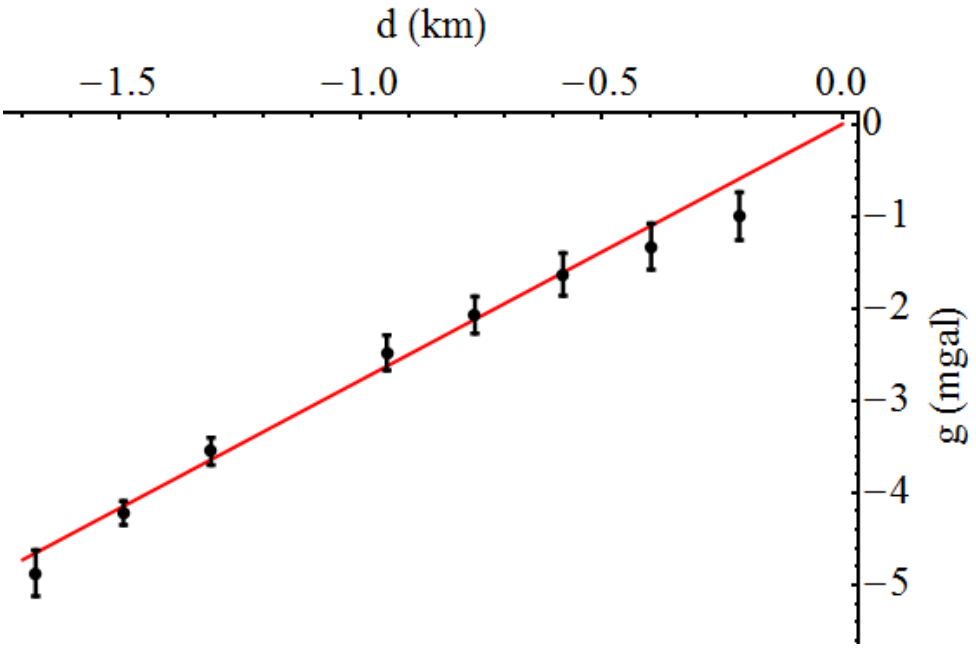

Figure 5.1: The Greenland Ice Shelf borehole g anomaly data, [101] giving $\alpha \approx 1/137$ from fitting the gravity residual $\triangle g(r)$ form in table 5.1. The misfit at shallow depths arises from the ice not having reached the ice-shelf full density, which is a snow compacting effect.

Shelf data, see figure 5.1. A similar result can be applied to the Nevada borehole data.[102, 111]

A redefinition of $G_N \equiv (1 + \pi^2\alpha/2)G$ is also required, since this is the definition of Newton's gravitational constant in [111]. Here G_N implies that a two parameter fit consisting of G and α applies to experiments including studying galaxy dynamics, borehole gravity gradients and also those which determine G experimentally. Newtonian physics only contains the single parameter G_N to base G measurements from. The inflexibility of NG when applied to gravitational studies then yields differing values of G_N with large uncertainties, created as a result of using differing matter density distributions between experiments. These matter distributions would instead need to be modelled using velocity fields (of both test particle and Earth/Sun/galaxy environment) in an effort to then predict the acceleration fields involved. These fields would certainly become non-Newtonian as one deviates from spherical symmetry. This should then allow laboratory Cavendish-type experiments in conjunction with astrophysical data for example to determine

both G and α to high accuracy. The Dynamical 3-Space model predicts that G will be reduced by a factor of $(1+\pi^2\alpha/2) \approx 3.5\%$ than currently reported, and so $G \approx 6.442 * 10^{-11}$ m^3/kg/s^2, using $\alpha = 1/137$. It is important to revisit both the solutions to the Dynamical 3-Space theory as well as any other experimental data that the model has been applied to, in order to check that the theory still holds.

5.2 Methodology

All solutions and figures were plotted using Mathematica version 9.0. The references for all data presented can be found in the figure captions. Generation of the plot fits will be discussed as they are presented. Modelling equation (5.1) in time independent cases was achieved differently for different solutions:

- Spherically symmetric cases involve setting up the x, y and z components of $\mathbf{v}(\mathbf{r}, t)$ (e.g. $\mathbf{v}_x(r) = v(\sqrt{x^2+y^2+z^2})\hat{\mathbf{x}}$ etc.) and then solving (5.1) for $\mathbf{v}(\mathbf{r}, t)$ as $x \to r$, $y \to 0$ and $z \to 0$ for simplicity.

- For filament solutions $\mathbf{v}_x(r) = v(\sqrt{x^2+y^2})\hat{\mathbf{x}}$, $\mathbf{v}_y$ is similar and $\mathbf{v}_z = 0$ to generate cylindrical symmetry - see section 5.3.1 for the new black hole and cosmic filament solutions.

- When $\delta \neq 0$, Mathematica is unable to solve for $v(r)$ directly. In this case substituting $v(r) = \sqrt{f(r)}$ allows Mathematica to retrieve a general solution for $f(r)$ and hence $v(r)^2$ in terms of 2 hypergeometric functions in the form below, after rearranging the solution provided by Mathematica:

$$v(r)^2 = v_0^2 \left(\frac{c_1}{r} + \frac{\delta}{r} \left(\kappa(c_2, c_3) - 1 \right) (1 - A) - \frac{r^2}{\delta^2} \kappa(c_2) X B \right). \tag{5.2}$$

  Here A and B are confluent hypergeometric functions which are part of the solution Mathematica provides. The first term contains a singularity at

$r = 0$ which was removed by setting constant $c_1 = 0$. The strength of the two hypergeometric terms $\frac{\delta}{r}(1 - A)$ and $\frac{r^2}{\delta^2}B$ were related by $\kappa - 1$ and κ which contain constants c_2 and c_3 in their expressions. By taking the ratio $\frac{\kappa-1}{\kappa}$ and setting $c_3 = 0$ the remainder X was found, which then relates the two hypergeometric terms together, the structure which can be changed by varying κ. See section 5.3.3 for the new black hole $\delta \neq 0$ solutions.

- The new solutions for $g(r)$ are all related by $g(r) = \frac{1}{2}\frac{d}{dr}v(r)^2$, see equation (3.11) in section 3.6.1.

- In the case of spherically symmetric and time dependent Hubble solutions, $\mathbf{v}(\mathbf{r}, t) = H(t)\mathbf{r} = H(t)\sqrt{x^2 + y^2 + z^2}$ and then solving for $H(t)$ as $x \to r$, $y \to 0$ and $z \to 0$ for simplicity.

5.3 Revisiting Predictions and Experimental Data

5.3.1 Spatial Flow $(\alpha \neq 0, \delta = 0, \rho = 0)$ Effects

The primordial black hole solutions shown in equation (3.11) now instead have the following characteristics shown in table 5.2. At long range $v(r)$ still behaves like a constant as indicated by the $1/r^{\alpha\pi^2/4}$ term and $\alpha \approx 1/137$. As shown in figure 5.2a this new inflow is weaker than a $v(r) \propto 1/r^{\alpha/4}$ strength BH at the same distance r from a BH. At a distance of our solar system 8 kpc from the Milky Way black hole, the predicted inflow speed is some 47% weaker then previously predicted. The acceleration of space now instead appears stronger for all r due to the presence of π^2 in the new solutions. Due to the new $g(r) \propto 1/r^{1+\alpha\pi^2/2}$ dependence of $g(r)$ on r, the relative strength of the new black holes when compared to the previous $g(r) \propto 1/r^{1+\alpha/2}$ dependence decreases with distance, as shown in figure 5.2b. At

Table 5.2: New Dynamical 3-Space black hole and filament solutions for long range $\alpha \neq 0, \delta = 0, \rho = 0$

BH Property	**Eqn. Ref.**	**New Solution**
3-Space Velocity	(3.11)	$v(r) = -\frac{\beta}{r^{\alpha\pi^2/4}}$
3-Space Gravity	(3.11)	$g(r) = -\frac{\alpha\pi^2\beta^2}{4r^{1+\alpha\pi^2/2}}$
Dark Matter Density	(3.12)	$\rho_{DM}(r) = -\frac{\alpha\pi\beta^2(2-\pi^2\alpha)}{256Gr^{2+\alpha\pi^2/2}}$
Matter Orbital Velocity	(3.13)	$v_O(r) = \frac{\pi\alpha^{1/2}\beta}{2r^{\alpha\pi^2/4}}$
	(3.15)	$v_O(r) = \frac{K}{2}\left(\frac{1}{r} + \frac{\pi^2\alpha}{2R_s}\left(\frac{R_s}{r}\right)^{\pi^2\alpha/2}\right)^{1/2}$
Filament Property		
3-Space Velocity	(3.16)	$v(r) = -\frac{\mu}{r^{\alpha\pi^2/8}}$
3-Space Gravity	(3.16)	$g(r) = -\frac{\alpha\pi^2\mu^2}{8r^{1+\alpha\pi^2/4}}$
Dark Matter Density	(3.16)	$\rho_{DM}(r) = -\frac{\alpha\pi\mu^2}{1024Gr^{2+\alpha\pi^2/4}}$

the Solar System - Milky Way BH distance of 8 kpc, $g(r)$ is now predicted to be 2.15 times stronger than predicted by the previous solutions.

The orbital velocity of an object around a black hole is affected in an interesting manner - figure 5.3 shows the NGC3198 spiral galaxy rotation curve data. In GR these plots are typically predicted by a universal rotation curve empirically determined by Persic, Salucci and Stel;[112]

$$v_O(x) = v(R_{opt})\left[\gamma\frac{1.97x^{1.22}}{(x^2+0.78^2)^{1.43}} + 1.6e^{-0.4(L/L_*)}\frac{x^2}{x^2+1.5^2\left(\frac{L}{L_*}\right)^{0.4}}\right]^{1/2} \tag{5.3}$$

where $\gamma = \left(0.72 + 0.44\log\frac{L}{L_*}\right)$, $x = r/R_{opt}$ where R_{opt} is the optical radius, i.e. 83% of the matter limit and $L/L*$ is mass to light ratio. The first term is the Newtonian contribution from an exponential matter disk and controls the initial upper slope of the generated rotation curve, which then drops off rapidly as shown

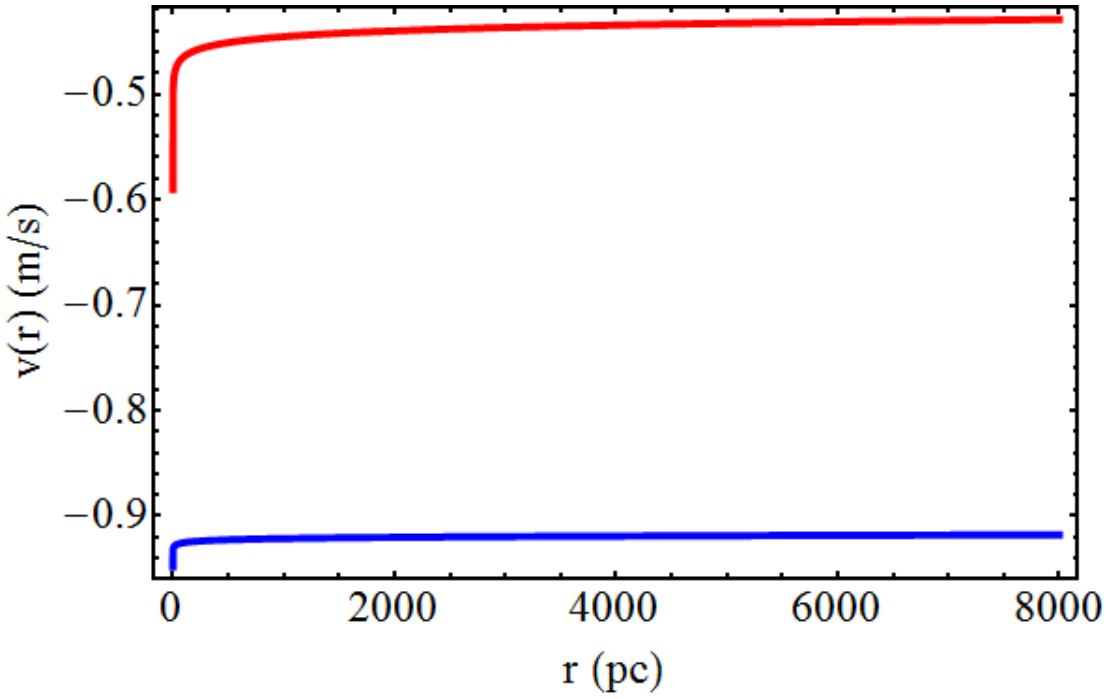

(a) Velocity profile

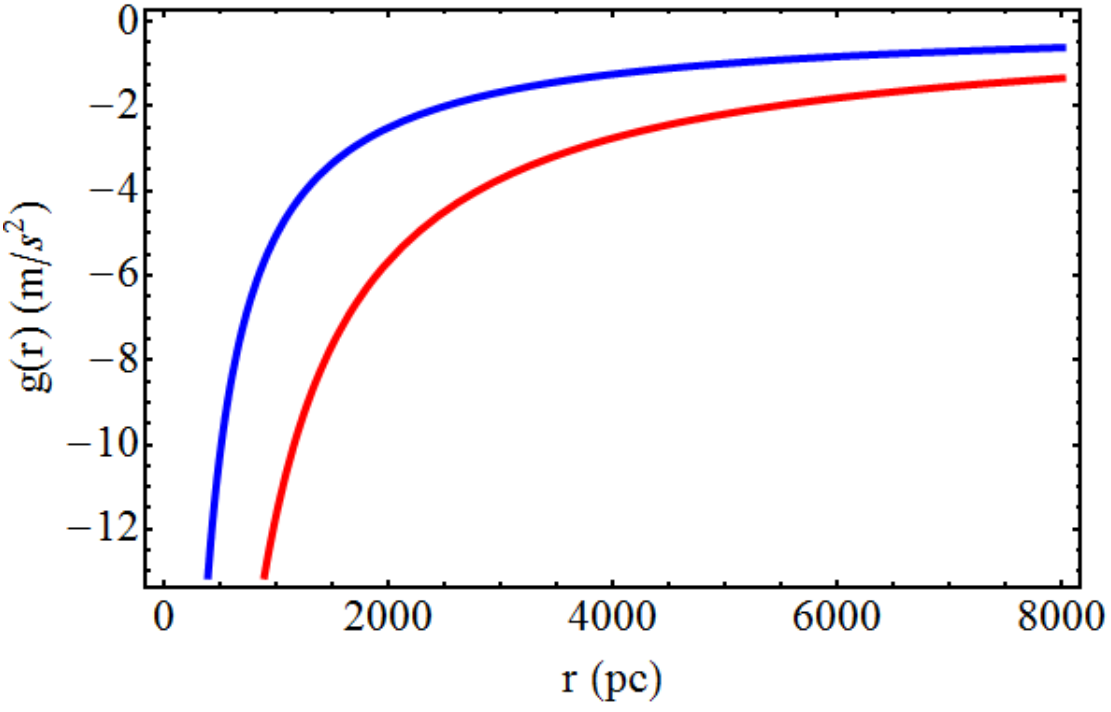

(b) Acceleration profile

Figure 5.2: Inflow velocity (a) and acceleration (b) profiles for black holes predicted by the previous (blue) and modified (red) Dynamical 3-Space theory. Here the black hole strength $\beta = 1$ for the velocity profile and $\beta = 3.16 * 10^{11}$ for y axis aesthetics only.

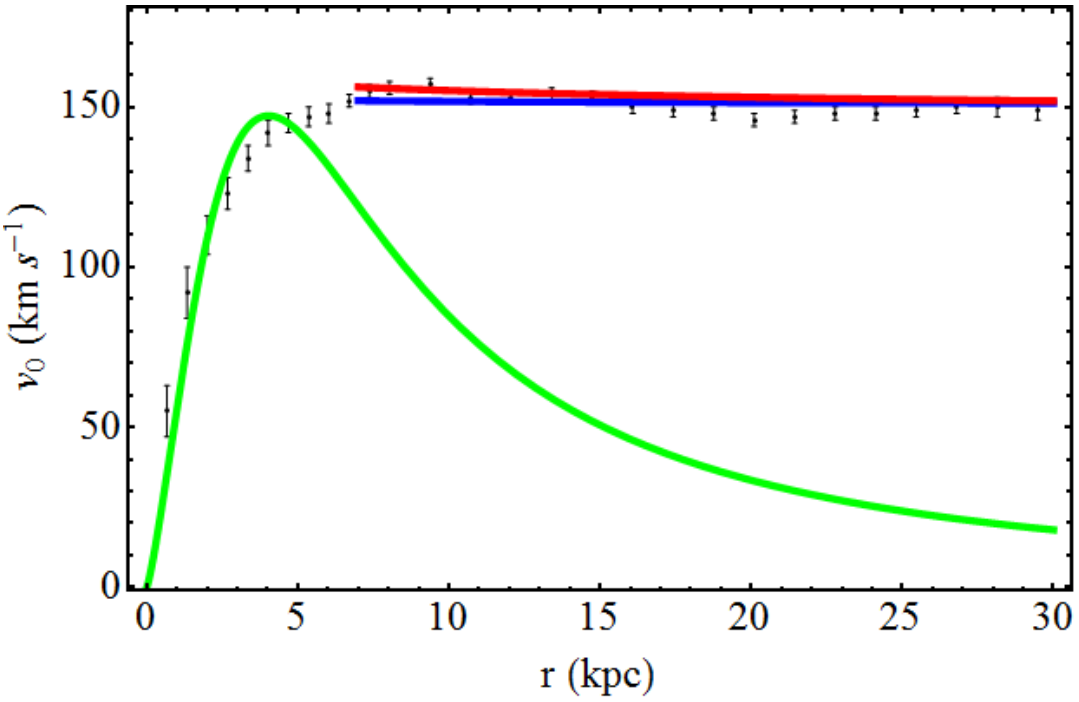

Figure 5.3: Spiral galaxy rotation curve for the NGC3198 data.[113] Green plot is best fit by Newtonian Gravity, blue plot is the former Dynamical 3-Space theory fit for $\beta = 3550$ and red plot is for the modified version and $\beta = 1165$.

by the green plot in figure 5.3. The second term is the 'dark matter' contribution, which generates a flat asymptotic region sufficiently far away from the centre of a galaxy and is required to explain the flat outer arms of the rotation curves. To generate the asymptotic regions of the data using Dynamical 3-Space theory the second 'dark matter' term in (5.3) was replaced with the expression for v_O shown in table 5.2 to produce the following

$$v_O(x) = \left[260 \frac{x^{1.22}}{(x^2 + 0.78^2)^{1.43}} + \left(\frac{\pi \alpha^{1/2} \beta}{2x^{\alpha\pi^2/4}} \right)^2 \right]^{1/2}. \tag{5.4}$$

This then mimics the dark matter effects required by NG, but where the effects are purely space self interactions, and require no actual matter. Alternatively the two parameter analytic solution for v_O in terms of K and R_S in table 5.2 could be used to generate a similar result. The predictions of the rotation curves made by Dynamical 3-Space theory are asymptotic only. This means that they are only able to account for the outer regions of the spiral galaxy data, as they

are solutions containing only the long range α effects of black holes, which have an inflow singularity. The rotation curve solution to (5.1) when also accounting for both nonzero α and δ are unknown, i.e. when accounting for both long and short range inflow effects. As the inflow speeds for these black hole solutions (see table 5.3) decrease smoothly to zero as $r \to 0$ this then suggests that the predicted rotation curves will also decrease to zero as $r \to 0$. The red orbital velocity plot was obtained using (5.4) with black hole strength $\beta = 1165$, and the blue plot is that when substituting the previous expression for v_O, namely equation (3.13) into the dark matter expression in (5.3), using $\beta = 3350$. The previous orbital velocity prediction by the Dynamical 3-space model (blue plot) shows very flat rotation curves. The velocities in the NGC3198 spiral galaxy curve however appear to slowly decrease with distance which is arguably better represented by the new 3-space solutions in table 5.2, see the red plot, since the orbital speeds drop off more slowly with distance as suggested by [112]. The NGC3198 black hole is predicted to be 67% weaker than previously predicted, as shown by the difference in BH strength parameters β used between previous and modified orbital velocity solutions.

5.3.2 The 'Dark Matter' Effect

In the case for the effective 'dark matter' density, i.e. the space self interaction effects, equation (3.3) now becomes

$$\rho_{DM}(\boldsymbol{r}, t) \equiv \frac{\pi\alpha}{32G}\left((trD)^2 - tr(D^2)\right) + \frac{\delta^2}{4\pi G}\nabla^2\left((trD)^2 - tr(D^2)\right) \tag{5.5}$$

and so the effective dark matter effects observed are at most π^2 times stronger than predicted by the previous Dynamical 3-Space equation. Figure 5.4 shows the dark matter profile predicted for the black hole inflows generated, (for $\delta \neq 0$) and they

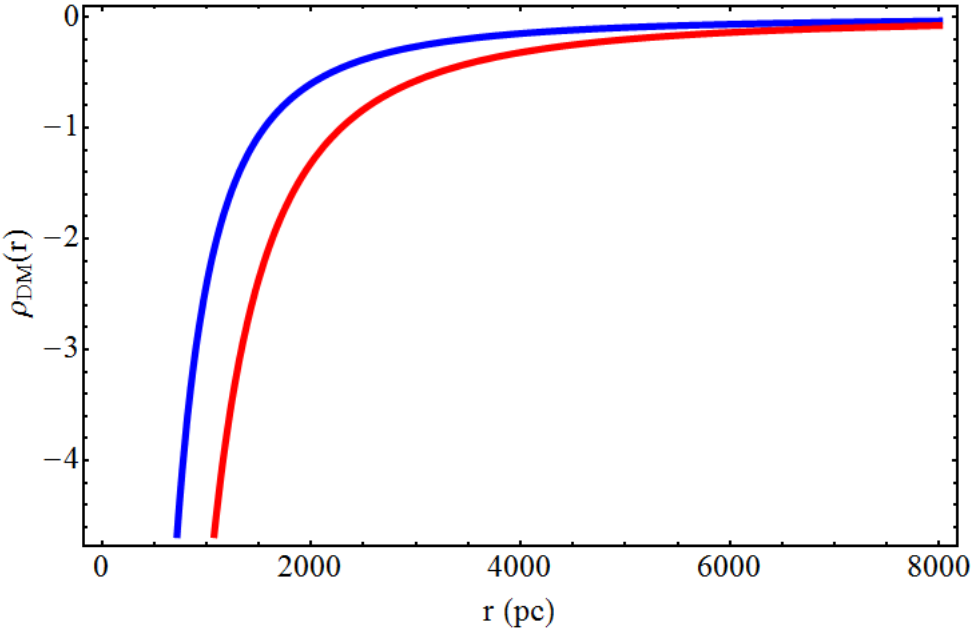

Figure 5.4: Dark matter density profiles for black holes predicted by the previous (blue) and modified (red) Dynamical 3-space theory. Here the black hole strength $\beta = 10^{17}$ is purely for y axis aesthetics.

show that ρ_{DM} is indeed stronger than previously predicted. The decrease is still approximately $1/r^2$ as determined by the 'dark matter' interpretation of the flat rotation curves of galaxies. Here it is still purely a space self interaction effect. The dark matter density at 8 kpc away from a black hole is estimated to be twice than that previously predicted. Figure 5.5 illustrates that for globular clusters and spherical galaxies the observational data implies the relationship $M_{BH} = \frac{\alpha}{2}M$, where M_{BH} is the apparent black hole mass and M is the mass of the star system. Here the α- dynamics appear to be the cause of this result, and would imply that the minimal black hole strength induced by the system is proportional to its mass. This relationship is yet to be derived from the Dynamical 3-Space theory however it now predicts a relationship between the dark matter mass M_{DM} of a black hole and its observable mass to be

$$M_{DM} = 4\pi \int_0^\infty r^2 \rho_{DM}(r) dr = 5\alpha M + O(\alpha^2) \tag{5.6}$$

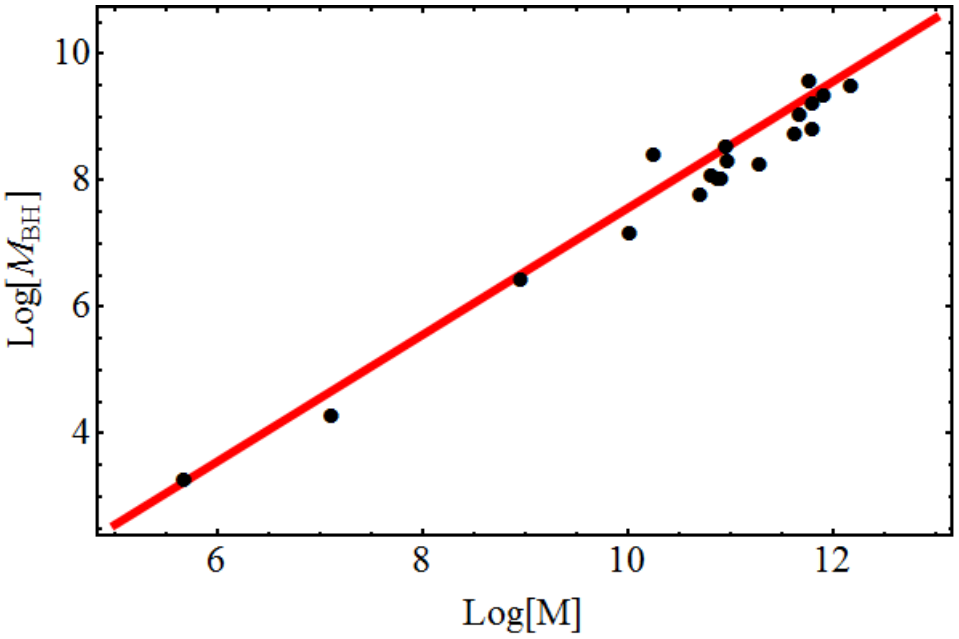

Figure 5.5: Black hole masses M_{BH} vs mass M, in solar masses, for globular clusters M15 and G1, and spherical galaxies.[114] The straight line is the relation $M_{BH} = \frac{\alpha}{2}M$ with $\alpha \approx 1/137$.

for a spherical galaxy. Dynamical 3-Space theory currently defines $M_{DM} = M_{BH}$ although there is no derivation of this; it is only conjecture. For any spherical matter distribution this result will still apply, meaning that planets and stars also contain an inflow singularity at their centre. This affects the effective mass of planets and hence their gravity profiles such as what the borehole data suggests. As backed up by the spherical galaxy data the minimal BH effects become more prominent in larger star systems.

The 3-space velocity, gravity and effective dark matter density solutions for the new filaments are also mentioned in table 5.2. All of the characteristics essentially display similar behaviour to that of the black holes mentioned, and are so not required to be discussed any further.

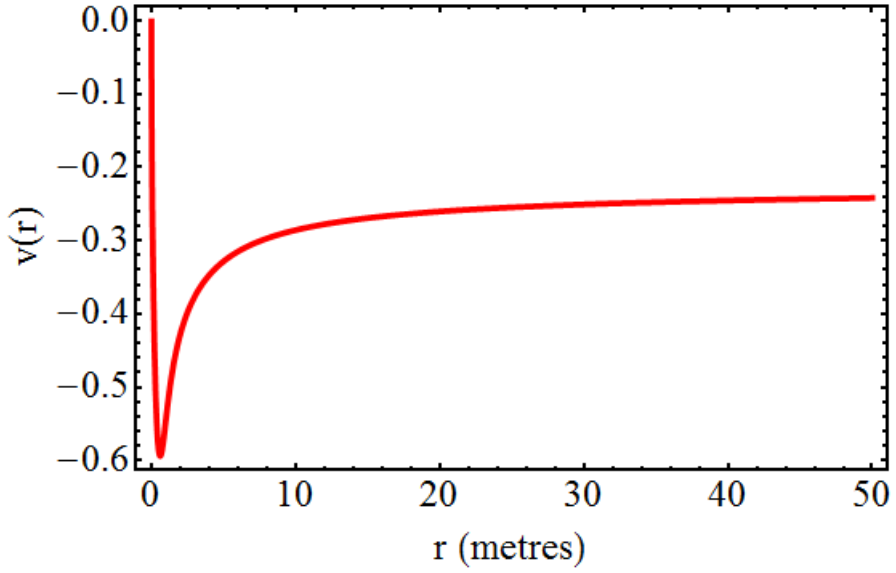

Figure 5.6: Black hole velocity profile for the full Dynamical 3-Space model for $\alpha \neq 0$ and $\delta \neq 0$, with the inflow speed smoothly reducing to zero at the centre. Here $\delta = 0.5$ as Mathematica is unable to accurately determine hypergeometric calculation for very small δ due to underflow problems.

5.3.3 Spatial Flow ($\delta \neq 0, \rho = 0$) Effects and the SgrA* BH Data

Table 5.3 shows a summary of the new solutions to the full Dynamical 3-Space theory, i.e. equation (5.1) for $\delta \neq 0$. Both the black hole and filament solutions still contain hypergeometric functions as expected. The parameter v_0 sets the BH/filament inflow strength and κ sets the structure of the BH by adjusting the relative strength of the two hypergeometric terms present. As before, at large distances $r \gg \delta$ the inflow increases as $v(r)^2 \approx A\frac{\delta}{r} + B\left(\frac{\delta}{r}\right)^{\alpha\pi^2/2}$. The solutions are still well behaved however, and $v(r) \to 0$ as $r \to 0$, as shown in figure 5.6, therefore removing the singularity at the centre. The δ self interaction effects have a characteristic radius of $O(\delta)$, which act as to self regulate the interior structure of the BH and filaments. The new BH velocity profiles are still a generalisation of that in table 5.2, and so from (3.7) i.e. the gravitational acceleration of matter

Table 5.3: New Dynamical 3-Space theory solutions for $\alpha \neq 0, \delta \neq 0$ and $\rho = 0$.

Property	Eqn. Ref.	New Solution
BHs	(3.18)	$v(r)^2 = v_0^2(\kappa - 1)\frac{\delta}{r}\left(1 - {}_1F_1\left[\frac{-2+\pi^2\alpha}{4}, -\frac{1}{2}, -\frac{r^2}{\delta^2}\right]\right)$ $-v_0^2\kappa\frac{8}{3}\frac{r^2}{\delta^2}\frac{\Gamma(\frac{6-\pi^2\alpha}{4})}{\Gamma(\frac{-\pi^2\alpha}{4})}{}_1F_1\left[1 + \frac{\pi^2\alpha}{4}, \frac{5}{2}, -\frac{r^2}{\delta^2}\right]$
	(3.19)	$v(r)^2 \approx A\frac{\delta}{r} + B\left(\frac{\delta}{r}\right)^{\pi^2\alpha/2} \quad , \quad r \gg \delta$
Eff. BH Mass	(3.20)	$M(r) = M_0 + M_0(\frac{r}{r_s})^{1-\pi^2\alpha/2}$
Orbital Velocity	(3.21)	$v_{orb}(r)^2 = GM_0(\frac{r_s}{r})^{\pi^2\alpha/2}\frac{1}{r_s} \quad , \quad r \gg \delta$
Filaments	(3.22)	$v(r)^2 = v_0^2\frac{r^2}{\delta^2}{}_1F_1\left[1 + \frac{\pi^2\alpha}{8}, 2, -\frac{r^2}{4\delta^2}\right]$

this then gives $g(r) = GM(r)/r^2$, where $M(r)$ defines an 'effective mass',

$$M(r) = M_0 + M_0\left(\frac{r}{r_s}\right)^{1-\pi^2\alpha} \tag{5.7}$$

where r_s is the distance where $M(r_s) = 2M_0$. This 'effective mass' mimics the amount of matter enclosed within radius r outside a black hole, however this is now completely induced by space interaction effects, and does not contain any actual matter.

Equation (5.7) can be used to test whether these space interactions can account for the increasing matter density outside the SgrA* supermassive black hole at the centre of our Milky Way galaxy. This is achieved by creating an effective mass density function $M(r, \kappa, \alpha, \delta)$ then finding the best fit for κ, α and δ via comparison with the SgrA* mass data. Firstly note that the following equality holds

$$g(r) = -\frac{GM}{r^2} = \nabla\frac{v(r)^2}{2} \tag{5.8}$$

where $v(r)$ is the BH solution shown in table 5.3. An effective matter density can

then be defined in terms of the 3-space inflow velocity, radius and the gravitational constant G, i.e.

$$M(r) = -\frac{r^2}{2GM_\odot}\nabla v(r)^2 \tag{5.9}$$

which is in terms of solar masses $M_\odot$. The form for $v(r)^2$ shown in table 5.3 was written in a different form, namely $v(r)^2 = v_0^2 h(r)$ where $h(r)$ is a function including the entire remaining $(\kappa - 1)\frac{\delta}{r}(1 - {}_1F_1....)$ terms. Then (5.9) becomes

$$M(r) = M(r, \kappa, \alpha, \delta) = -\frac{r^2}{2GM_\odot}\frac{v(r_\infty)^2}{h(r_\infty, \kappa, \alpha, \delta)}\nabla\frac{v(r, \kappa, \alpha, \delta)^2}{v_0^2} \tag{5.10}$$

where r_∞ is an asymptotic value in relation to the SgrA* data, and here was taken to be 30 kpc, as the Milky Way's radius is 15 - 25 kpc. Here the presence of $v(r_\infty)/h(r_\infty) = v_0^2$ not only maintains the equality but allows the estimation of an asymptotic orbital speed $v(r_\infty) \approx v_{orb}(r)$ using the expression for the asymptotic velocity $v_{orb}(r)^2 = GM_0(\frac{r_s}{r})^{\pi^2\alpha/2}\frac{1}{r_s}$ in table 5.3. Here r_s is the distance where $M(r_s) = 2M_0 \approx 1$ pc as estimated from the SgrA* enclosed data shown in figure 5.7, and $\alpha = 1/137$ (only used here to determine an initial velocity of 105 km/s to assist the best fit calculation). The best fit between equation (5.10) and the SgrA* data was determined for κ, α and δ although the last value is unnecessary and only aids Mathematica in generating the fit to the data. These values along with the SgrA* data is shown in figure 5.7, and the source data is tabulated in table 5.4. Observed is that the best fit prediction of (5.10) for the modified Dynamical 3-Space model (red curve) matches that of the previous model, equation (3.20) (blue curve, barely visible) while the predicted $\alpha^{-1} = 144.0$ is only 5% higher than the expected value of 137. The gradual increase of $M(r)$ at the outer data points wrt the form predicted by (5.9) is presumably due to actual matter having an additional effect on the enclosed mass data, whereas (5.9) is a prediction for $\rho = 0$. The best fit for M_0 as observed in figure 5.7 is $4.21 \times 10^6 M_\odot$, is in good agreement with the $4.31 \pm 0.36 \times 10^6 M_\odot$ predicted by Gillessen *et al.*[115]

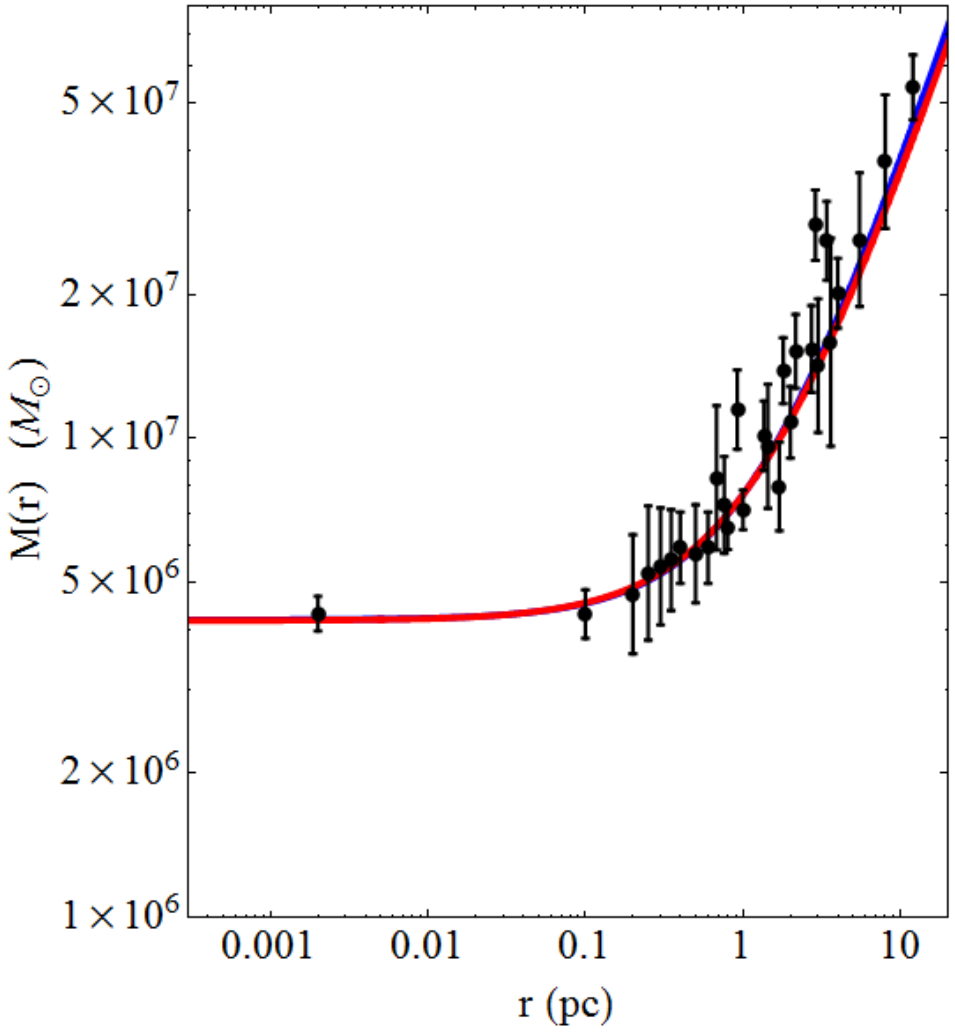

Figure 5.7: Effective mass data $M(r)$ for the Milky Way SgrA* black hole, from star and gas cloud orbital data, showing the flat regime that mimics a pointlike mass but for which there is no actual matter contained within the black hole, and the linearly rising form beyond r_s =1.33pc, as predicted by old (blue curve, see eq. (3.20) for best fit $\alpha^{-1} = 131.2$, $\kappa = 3.657$ and $\delta = 0.00001214$ and new (red curve, see $M(r)$ equation in table 5.3) for $\alpha^{-1} = 144.0$, $\kappa = 70.28$ and $\delta = 0.00002483$ but which is usually attributed to a constant 'dark matter' density. This form is a direct consequence of the 3-space self interactions in (5.1). Figure sources are shown in table 5.4.

Table 5.4: Enclosed mass distribution for the SgrA* Milky Way black hole, for a black hole mass predicted by Gillessen *et al.* of $4.31 \pm 0.36 \times 10^6 M_\odot$. All data sets apart from Beloborodov *et al.* were required to be scaled up by a factor of $4.31/2.5 = 1.7$. This is presumed to be due to these data sets fitting to a then predicted smaller initial $M_0 = 2.5 \times 10^6 M_\odot$ value, the scaling which then matches that of the prediction by Gillessen *et al.*

Data Source	r (pc)	$M(10^6 M_\odot)$	$\pm$ $(10^6 M_\odot)$
Gillessen *et al.* (2009)[115]	0.002	4.31	0.36
Beloborodov *et al.* (2006)[116]	0.1	4.3	0.5
Table 10 of Genzel *et al.* (1996)[117]	0.2	4.73	1.35
	0.25	5.24	1.69
	0.3	5.41	1.52
	0.35	5.58	1.35
	0.4	5.92	1.01
	0.5	5.75	1.35
	0.6	5.92	1.01
	0.8	6.51	0.68
	1	7.1	0.68
	2	10.82	1.86
	4	20.11	3.38
	12	54.09	8.45
Table 3 of McGinn *et al.* (1989)[118]	0.68	8.28	2.87
	0.76	7.27	1.69
	0.92	11.49	2.2
	1.36	10.14	1.69
	1.44	9.63	2.87
	1.8	13.86	2.2
	2.16	15.21	2.7
	2.72	15.38	3.21
	2.88	27.89	4.73
	3.4	25.86	4.9
	3.6	15.89	7.94
See abstract, figure 9 of Serabyn *et al.* (1986)[119]	3	14.2	4.56
	5.5	26.03	8.37
	8	37.86	12.17
Serabyn & Lacy (1985)[120]	1.7	7.94	1.69

The modified Dynamical 3-Space model therefore is still able to account for the Milky Way black hole mass data. Determining the contribution of the black hole inflow speed at the distance of our solar system, $r = 8$ kpc is required. Using (5.7) and the predicted flat rotation curve v_{orb} equation shown in table 5.3, r_s (defined as the point where $M(r_s) = 2M_0$) is 1.17 pc, using $\alpha^{-1} = 144.0$. This then yields $v_{orb} = 103$ km/s, which is 88% that of 117 km/s from the previous prediction.[52] Forcing $\alpha^{-1} = 137$ instead yields $r_s = 1.08$ pc and $v_{orb} = 106$ km/s, as a comparison, and so small changes in the α effects do not have huge impacts on the asymptotic inflow speeds.

As was discussed in [52], both α and δ are required to be nonzero in order for $M(r)$ to produce the flat and rising features observed in the SgrA* data in figure 5.7. If $\alpha = 0$ then the curve remains flat and does not rise, whereas if $\delta = 0$ then asymptotically the rising feature persists but does not become flat at smaller r. The δ- dynamics, i.e. the space self interactions close to the centre/interior of black holes are thus responsible for emitting an effective pointlike mass behaviour for a black hole although there is no actual matter present. With $\delta = 0$ the black hole effect is still apparent, but with $g(r) \propto 1/r^{1+\alpha\pi^2/2}$ which does not agree with the motion of inner star elliptical orbits found near the Milky Way's centre. For any value of δ used in $M(r)$ it is found that v_0 and κ rescale to give exactly the same plot, suggesting that δ must be small but nonzero, suggestive of a structure to space at the fundamental Planck length scale.

5.3.4 Universe Expansion

The new expanding universe solutions obtained from the modified Dynamical 3-Space theory, equation (5.1) are

$$H(t) = \frac{1}{\left(1 + \frac{\pi^2\alpha}{4}\right) t} \quad , \quad a(t) = \left(\frac{t}{t_0}\right)^{1/(1+\frac{\pi^2\alpha}{4})} . \tag{5.11}$$

Due to the low value of $\pi^2\alpha/4$, $H(t)$ still predicts a uniform expansion rate, and is still parameter free, i.e. does not require matter, let alone dark matter nor dark energy to explain its expansion. There are more implications of this result in which chapters 6 and 7 will further elaborate on, along with applying (5.11) to the type 1a supernova data to show that the new solution still predicts a uniform expansion in the same manner as the old solution. Because a uniform expansion is predicted, (5.11) gives the age of the universe as 13.7 Gyr, the same as that for the Newtonian and General Relativity models. Solutions for cosmic inflation will also be shown and discussed in the following chapter.

5.4 Concluding Remarks about Chapter 5

The inclusion of the π^2 factor into the α- terms of the Dynamical 3-Space theory alters all of the known solutions and mainly produces weaker black holes and filaments but which still maintain approximate long range $g(r) \propto 1/r$ effects which NG/GR cannot produce. These new solutions still have the necessary properties required to explain the shown astrophysical (and cosmological data - see chapter 6) and geophysical data, at least from a long range viewpoint. While the model still accounts for the effective black hole mass dynamics from the SgrA* Milky Way BH data at any scale, it has yet to still explain spiral galaxy rotation for stars closer to the centre of the galaxy. There is also still work to be achieved with for example the spherical galaxy and globular cluster data, in deriving the relationship between effective dark matter density with the observed black hole mass. The following chapter studies the application of the Dynamical 3-Space theory and its modification to the type 1a supernova data in more depth to show that this is too unaffected by the modification, and also to show that the supernova data alone suggests that the universe is expanding uniformly.

Chapter 6

Discovery of Uniformly Expanding Universe

6.1 Introduction

The major task in cosmology is to determine how the universe expands over time. The time evolution of the scale factor $a(t)$, i.e. the relative size of the universe at time t is then determined observationally through measurement of type 1a supernovae,[21, 22] and it is a simple process to extract $a(t)$ from that data. A secondary process is to then test different dynamical theories of the universe against that data. However this did not happen, and not for the first time in the history of astronomy was one predetermined theory forced onto the data fitting. The Babylonian planetary orbit data for example, was fitted using Ptolemy's geocentric model of the solar system. This required, and correctly so, that the orbits have epicycle components. When the heliocentric model replaced the geocentric model after roughly 1400 years, the epicycle phenomenon then vanished - it was merely an artifact of the incorrect geocentric model. Analysing the supernova data through the use of NG and GR has already lead to the introduction of the 'dark matter'

and 'dark energy' parameters. A third prediction is that of the future exponential acceleration of the universe, and so it appears that a similar confusion of data and model has happened in physics, as will be discussed here. Either NG or GR can be used to construct the Friedmann equation used to analyse the supernova data. This is because GR was constructed as a generalisation of NG, and reduces to NG in the limit of low matter speeds and densities. Here this chapter[121] shows in a few simple steps how a model independent result, and then the Dynamical 3-Space theory, both predict a uniformly expanding universe, and so dispenses with the 'dark matter' and 'dark energy' artifacts required by the Friedmann equation. This is in fact a major outcome of the observations of supernova events, and needs to be understood.

6.2 Methodology

6.2.1 Type 1a Supernova Magnitude-Redshift Data

The type 1a supernova data and fits were plotted using Mathematica 9.0. The data sets were taken from the ESSENCE data set, table 9 of [122] using only the supernovae that passed the light-curve-fit quality criteria and the HST data, table 6 of [123] using only the 'high confidence' supernovae classified as 'gold'. All models were plotted using the generic relationship between magnitude $\mu(z)$ and redshift z observables, namely

$$d_L(z) = (1+z)\int_0^z \frac{H_0 dz'}{H(z')} \tag{6.1}$$

and

$$\mu(z) = 5\log_{10} d_L(z) + m \tag{6.2}$$

where $m = 43.4$ and $d_L(z)$ is the dimensionless luminosity effective distance, or the 'Hubble-constant-free' luminosity distance as defined by Perlmutter.[21] The Hubble equation in terms of redshift z is defined as

$$H(z) = H_0\sqrt{\Omega_M(1+z)^3 + \Omega^\Lambda + \Omega_s(1+z)^{2+\alpha\pi^2/2}} \tag{6.3}$$

where H_0 is the Hubble constant, $\alpha = 1/137$ and the density parameters for dark energy Ω_Λ, matter/dark matter Ω_M, and space Ω_s (the radiation matter density here is negligible and not included for simplicity's sake) are related by

$$\Omega_\Lambda = 1 - (\Omega_M + \Omega_s)\,. \tag{6.4}$$

The parameters used for each of the plots is shown in table 6.1. The space parameter in (6.3) and (6.4) appears as a constant of integration in the Dynamical 3-Space model.[49] The derivation is equivalent to that from using the Friedmann equation to derive the NG/GR based Hubble equation, which contains a curvature integration constant.

Table 6.1: Density parameters used for the type 1a supernova magnitude-redshift plot shown in figure 6.1.

Plot	Ω_M	Ω_s	Ω_Λ
Dynamical 3-Space (Red)	0	1	0
Dark Matter Only (Black)	1	0	0
Dark Energy Only (Green)	0	0	1
NG/GR Best fit (Blue)	0.27	0	0.73

6.2.2 CMB Data

The actual data used for the Cosmic Microwave Background (CMB) angular power spectrum was taken from [124] and the resultant power spectrum is exactly that

shown in figure 1 of [35]. The July 2011 version of the Code for Anisotropies in the Microwave Background (CAMB) program was used to generate CMB power spectra predictions along with the use of version 1.5 of RECFAST, a model used to calculate the recombination history of hydrogen, helium and lithium throughout the universe's expansion. The 6 parameters used in CAMB for spectra calculation were obtained from Table 3 of [35] and also shown here in table 6.2. The 6 parameters were fixed, and Ω_Λ was then taken to be 0.0, 0.7331 and 1.0 to show the effects of varying the dark energy parameter on the CMB power spectrum.

Table 6.2: CAMB parameters used to generate the CMB angular power spectrum in figure 6.2. (The $\triangle^2_{\mathbb{R}}$ value used is different to the 2.43×10^{-9} value used in [35], likely due to the different versions of CAMB and RECFAST used here)

Parameter	**Description**	**Value**
H_0	Hubble constant (km/s/Mpc)	71.0
Ω_b	Baryonic matter density	0.0449
Ω_{DM}	Dark matter density	0.222
n_s	Scalar spectral index	0.963
τ	Reionization optical depth	0.088
$\triangle^2_{\mathbb{R}}$	Curvature fluctuation amplitude	2.18×10^{-9}

6.3 Model Independent Analysis Reveals Uniform Expansion

The scale factor $a(t)$ is the relative size of the universe at time t, and describes the time evolution of the universe assuming a homogeneous and isotropic description. It is defined as $a(t) = r(t)/r(t_0)$; ($a(t_0) \equiv 1$ by definition), where $r(t)$ are galactic separations on a sufficiently large scale, and t_0 is the present moment age of the universe. In principle it may be directly extracted from type 1a supernova magnitude-redshift data without the use of any particular dynamical model for

$a(t)$. To extract $a(t)$ we need to describe the relationship between the cosmological observables: the apparent energy-flux magnitudes and redshifts, and in a model independent manner. This relationship is that of equations (6.1) and (6.2), which are generic and was used in [21, 22] but here it is shown that the Dynamical 3-Space theory yields the same equations. The presence of an expanding dynamical space will affect travelling photons in the following ways:

- Reduction in photon count affects the energy-flux magnitude
- Reduction in photon energy affects the observed redshift

An embedding-space coordinate system is used with $r = 0$ at the location of a supernova event at time t_1, where the speed of light relative to this coordinate system is $c + v\left(r(t;t_1),t\right)$, i.e. c wrt the expanding space itself, where $r(t;t_1)$ is the photon embedding-space distance from the source. The distance travelled by a photon at time t after the supernova event at t_1 is determined implicitly by

$$r(t;t_1) = \int_{t_1}^{t} (c + v(r(t';t_1),t')dt'. \tag{6.5}$$

This has the solution, on using $v(r,t) = H(t)r$,

$$r(t;t_1) = ca(t)\int_{t_1}^{t} \frac{dt'}{a(t')} \tag{6.6}$$

where typically $H(t) \equiv \frac{\dot{a}(t)}{a(t)}$, $a(t)$ is not yet defined and so can be nonlinear, and an overdot represents a derivative with respect to time. The distance $r(t;t_1)$ gives directly the surface area $4\pi r(t;t_1)^2$ of the expanding sphere around a supernova event, and so the photon count per unit area on that surface decreases over time. With $t \to t_0$ (and dropping t_0 in the notation), $a(t_0) = 1$ and $a(t_1) = 1/(1+z(t_1))$, the photon distance in terms of redshift is

$$r(z) = c\int_{0}^{z} \frac{dz'}{H(z')}. \tag{6.7}$$

Due to the space expansion the flux of photons is reduced by the length scale $a = 1/(1+z)$ simply because they become spaced further apart by the expansion. The photon flux is then given by

$$\mathcal{F}_P = \frac{\mathcal{L}_P}{4\pi(1+z)r(z)^2} \tag{6.8}$$

where $\mathcal{L}_P$ is the source photon-number luminosity. Usually the energy flux is measured however, and because of the redshift the energy of each photon is reduced by the factor $1/(1+z)$. The energy flux in terms of the source energy luminosity $\mathcal{L}_E$ is

$$\mathcal{F}_E = \frac{\mathcal{L}_E}{4\pi(1+z)^2 r(z)^2} \equiv \frac{\mathcal{L}_E}{4\pi r_L(z)^2}. \tag{6.9}$$

This generates an effective sphere of radius $r_L(z)$ in terms of the observed photon energy emitted from a supernova. This effective energy-flux luminosity distance is therefore defined as

$$r_L(z) = (1+z)r(z) = c(1+z)\int_0^z \frac{dz'}{H(z')}, \tag{6.10}$$

where $H(z)$ is the Hubble term - equation (6.3) and derived in [125]. The dimensionless 'energy-flux' luminosity effective distance is then given by

$$d_L(z) = (1+z)\int_0^z \frac{H_0 dz'}{H(z')}. \tag{6.11}$$

Here $d_L(z)$ takes account of the reduced photon flux and energy loss caused by the expansion. Then the magnitude-redshift observables automatically follow, and are computable from

$$\mu(z) = 5\log_{10} d_L(z) + m \tag{6.12}$$

where m is determined by the intrinsic brightness of the supernova event. In principle $\mu(z)$ can be inverted to yield $a(t)$, without reference to any dynamical theory for $a(t)$. Notice that (6.11) and (6.12) match that of (6.1) and (6.2).

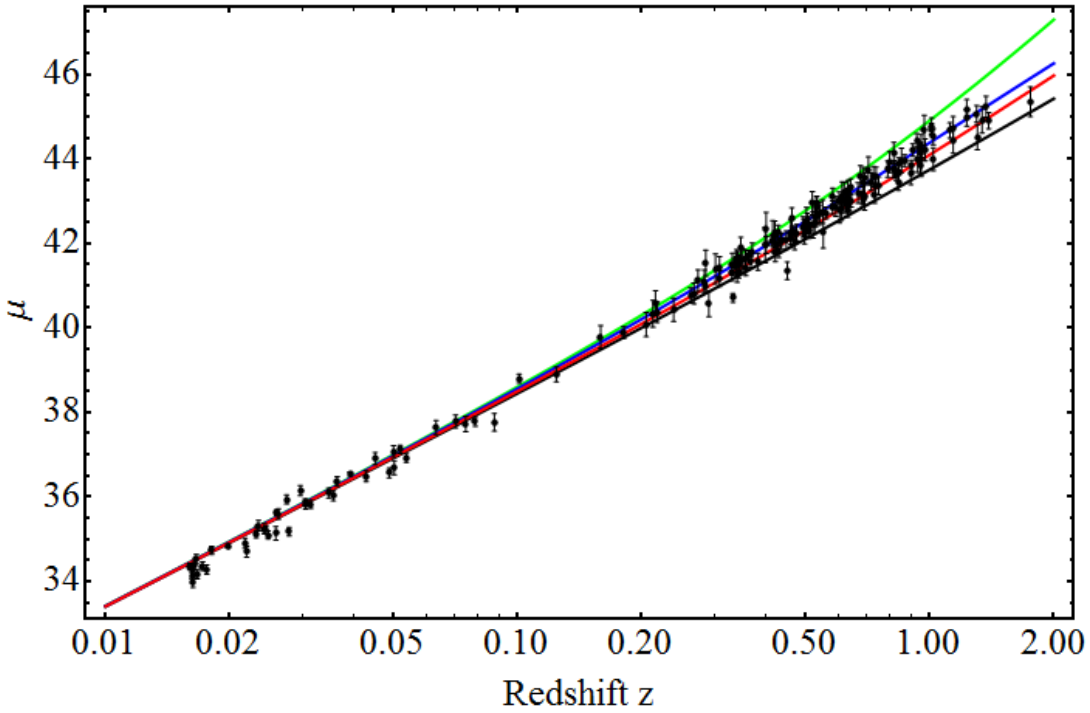

Figure 6.1: Type 1a supernova magnitude-redshift data. Upper curve (green) is 'dark energy' only $\Omega_\Lambda = 1$. Next curve (blue) is best fit of 'dark energy'-'dark-matter' $\Omega_\Lambda = 0.73$. Lowest curve (black) is 'dark matter' only $\Omega_\Lambda = 0$. Second lowest curve (red) is the uniformly expanding universe, and also predicted by Dynamical 3-Space theory (5.1).

A simple first analysis of the data tries a uniform expansion $a(t) = t/t_0$, which involves one parameter $t_0 = 1/H_0$ that sets the time scale. Figure 6.1 shows that this uniform expansion (shown by red plot) gives an excellent account of the data, and so further, more complex solutions are unnecessary. For a uniformly expanding universe $H(z) = (1 + z)H_0$ and $d_L(z) = (1 + z)\ln(1 + z)$. It is therefore concluded that the supernova magnitude-redshift data reveals a uniformly expanding universe. So why did the Perlmutter[21] and the Schmidt - Riess teams[22] report an accelerating expansion for the universe? According to the Nobel Prize briefing notes, this is because *"The evolution of the Universe is described by Einstein's theory of general relativity."*[126] To the contrary it is argued that the data should be used to test possible theories of the universe, as in the usual scientific method, and not *a priori* demand that one theory, with *ad hoc* adjustments, be defined to be the only correct theory.

6.4 NG / GR Universe Models

The analysis in [21, 22] used the GR-based Friedmann equation for $a(t)$, i.e. the 00 (temporal) component of the field equations mentioned in chapter 1,

$$\dot{a}^2 = \frac{8}{3}\pi G a(t)^2 \rho(t) \tag{6.13}$$

where the overdot represents a derivative with respect to time, and $\rho(t)$ is the matter/energy density. However this equation follows trivially from Newtonian gravity, by considering a uniform matter density moving radially with speed $v(r,t)$, at distance r, away from an origin. The kinetic + gravitational potential energy, with total energy E, of a test particle of mass m is given by

$$\frac{1}{2}mv^2 - \frac{GmM(r)}{r} = E \tag{6.14}$$

where $M(r) = \frac{4}{3}\pi r^3 \rho$ is the mass enclosed within radius r - this follows simply from Newton's inverse square law. Using $r(t) = a(t)r_0$, $v = \dot{r}$ and the so-called critical case $E = 0$, immediately gives (6.13). The reason for this simple derivation is that GR was constructed as a generalisation of NG, that reduces to NG in the limit of low speeds and matter densities. The Friedmann equation therefore inherits all of the fundamental problems with NG. As well the redshift z is actually a Doppler shift effect, caused by the motion of the source relative to the observer. Consider then some of the implications of (6.13):

1. If $\rho = 0$, i.e. no matter, then there is no expanding universe possible: $\dot{a} = 0$. This arises because (6.13) is about the effects of matter-matter gravitational attraction, and without matter there are no gravitational effects.

2. It is not about the expansion of space, for it arises from NG in which matter moves through a Euclidean and unchanging space.

3. (6.13) requires, at $t = t_0$, that

$$H_0^2 = \frac{8}{3}\pi G\rho_c \tag{6.15}$$

where ρ_c is the so-called critical density. However (6.15) is strongly violated by the data; the observed baryonic matter density is 20 - 25 times smaller than ρ_c, and so ρ must be padded out to satisfy (6.15).

4. No uniformly expanding solutions for (6.13) exist unless $\rho \sim 1/a^2$, a form not considered in [21, 22].

To fit the data [21, 22] used the restricted *ad hoc* form

$$\rho(a) = \left(\frac{\Omega_M}{a^3} + \Omega_\Lambda\right)\rho_c \tag{6.16}$$

where Ω_Λ is the dark energy density parameter, and Ω_M is the matter density parameter. There is no theoretical underpinning for this dark energy parameter. The relationship for the critical density in equation (6.15) relationship requires that $\Omega_\Lambda + \Omega_M = 1$, resulting in a two parameter model containing H_0 and Ω_Λ. Fitting the data, by solving (6.13), and then using (6.1) and (6.2), gives $\Omega_\Lambda = 0.73$, and so $\Omega_M = 0.27$. This fitting is shown as the blue curve in figure 6.1. Since it was argued earlier that the data alone suggests that the universe is expanding uniformly, $\Omega_\Lambda = 0.73$ is essentially the value for which NG best mimics a uniformly expanding universe, despite its inherent weakness as a model of the universe. The known baryonic matter density, corresponding to $\Omega_b = 0.04$, then requires that $\Omega_M - \Omega_b = 0.23$ be interpreted as the dark matter composition Ω_{DM}. However (6.13) has another strange feature, namely that $a(t)$, as a consequence of the dark energy parametrisation, possess an exponential component; neglecting Ω_M (which becomes increasingly valid into the future) we obtain

$$a(t) \sim e^{H_0\sqrt{\Omega_\Lambda}t}. \tag{6.17}$$

The Nobel Prize for Physics in 2011 was awarded for the discovery of this *"accelerated expansion of the universe"*,[126] despite the fact that the model independent analysis in section 6.3 shows no such effect.

6.5 Dynamical Space Universe Model

6.5.1 Uniformly Expanding Universe Solutions

The Dynamical 3-Space theory contains a solution for the expansion of space in all directions. Substituting the Hubble form $\mathbf{v}(\mathbf{r},t) = H(t)\mathbf{r}$, and then $H(t) = \dot{a}/a$, we obtain[121]

$$4a\ddot{a} + \pi^2\alpha\dot{a}^2 = -\frac{16}{3}\pi G a^2\rho \tag{6.18}$$

This has a number of key features:

1. Even when $\rho = 0$, i.e. no matter, $a(t) \neq 0$ and monotonically increasing. This is because the space itself is a dynamical system, and the (small) amount of actual baryonic matter merely slightly slows that expansion, as the matter dissipates space.

2. Relation (6.15) no longer applies, and so there is no 'critical density'.

3. The redshift z is no longer a Doppler shift; now it is caused by the expansion of the space removing energy from photons.

4. As mentioned in chapter 5, in the absence of matter $\rho = 0$ (6.18) has the solutions

$$H(t) = \frac{1}{(1+\frac{\pi^2\alpha}{4})t} \quad , \quad a(t) = \left(\frac{t}{t_0}\right)^{1/(1+\frac{\pi^2\alpha}{4})} . \tag{6.19}$$

Because of the small value of $\alpha = 1/137$, the α term only plays a significant role in extremely early epochs, but only if the space is completely homogeneous.

Neglecting the α dynamics, the solution $a(t) = t/t_0$ is obtained, which remarkably is a uniformly expanding universe solution. This solution is exactly the form directly determined in section 6.3 from the supernova data, and the extra π^2 factor from equation (5.1) has no observable effect on the model independent plot in figure 6.1. It requires neither 'dark energy' nor 'dark matter' - these parameters have evaporated, and are clearly revealed as nothing more than artifacts of the NG model. The 'accelerating expansion of the universe' in the future has also disappeared, as can be noticed by observing that $\dot{a}(t) = 1/t_0$ and $\ddot{a}(t) = 0$.

6.5.2 CMB Fluctuations

Another technique for determining the expansion rate and density composition of the universe is to use the Cosmic Microwave Background (CMB) temperature angular fluctuation spectrum. The thermal fluctuations observed in the sky provides a snapshot of the anisotropic primordial plasma densities at the time of decoupling, or recombination of hydrogen when the universe was around 3000 K ($z \approx 1100$). As briefly mentioned in chapter 1 this spectrum is computed as a perturbation of the primordial plasma relative to an assumed homogeneous background universe dynamical model. The background model used is the Friedmann equation (6.13). The computed angular fluctuation power spectrum from CAMB is shown in figure 6.2 for the same three values $\Omega_\Lambda = 0.73$, 0 and 1, as also used in figure 6.1. Increasing the dark energy parameter does nothing to the shape of the plot; it merely compresses its form. As already noted in section 6.4, this homogeneous background dynamics is merely a NG/GR model, with the dark energy and dark matter parameters used to pad out the critical density and mimic a uniform expansion. In the presence of a dynamical space the CMB power spectrum should then yield information about the space self interaction effects that mimic the dark matter density, without requiring an extra padding parameter to stretch the predicted power spectrum form, which the dark energy parameter achieves in

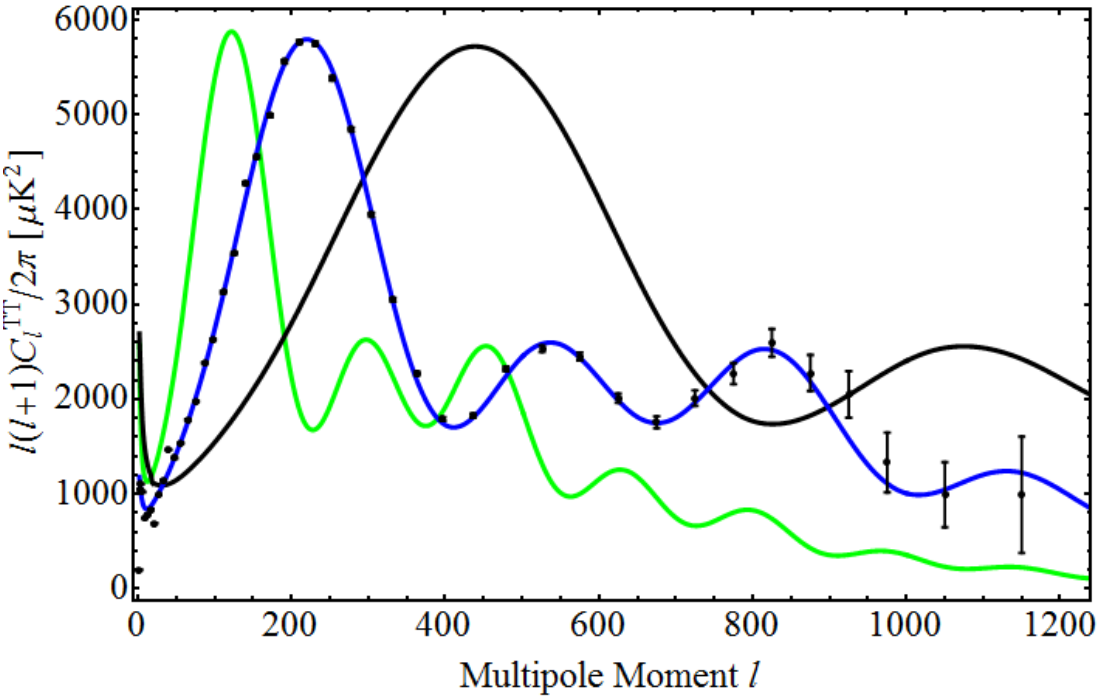

Figure 6.2: CMB angular power spectrum for (i) $\Omega_\Lambda = 1$ (green curve), (ii) $\Omega_\Lambda = 0.73$ (blue curve), and (iii) $\Omega_\Lambda = 0$ (black curve), confirming that the background space is uniformly expanding due to the appearance of the reoccurring $\Omega_\Lambda = 0.73$ and $\Omega_M = 0.27$ best fit parameters.

GR. The baryonic matter density Ω_b is responsible for the relative heights of the first and second peaks in the CMB power spectrum, as well as the position of the first peak. Decreasing the $\Omega_b : \Omega_{DM}$ ratio decreases the heights of all observed peaks as well as dampens the heights of the second and third peaks. Observing the relative heights and location of the first 3 peaks therefore yields information about the $\Omega_b : \Omega_s$ ratio observed within the primordial plasma. Because Ω_s indicates the strengths of space self interactions present and is determined by α, the value of α should therefore also be obtained from the power spectrum. Predicting the CMB power spectrum using Dynamical 3-Space theory is currently not possible due to the lack of knowledge of how perturbations in space self interaction effects develop. These might potentially be modelled in a similar fashion as to how dark matter is currently perturbed in cosmology textbooks. It may certainly be possible to modify the Hubble equation used in CMB anisotropy programs, such as CAMB (which also requires modifying Hubble equations in RECFAST) in order to model

that of a uniformly expanding universe in order to predict the CMB anitostopies. This would then entail modelling 'dark matter' effects which drop off as $\approx 1/a^2$ as predicted in equation (6.3) for example, instead of $1/a^3$ using the standard model of cosmology.

6.5.3 Age of Universe and Cosmic Inflation

The Newtonian model and the Dynamical 3-Space model give the same age for the universe, 13.7 Gyr, as they both describe the same uniform expansion rate, with the minor variations in the Newtonian model expansion rate cancelling out. However they give different decoupling times, which can be determined from the respective models for the scale factor. The Newtonian and Einstein models give the well known decoupling of 0.38 Myr. The decoupling time for the Dynamical 3-space theory can be computed straight from equation (6.19) for $a(t) = 1/1100$ since $z \approx 3000/2.725 \approx 1100$ at time of recombination. The previous Dynamical 3-Space model, equation (3.17) predicts a decoupling time of 12.3 Myr while the new model predicts 11.0 Myr. This suggests that in the modified model the universe expanded faster in its infancy, and has therefore cooled down faster. It is therefore important to note that the decoupling time is very model dependent.

The presence of α in solutions (6.19) suggest that at very small t the rate of space expansion becomes nonuniform, suggesting an 'inflation epoch' emergent from the Dynamical 3-Space model. Certainly if $\alpha = 0$ then $\dot{a}$ becomes constant and $\ddot{a} = 0$. With the presence of α the following solutions for the rate and acceleration of the universe's expansion are

$$\dot{a} = \frac{\left(\frac{t}{t_0}\right)^{\frac{1}{1+\frac{\alpha\pi^2}{4}}}}{t(1+\frac{\alpha\pi^2}{4})} = \frac{4.6636 \times 10^{-18}}{t^{0.0177}} \tag{6.20}$$

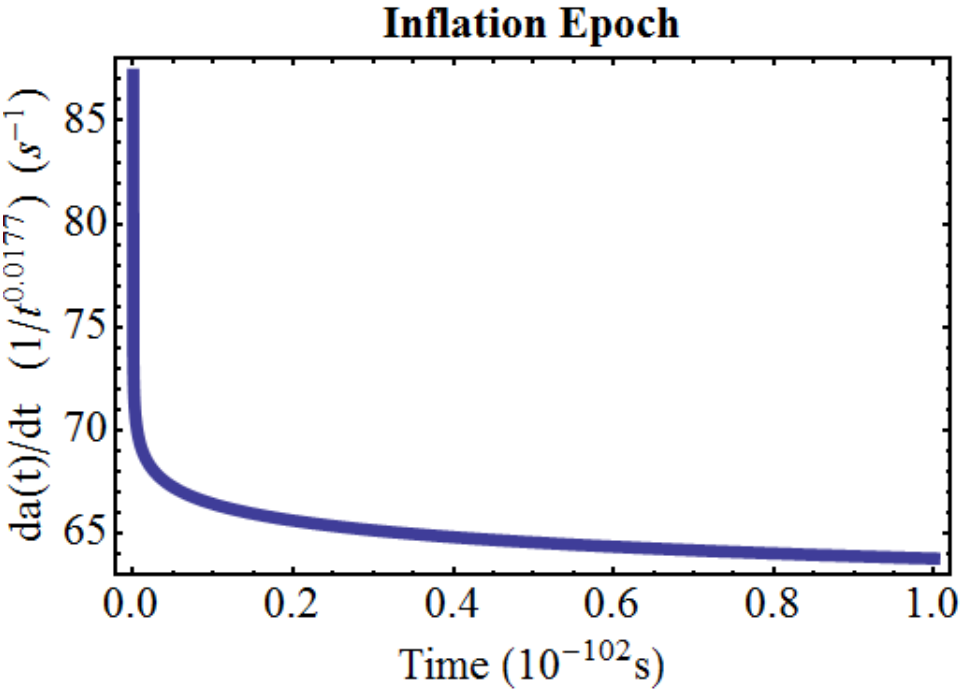

Figure 6.3: Plot of $\dot{a} = 1/t^{0.0177}$, the rate of expansion showing the inflation epoch (without the 4.6636×10^{-18} coefficient in equations (6.20) and (6.21)). This inflation epoch is intrinsic to the Dynamical 3-Space.

and

$$\ddot{a} = \frac{\pi^2 \alpha \left(\frac{t}{t_0}\right)^{\frac{1}{1+\frac{\alpha\pi^2}{4}}}}{4t^2(1+\frac{\alpha\pi^2}{4})^2} = -\frac{8.2507 \times 10^{-20}}{t^{1.0177}} \tag{6.21}$$

when substituting $\alpha = 1/137$ and $t_0 = 13.7$ Gyr as this is predicted by the supernova data. By studying the rate of expansion of the universe, i.e. $\dot{a}$ at early times one can deduce the epoch of inflation, which is intrinsic to the Dynamical 3-Space theory and shown in figure 6.3. This is different to cosmic inflation theories in NG and GR which are created as a way to explain various problems such as horizon and flatness problems, and also requiring a mechanism to introduce primordial perturbations into the universe. These models suggest that inflation occurs through a mechanism which causes space to expand exponentially for a fraction of a second, before settling to a more uniform expansion. Equations (6.20) and (6.21) instead suggest such an epoch would see space expanding rapidly at the universe's beginning but always at a decelerating rate, until at sufficiently large time t such that the acceleration is negligible and the universe expands uniformly.

Table 6.3: Relative size, speed and acceleration of the universe's expansion over time.

Time t	**Size** $a(t)$	**Speed** $\dot{a}(t)$	**Acceleration** $\ddot{a}(t)$
10^{-102} s	3.03×10^{-118}	2.27×10^{-16}	-5.26×10^{84}
1 s	4.75×10^{-18}	4.47×10^{-18}	-8.25×10^{-20}
13.7 Gyr	1	2.27×10^{-18}	-9.31×10^{-38}

Process Physics[47] and Dynamical 3-Space theory suggest that at very fast inflow speeds during this very early epoch such a space flow would be turbulent, and would introduce perturbations into the universe. The inflation epoch predicted by Dynamical 3-Space theory however does contain a singularity at $t = 0$ suggesting that the expansion of space becomes infinite at the Big Bang, and so the model currently breaks down at very early times. The only explanation for this would be dependent on modelling any phase transitions that triggered the early stages of the Big Bang, which there is no test for. The inflation epoch according to figure 6.3 ends at around $t = 0.1 \times 10^{-102}$ s, some 70-75 orders of magnitude earlier than conventional physics inflation models. This value was earlier reported to be related to $t = 0.1 \times 10^{-101} t_0 = 4.4 \times 10^{-83}$ s,[84] here the additional π^2 factor predicts an inflation epoch an order of magnitude earlier. The t_0 constant however only affects the magnitude of the relative rate of expansion, and not t directly, and so is not plotted here on the $x-$ axis.

Table 6.3 shows information about the relative size, rate and acceleration of the universe's expansion. The universe's relative deceleration at $t = 10^{-102}$ s is around 122 orders of magnitude higher to the current time of 13.7 Gyr while the relative expansion rate of expansion of the universe was only 2 orders of magnitude higher in the same period. After only one second the universe's expansion rate is comparable (roughly double) to what is observed today, and the acceleration is negligible, showing how rapidly the universe's expansion becomes uniform. So the α effects gradually slow the universe's expansion, but at essentially a negligible rate.

6.6 Concluding Remarks about Chapter 6

The supernova magnitude-redshift data is of great significance to cosmology. From a model independent approach it reveals that the universe is undergoing a uniform expansion. This represents a major challenge to theories of the universe, particularly as GR does not have such solutions. To mimic the uniform expansion the canonical value $\Omega_\Lambda = 0.73$ emerges by fitting the NG model to either the data, or more revealingly, by fitting to the Dynamical 3-Space theory. However the *ad hoc* introduction of the dark energy parameter results in a spurious accelerating expansion. These spurious effects, namely dark energy, dark matter, and the universe's future accelerating expansion, are today's 'epicycles' when an incorrect model of reality is forced to fit the data, instead of using the data to test different models of the universe. Astronomers are now committing major resources to 'explaining' these new epicycles instead of potentially exploring alternative models. The Dynamical 3-Space theory gives a uniformly expanding universe without the introduction of any *ad hoc* parameters, and disagrees in general with NG, even in the low matter density, low speed limits, while nevertheless reproducing the NG restricted successes within the solar system. It also predicts an intrinsic early epoch where space is rapidly expanding at a decelerating rate, as opposed to current cosmic inflation theories which introduce an accelerating universe expansion phase early on. Introducing the dark matter and dark energy parameters amounts to the belief that Newton had correctly and completely described space and gravity some 300 years ago, requiring only the identification of new matter/energy. The supernova data, and potentially the CMB data, is now showing that this is not the case.

Chapter 7

Black Holes in an Expanding Universe

7.1 Introduction

The type 1a supernova magnitude-redshift data permits the study of the universe's evolution up to redshifts of about 2, i.e. when the universe was a third of its current size. Gamma ray burst data can provide information about $a(t)$, up to redshifts of 5-7[127] thus providing more information about the universe's evolution. Recession of distant galaxies from a central larger galaxy cluster, for example those receding from the M81 group[128] or from the CenA/M83 complex[129] can also study the same phenomenon however at a lower redshift. These data sets are referred to as velocity-distance relationships similarly to those Hubble discovered in the 1920s, but are more used to determine both the dynamics and mass of galaxies in clusters. Today they are studied using a 2 parameter fit typically involving attractive and repulsive parameters, i.e. a gravitational attraction associated with the large central mass and the cosmic repulsion suggested by both Hubble expansion and dark energy parameters in the GR model.[31] As briefly discussed in

chapter 1 there then defines a zero velocity surface, i.e. the radial distance from the central mass where these two effects cancel, and this radius is then used to calculate the enclosed mass of the cluster. This chapter will extend on Dynamical 3-Space theory, and present how the model demands the combination of black hole and expanding universe solutions. These combined solutions will be discussed and shown how they could potentially be used to study the dynamics of galaxy cluster data and also the large scale structure of the universe.

7.2 Black Hole/Expanding Universe Solutions

Chapter 6 discussed expanding universe solutions which are emergent from Dynamical 3-Space theory. This Hubble flow, equation (6.19) does not contain a free parameter, and so in this theory the universe necessarily expands, and hence it cannot be ignored when considering BH and filament solutions, for example. Since any radially flowing and time dependent $v(r,t)$ (i.e. containing both outflows and inflows) has spherical symmetry, (5.1) becomes, in the absence of matter

$$\begin{aligned}\frac{\partial}{\partial t}\left(\frac{2v}{r}+v'\right)+vv''+2\frac{vv'}{r}+(v')^2+\frac{\pi^2\alpha}{4}\left(\frac{v^2}{r^2}+\frac{2vv'}{r}\right)\\ +\frac{4\delta^2}{r^4}\left(v^2+r^2(v')^2+3r^3v'v''\right)\\ +\frac{4\delta^2}{r^4}\left(-2rvv'+r^2vv''+r^3vv'''\right)=0\end{aligned} \tag{7.1}$$

where $v' \equiv \partial v/\partial r$. General black hole / expanding universe solutions would require the following ansatz

$$\mathbf{v}(\mathbf{r},t) = H(t)\mathbf{r} + w(r,t)\hat{\mathbf{r}} \tag{7.2}$$

where $w(r,t)$ is the spherically symmetric black hole inflow. After substituting this form into (5.1), a time dependent equation for $w(r,t)$ was found, however solutions for $w(r,t)$ are currently unknown. By setting $w(r,t) = R(r)/t$ however this time

dependence is completely resolved, and (5.1) now may be solved for $R(r)$, implying that the Hubble expansion and black hole inflow are inseparable and compatible phenomena. There are two cases for potential solutions that must be discussed, namely the long range $\delta = 0$ and short range $\delta \neq 0$ cases.

7.3 Long Range $(\delta = 0)$ Solutions

Asymptotically, when $r \gg \delta$, then δ may be set to zero for the purposes of determining black hole / expanding universe solutions which hold sufficiently far away from the centre of a black hole. The resulting equation for $R(r)$ has the solution

$$R(r) = -\frac{\nu}{r^{\frac{\pi^2\alpha}{4}}}, \quad \text{and so} \quad v(r,t) = \frac{r}{(1+\frac{\pi^2\alpha}{4})t} - \frac{\nu}{r^{\frac{\pi^2\alpha}{4}}t} \tag{7.3}$$

which contains the original black hole solution (see table 5.2 in chapter 5.3.1), but now with an inverse time dependence, and where ν is a parameter for the black hole strength. Eqn (7.2) is for the black hole located at $\mathbf{r} = \mathbf{0}$. For a black hole comoving with the local Hubble space flow the solution of (5.1) is

$$\boldsymbol{v}(\boldsymbol{r},t) = H(t)\mathbf{r}' + \mathbf{w}(\mathbf{r}',\mathbf{t})\hat{\mathbf{r}}' \tag{7.4}$$

where $\mathbf{r}' = \mathbf{r} - a(t)\mathbf{r}_{BH}$ when the observer is at $\mathbf{r} = \mathbf{0}$, and the black hole is located at $a(t)\mathbf{r}_{BH}$. A consequence of (7.2) and (7.3) is that for any BH there exists a critical radius r_c where the spatial inflow into the BH is equal and opposite to the Hubble expansion, figure 7.1, so defining a sphere of influence where $v(r,t) = 0$,

$$v(r_c,t) = 0 \implies \frac{r_c}{t(1+\frac{\alpha\pi^2}{4})} - \frac{\nu}{r_c^{\frac{\pi^2\alpha}{4}}t} = \nu\left(1+\frac{\alpha\pi^2}{4}\right) - r_c^{1+\frac{\alpha\pi^2}{4}} = 0. \tag{7.5}$$

Inside the sphere the space is moving towards the black hole, and outside the space appears to recede from it due to universe expansion effects. This does not

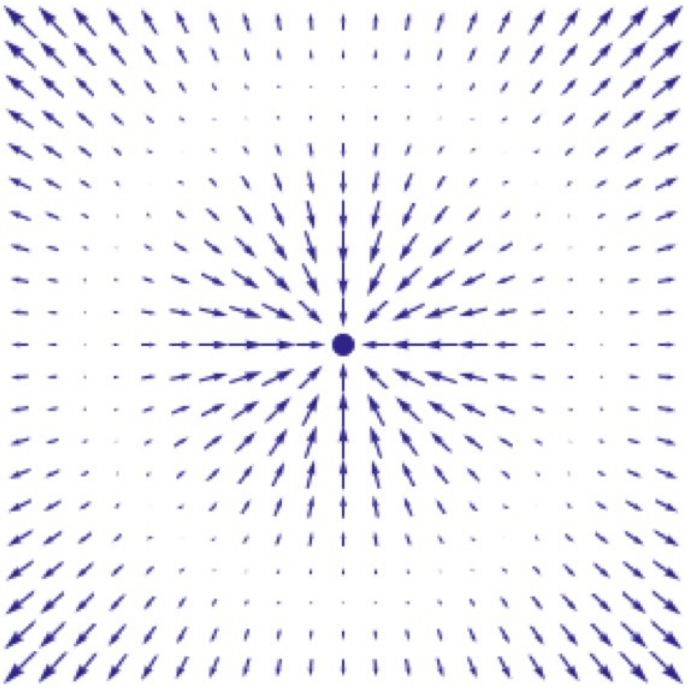

Figure 7.1: Schematic 3-space velocity for an isolated black hole embedded in an expanding universe, see (7.2), showing radius at which flow reverses, defining the black holes sphere of influence at radius r_c.

necessarily mean that test particles will behave in the same way as that of space, as their motion is affected by the gravitational acceleration of the dynamical space and potentially due to a galaxy cluster environment, for example. Additionally the two effects present are physically different, namely the black hole effect is space flowing into a singular point, and is a real velocity, whereas the Hubble expansion is the centreless expansion of space everywhere, the magnitude of this which is relevant to an observer's position. It is important to emphasise that sufficiently far away from a black hole an observer would view an apparent space velocity, and then ultimately the recession of galaxies due to the universe's expansion (sufficiently far away), and not an actual space flow velocity superposition. This is also illustrated in figure 7.2a which plots the velocity profile of the 3-space flow with decreasing Hubble constant, while holding the black hole strength ν fixed. The two separate inflow and 'outflow' regions are clear from this figure. What is also evident from figure 7.2a is that the critical radius r_c is found to remain independent of time, i.e.

r_c depends only on the strength of the black hole as suggested by (7.5) and figure 7.2b. Increasing the black hole strength ν only affects the 3-space inflow profile, and not that of the outflow/expanding universe as denoted by the asymptotic parallel plots in figure 7.2b.

The acceleration of the new black holes can be derived simply from

$$g(r,t) = \frac{\partial v(r,t)}{\partial t} + v(r,t)\frac{\partial v(r,t)}{\partial r} \equiv \frac{\partial v(r,t)}{\partial t} + \frac{\nabla v(r,t)^2}{2}. \tag{7.6}$$

This then predicts coupled interactions between the spatial inflows and 'outflows' present near the black hole, as the $H(t)$ and $w(r,t)$ terms will cross multiply. For the known black hole (7.3) and Hubble solution (6.19) the gravitational acceleration is, from (7.2),

$$\begin{aligned} g(r,t) &= -\frac{\pi^2\alpha}{4}\frac{H(t)^2}{r^{1+\frac{\pi^2\alpha}{2}}}\left(\left(1+\frac{\pi^2\alpha}{4}\right)\nu - r^{1+\frac{\pi^2\alpha}{4}}\right)^2 \\ &= -\frac{\pi^2\alpha}{4r}v(r,t)^2. \end{aligned} \tag{7.7}$$

This solution appears quite complex however with some manipulation it reduces to a more elegant form, namely to g in terms of v^2, with an inverse dependence on distance. This also occurs for the gravitational acceleration due to static black holes upon closer inspection, where similarly $g(r) = -\frac{\pi^2\alpha}{4r}v(r)^2$, see table 5.2 in chapter 5.3.1, and so this new result appears to be correct and in trend with the previously known solutions. Figure 7.3 shows the acceleration profiles of the 3-space, using the same values as those for the velocity profiles in figure 7.2. Note that from figure 7.3a the critical radius r_c still remains independent of time, which is expected as the predicted 3-space acceleration (7.7) can be written in terms of its velocity, and inherits this property. A peculiar result may be apparent here, namely that the 3-space acceleration is always negative. Certainly for $r < r_c$ the acceleration is always towards the black hole but it may be unclear as to why this is

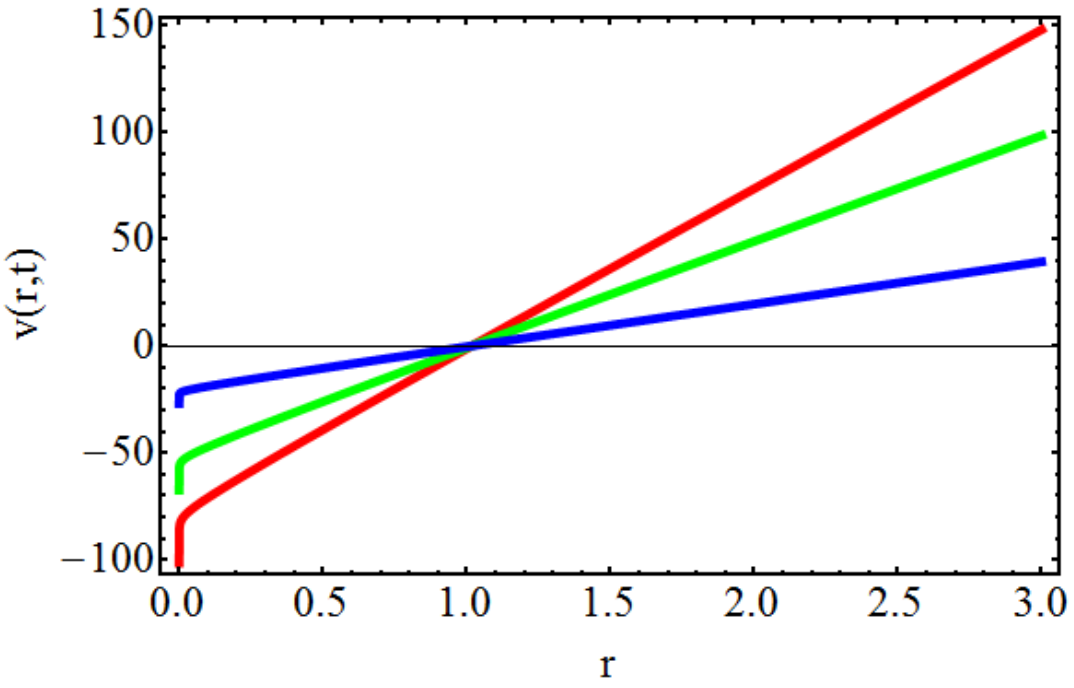

(a)

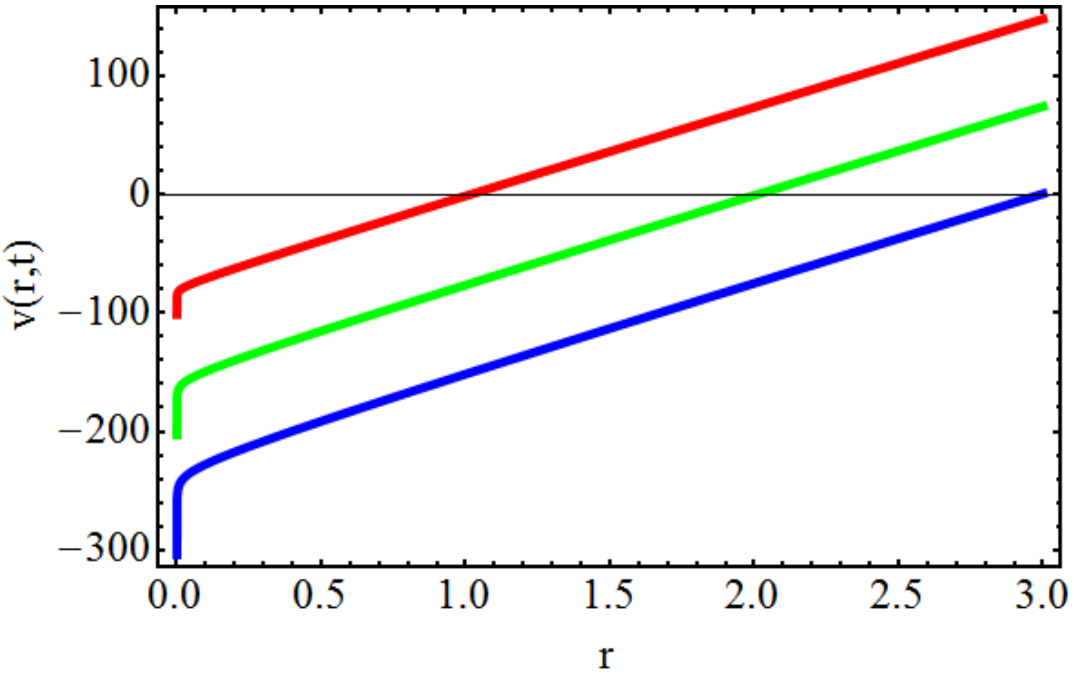

(b)

Figure 7.2: (a) Typical 3-space velocity profile for a single black hole embedded in an expanding universe, (7.2) and (7.3), for fixed $\nu = 1$, and $H(t) = 75$ (red), $H(t) = 50$ (green), and $H(t) = 20$ (blue). (b) Velocity profiles for fixed $H(t) = 75$ and $\nu = 1$ (red), $\nu = 2$ (green) and $\nu = 3$ (blue). The values used here are for schematic purposes only.

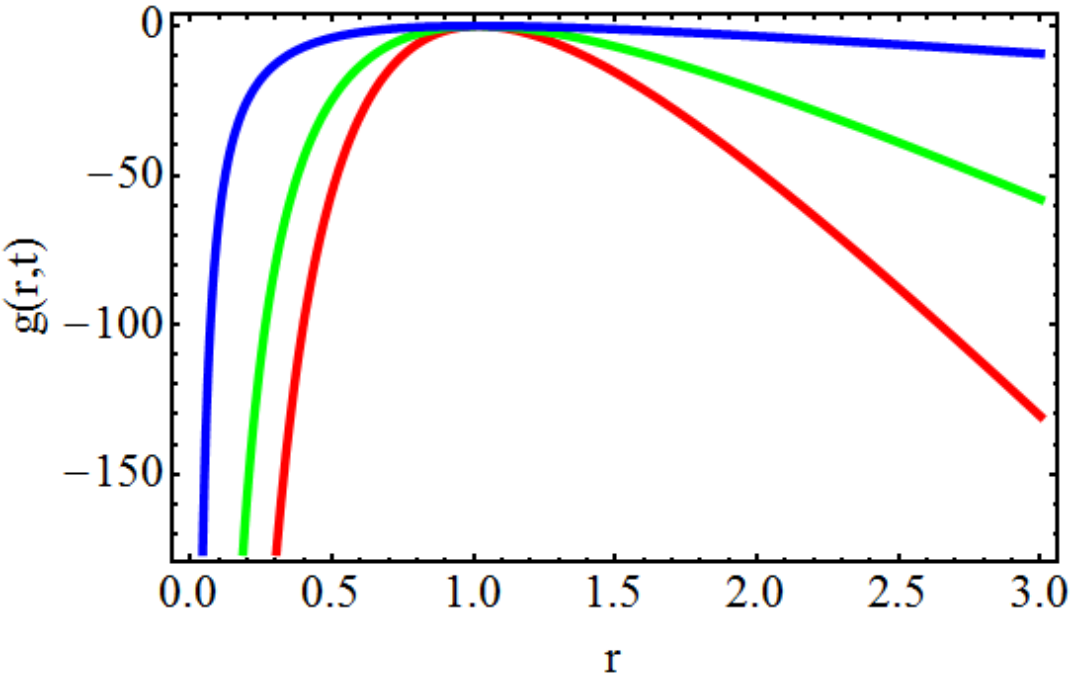

(a)

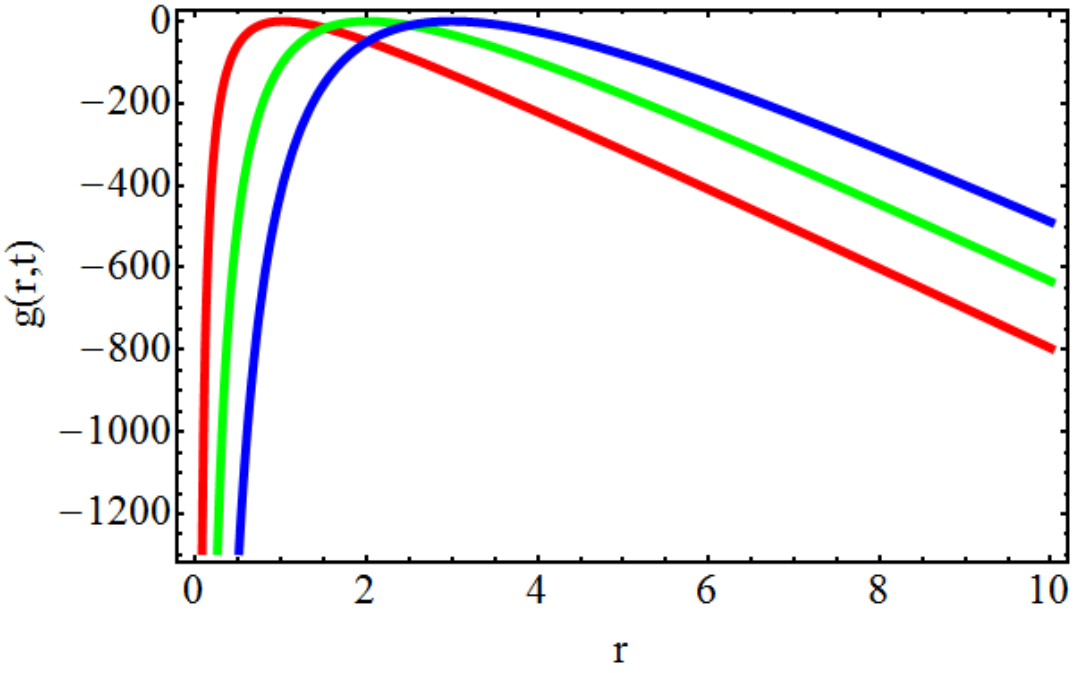

(b)

Figure 7.3: (a) Typical 3-space acceleration profile for a single black hole embedded in an expanding universe, (7.2) and (7.3), for fixed $\nu = 1$, and $H(t) = 75$ (red), $H(t) = 50$ (green), and $H(t) = 20$ (blue). (b) Acceleration profiles for fixed $H(t) = 75$ and $\nu = 1$ (red), $\nu = 2$ (green) and $\nu = 3$ (blue). The values used here are the same used in figure 7.2.

the case for $r > r_c$. To an observer viewing space at great distances, equation (7.2) suggests that space recedes faster at larger distances from the observer. This then implies that the apparent acceleration of expanding space will always be towards the observer. This is not to be confused with the acceleration of the scale factor $a(t)$ which is related to the Hubble term $H(t)$, as this is a derivative with respect to time whereas here it is with respect to distance, and is therefore different. Stronger black hole inflows are also predicted for higher values of $H(t)$ (obtained by varying t to yield $H(t)$) as shown by comparing for example, the red curve to the blue curve in figure 7.3a for $r < r_c$, or $r \approx 1$ in this case, as well as faster outflows for $r > r_c$. This occurs because of the inverse dependence on t for both black hole inflows and the Hubble expansion now - a higher Hubble constant then also dictates the black hole strength (flow strength only, not the value of r_c) implying that these two phenomena cannot be separated, and are indeed compatible. Increasing the value of ν yields stronger and longer range gravitational black hole strengths as observed in figure 7.3b, for $r < r_c$, while outside of this the behaviour is similar to that of the velocity profiles observed in figure 7.2b.

To clarify, the critical radius r_c where $v(r,t) = 0$ is the same for both the velocity and gravitational properties of the Dynamical 3-space. This implies that test particles placed **at rest** inside r_c are attracted to the black hole due to gravity, while those placed outside r_c, and at rest wrt the local space, recede from it due to expansion. This also gives the smallest possible radius at which an object could theoretically orbit a black hole without being drawn to it gravitationally. This was previously reported by [30, 31] who predicted a similar critical radius defined as r_F from galaxy cluster data, and induced by gravity and expansion/dark energy effects canceling out. Objects with initial velocities would violate this rule - for example two galaxies separated by $r > r_c$ but traveling towards each other would still do so provided their relative velocities overcame that of the universe's

expansion. Solution (7.3) therefore cannot immediately be applied to the velocity-distance relationships from galaxy cluster data as the initial cluster dynamics are unknown. The critical radius is found to remain independent of time, i.e. r_c only depends on the black hole strength ν. r_c is expected to be sufficiently large that the black hole - star distance r in a galaxy today is negligible compared to r_c, i.e. $r \ll r_c$, therefore not affecting the size of galaxies themselves. This effect would more likely be evident at a distance which galaxies are separated by, as suggested by the galaxy cluster data in [31]. For a Hubble constant $H_0 = 74$ km/s/Mpc, and using the new $v_{orb} = 103$ km/s calculation for the asymptotic inflow speed from table 5.3 in chapter 5, solving for $v_{orb}(r_c) = H_0 r_c$ for the Milky Way SgrA* black hole data (figure 5.7) yields $r_c = 1.39$ Mpc. This value is of the same order of magnitude as those obtained experimentally in [31, 128] which suggest r_c values around 0.7 - 1.25. This value is however assuming that the orbital speed of stars in the Milky way galaxy remains constant over such large distances (this calculation is for our location 8 kpc from the Milky Way black hole), which might not be the case at 1.39 Mpc. For example, at a distance 1.31 Mpc from the SgrA* black hole, $v_{orb} = 96.7$ km/s which then yields $r_c = 1.31$ Mpc. Indeed the orbital speed contributed by v_{orb} would weaken at further distances, which ultimately reduces r_c. There is currently no known way to derive the black hole strength ν in order to accurately determine r_c. For multiple black holes in the expanding space, (5.1) implies a more complex time evolution.

7.4 Short Range ($\delta \neq 0$) Solutions

As mentioned earlier the obtained black hole/expanding universe solution (7.3) is predicted to hold sufficiently far away from a black hole, however the singularity at $r = 0$ means the inflow speed at the black hole becomes infinite, and so these solutions break down at small distances. For the current full Dynamical 3-Space

equation there exist a class of time independent (non expanding universe) black hole solutions in which the inflow speed smoothly reduces to zero at $r = 0$, namely those in table 5.3 in chapter 5 but shown here again just to reiterate

$$v(r)^2 = v_0^2(\kappa - 1)\frac{\delta}{r}\left(1 - {}_1F_1\left[\frac{-2+\pi^2\alpha}{4}, -\frac{1}{2}, -\frac{r^2}{\delta^2}\right]\right) - v_0^2\kappa\frac{8}{3}\frac{r^2}{\delta^2}\frac{\Gamma(\frac{6-\pi^2\alpha}{4})}{\Gamma(\frac{-\pi^2\alpha}{4})}{}_1F_1\left[1+\frac{\pi^2\alpha}{4}, \frac{5}{2}, -\frac{r^2}{\delta^2}\right]. \tag{7.8}$$

To find black hole / expanding universe solutions which are valid for all r requires setting both $\alpha \neq 0$ and $\delta \neq 0$. It was expected that $w(r,t)$ for the $\delta \neq 0$ case would be simply (7.8) with an inverse time dependence, however Mathematica was unable to completely simplify the result after substituting this form into (7.1). Neither could Mathematica produce a solution to (7.1) for $R(r)$ suggesting that either the necessary solution classes are unavailable to Mathematica to allow it to solve this equation, or that the generated equation is in a too unfamiliar form for Mathametica to reduce to a solvable form. Whether (7.8) with an inverse time dependence is a solution to (7.1) or not is therefore unknown. It is expected however that the solution will have hypergeometric properties just as in the case of time independent and static black holes and so the black holes will retain the same or at least similar properties as discussed in [52], such as removing the inflow speed singularity at the black hole's centre as mentioned in chapter 3.

7.5 Large Scale Structure - Induced Filaments and Bubble Networks

We have seen that the Dynamical 3-Space theory offers possible explanations for many phenomena, including a uniformly expanding universe with no additional parameters, and that of an isolated black hole coexisting with this Hubble expansion.

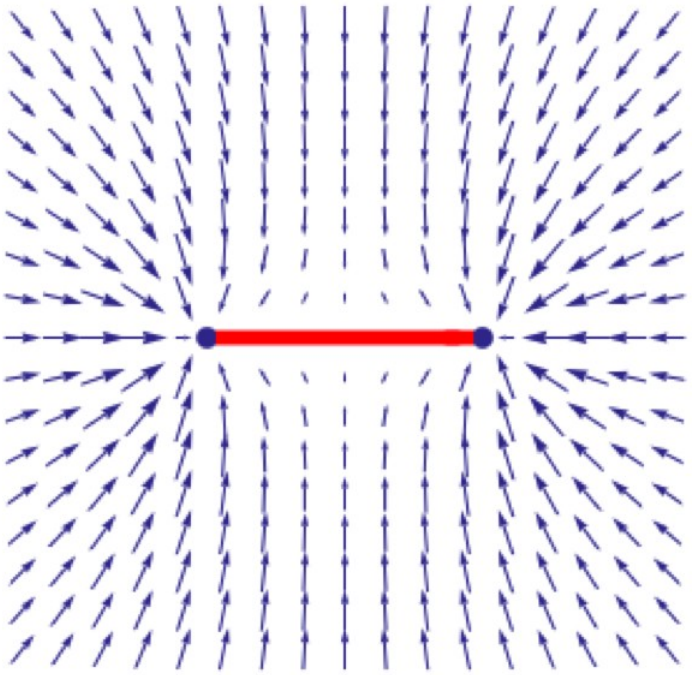

Figure 7.4: 3-space in-flow velocity schematic for two black holes located within their spheres of influence. Note the emergence of a filament forming between the black holes, indicative of a BH - filament network formation, see figure 7.5.

It also has filament solutions, in the absence of the Hubble expansion. However with multiple black holes embedded in this Hubble expansion a new feature appears to emerge, namely cosmic networks of black holes and induced filaments. First note that the black hole inflow speed in table 5.3 and (7.3) is essentially very long range, resulting in the matter acceleration $g(r) \sim -1/r$, which is a key feature of these black holes, and may explain the 'dark matter' effect. However this long range in-flow then raises the question of how multiple black holes coexist when located within one another's sphere of influence, i.e. the critical radius r_c. Figure 7.4 shows the vector addition of the inflows for two black holes. This cannot be a solution of (5.1) as it is non-linear and so does not have a superposition property, from which this flow must evolve over time. Indeed the evolving flow appears to form a filament connecting the two black holes, however even then there remains a long range inflow, which would lead to further filaments connecting black holes

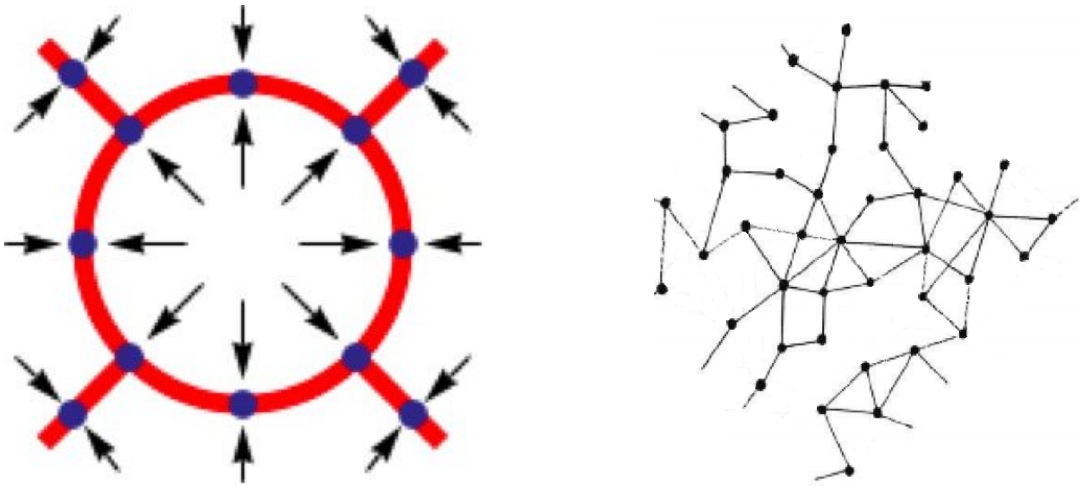

(a) (b)

Figure 7.5: (a) 2D schematic cross section of a symmetrical cosmic network of black holes and induced filaments. Vectors indicate 3-space flow, both within the bubble from the Hubble space expansion, and inwards to black holes (dots) and filaments (red lines). (b) A bubble structure schematic of how the universe would more likely behave as, with solid filament lines connecting black holes but where not all black holes influence each other.

within their range of influence. These black holes are remnants of the early formation of space, and imply that (5.1) will undergo a dynamical breaking of symmetry, from an essentially homogeneous and isotropic 3-space, to a network of black holes and induced filaments. Note that the matter content of the universe is very small, and does not play a key role in this structure formation. Mini primordial black holes sufficiently close to each other would likely coalesce into larger macroscopic black holes due to gravitational forces overcoming the universe's expansion. This could either instantly or rapidly affect the local inflow properties of the new black hole, especially if the coalesced black hole properties have now changed. A possible dynamically stable 3-space structure is shown in fig.7.5a, which entails this network forming a bubble structure with the network defining a 'surface' for the bubbles. The stability of this is suggested by noting that the Hubble expansion within the interior of each bubble is now consistent with the inflow into the black holes and filaments, and so there is no longer a dynamical clash between the long range flows. This is not observed in reality however; we observe other currently dynamically stable structures formed since the beginning of the universe which

may look like that shown in figure 7.5b, where galaxies are observed to be joined by filaments lying on spherical surfaces, filled with large voids. This is indeed found at least for our observable universe, such as that for the Coma[130] and Lynx-Ursa Major filaments[131] for example.

7.6 Concluding Remarks about Chapter 7

Instead of studying black-hole only cases, we need to model astrophysical and cosmological phenomena embedded in an expanding universe. The Dynamical 3-Space theory naturally forces us to do this, as there is no free parameter to switch off the emergent expanding universe solution, and so must be included. It has been shown that the long range black hole solutions found previously hold while embedded in an expanding universe, and predict a critical radius at which gravity and universe expansion effects cancel. This critical radius is predicted to be in the order of $\approx$ Mpc. It is suggested that the time dependent nature of these new solutions explains in part the observed cosmic web. It appears that the dynamics of the 3-space in the presence of primordial black holes, essentially defects in the space emerging from the quantum foam, renders a homogeneous and isotropic universe dynamically unstable, even without the presence of matter, resulting in a spatial bubble network. The long range $g \sim 1/r$ of both the black holes and induced filaments will cause matter to rapidly infall and concentrate around these spatial structures, resulting in the earlier formation of galaxies than expected from conventional physics models.

Chapter 8

Conclusions and Future Work

8.1 Conclusions

The Dynamical 3-Space theory, which is based from *Process Physics* is a unique generalisation of Newtonian gravity cast into an inflow formalism, and while it is relatively new in its development it has been able to predict the emergence of many linked phenomena. Some of these phenomena such as gravity, black holes and filaments, conventional physics only assumes to exist and doesn't actually predict. The Dynamical 3-Space theory is also able to predict these phenomena without the requirement of additional parameters, something which is remarkable. Here we have shown to not only extend on this theory and discuss its implications but also show a new method using two different phenomena to study this effect, aided with the discovery of Simon Shnoll's work and methods a couple of years ago now.

The study of the RF EM dual coaxial cable data and the Zener diode tunneling current fluctuation data was successful, with showing nonrandom effects in layered histograms generated for the two data sets. The coaxial cable experiment was first studied to understand how the long term Shnoll effect works, and then using the

Zener diode experiment that has a better timing resolution to further study this. We then gave an explanation of the fine structure observed in the data in terms of a dynamical and fractal space present affecting tunneling current fluctuations, and then predicted how the short term Shnoll effects would manifest from space fluctuations.

The discovery that the α effects in the borehole g anomaly data were approximately ten times stronger than previously reported allowed the revision of the Dynamical 3-Space equation to allow for an additional π^2 factor in the α space self interaction effects. New black hole, filament and effective dark matter density solutions were reported, where the predicted black hole inflow is now weaker than previously predicted however their acceleration is stronger. We then showed that the new orbital velocity solutions would still asymptotically predict the flat rotation curves observed in spiral galaxies. The inflow dynamics were still observed to mimic an effective matter density that predicted the enclosed mass observed in the Milky Way SgrA* black hole data, and successfully predicted the $M_0 = 4.21 \times 10^6 M_\odot$ pointlike black hole mass observed at its centre.

The type 1a supernova data used to study the universe's evolution over time is able to be predicted from a model independent point of view, and we showed that the data suggests that the universe is undergoing a uniform expansion. This is in contradiction to that predicted by Newtonian Gravity and General Relativity which do not have a simple uniform expansion solution. It is only when the dark matter and dark energy parameters are forced onto the models that a uniform expansion is mimicked, which then also generates a predicted future accelerating expansion of the universe. Dynamical 3-Space theory now possesses new solutions for a uniform universe expansion, even without requiring the presence of matter, and such a solution has negligible universe acceleration except at very early times ($t < 10^{-103}$ s), which is dubbed the inflation epoch. This epoch is one where space

is rapidly expanding but always at a decelerating rate, as opposed to current inflation models which contain accelerating phases in the universe's infancy.

That the Hubble solutions do not contain a free parameter forces any phenomena emergent from the Dynamical 3-Space theory to be embedded in the centreless Hubble expansion. New black hole / expanding universe solutions were obtained and suggest that the black hole inflow is compatible with the Hubble expansion in that a critical radius in the order of $\approx$ Mpc exists where both the 3-space velocity and acceleration are zero. At this critical radius an object at rest will remain at a fixed distance from a black hole. This was at least found for the asymptotic $\delta = 0$ case; solutions to the full Dynamical 3-Space equation were not obtained. Embedding multiple black holes in an expanding universe was predicted to produce filaments between two black holes located within their spheres of influence, or within their critical radii. This would predict a cosmic network of black holes connected by filaments, located on the surface of large empty voids produced by the universe's expansion.

8.2 Future Work

There is a vast amount of work which can be achieved, with regards to the application of the Dynamical 3-Space theory to phenomena and also extending on the model itself. We know the approximate velocity of space i.e. its speed and direction, which changes throughout the year, and it would be a huge but rewarding task to further map out the change in velocity throughout the year as the Earth changes position. This could be achieved for example through repeating the experiments performed by Cahill and DeWitte, which use coaxial cables to measure the periodic change in travel time of signals as they travel through coaxial cables. Repeating the anisotropic Brownian motion study performed by Dai could potentially offer further insight as to how the right ascension changes with

time. Reanalysing Courvoisier's extensive research would also be beneficial, as his understanding of relativistic effects contradicted Lorentz however he studied light speed anisotropy effects in several different ways. Being able to further replicate the directional results predicted by Miller and from NASA flyby data would reinforce the argument justifying a dynamical space theory.

The characteristics of space and its turbulence effects can potentially be studied by observing fluctuations in virtually any data set. The fractal nature of the fluctuations however makes it very difficult to characterise the properties of space in depth. This could be achieved by studying the tunneling current fluctuations in Zener diodes or possibly through using the extensive data (over 17 years' worth) available through the Global Consciousness Project. There are many studies which can be performed here, including real time experiments to study the evolution of space fluctuations, or those made in parallel to also study correlations in the fluctuations. Alternatively, the histogram similarity approach by Shnoll could be implemented, as his histogram analysis reveals the evolutionary nature of space fluctuations in 60 - 100 measurement blocks, the technique which differs from the real time study approach. For example, studying the characteristic histogram shapes generated during solar eclipses would yield valuable information about the nature of space fluctuations when the relative positions of Sun, Earth and Moon are locked.

There are some data sets which Dynamical 3-Space has yet to completely explain. An important result observed from the spherical galaxy data is that of the $\alpha/2$ proportionality between black hole and spherical galaxy cluster mass, which has yet to be derived from Dynamical 3-Space theory. The CMB anisotropies could potentially be predicted through modifying the Hubble equation to mimic uniform expansion. This would likely require modelling 'dark matter' effects to fall as $1/a^2$ instead of the currently predicted $1/a^3$, while keeping the current equations for how dark matter density perturbations evolve in time. If this was successful, then

including the α effects into the Hubble equation should then predict the value of α, and the dark matter perturbations would instead mimic space self interaction perturbations.

Much is unknown about the Dynamical 3-Space theory for $\delta \neq 0$. This is simply because the inclusion of δ effects produces extremely complex equations, which aren't currently able to be reduced to a form that Mathematica can solve. Knowing the $\delta \neq 0$ black hole solutions while embedded in an expanding universe could allow the study of the velocities of galaxies in clusters, for example. The spiral galaxy rotation curves for $\delta \neq 0$ orbital velocity solutions have not been studied, along with the solutions where matter is present, i.e. for $\rho \neq 0$. A starting point here could be to use the $\delta \neq 0$, $\rho = 0$ black hole solutions, determine $v_O(r)$ and observe whether the orbital speeds or the best fit predicted rotation curve matches that of the data. The work presented here will hopefully gain an insight as to how to approach these problems, in order to further our understanding of the dynamics of space.

Bibliography

[1] G. Galilei and S. Drake. *Dialogue Concerning the Two Chief World Systems, Ptolemaic and Copernican*. Random House Digital, Inc., 1953.

[2] R. T. Cahill. Dynamical 3-Space: neo-Lorentz Relativity. *Physics International*, 4(1):60–72, 2013.

[3] I. Newton and F. Cajori. Philosophia Naturalis Principia Mathematica. Mathematical Principles of Natural Philosophy and his System of the World. Translated into English by A. Motte in 1729; The translations revised and supplied with a historical and explanatory appendix by F. Cajori. 1962.

[4] P. J. Mohr and B. N. Taylor. CODATA Recommended Values of the Fundamental Physical Constants. *Rev. Mod. Phys*, 77(1):1–107, 2002.

[5] J. C. Maxwell. *A Treatise on Electricity and Magnetism*, volume 1. Clarendon Press, Oxford, 1881.

[6] A. A. Michelson and E. W. Morley. On the Relative Motion of the Earth and the Luminiferous Ether. *American journal of science*, 203:333–345, 1887.

[7] A. Einstein. On the Electrodynamics of Moving Bodies. *Annalen der Physik*, 17(891):50, 1905.

[8] K. Schwarzschild. On the Gravitational Field of a Mass Point according to Einstein's Theory. *arXiv preprint physics/9905030*, 1999.

[9] S. Chandrasekhar. The Maximum Mass of Ideal White Dwarfs. *The Astrophysical Journal*, 74:81, 1931.

[10] J. R. Oppenheimer and G. M. Volkoff. On Massive Neutron Cores. *Physical Review*, 55(4):374, 1939.

[11] J. H. Oort. The Force Exerted by the Stellar System in the Direction Perpendicular to the Galactic Plane and some Related Problems. *Bulletin of the Astronomical Institutes of the Netherlands*, 6:249, 1932.

[12] F. Zwicky. On the Masses of Nebulae and of Clusters of Nebulae. *The Astronomical Journal*, 86:217, 1937.

[13] S. Smith. The Mass of the Virgo Cluster. *The Astronomical Journal*, 83:23, 1936.

[14] H. W. Babcock. The Rotation of the Andromeda Nebula. *Lick Observatory Bulletin*, 19:41–51, 1939.

[15] V. C. Rubin and W. K. Ford Jr. Rotation of the Andromeda Nebula from a Spectroscopic Survey of Emission Regions. *The Astrophysical Journal*, 159:379, 1970.

[16] M. S. Roberts and R. N. Whitehurst. The Rotation Curve and Geometry of M31 at Large Galactocentric Distances. *The Astrophysical Journal*, 201:327–346, 1975.

[17] J. P. Ostriker and P. J. E. Peebles. A Numerical Study of the Stability of Flattened Galaxies: or, can Cold Galaxies Survive? *The Astrophysical Journal*, 186:467–480, 1973.

[18] J. P. Ostriker, P. J. E. Peebles, and A. Yahil. The Size and Mass of Galaxies and the Mass of the Universe. *The Astrophysical Journal*, 193:L1–L4, 1974.

[19] H. Bondi and T. Gold. The Steady-State Theory of the Expanding Universe. *Monthly Notices of the Royal Astronomical Society*, 108:252, 1948.

[20] R. H. Brandenberger. Introduction to Early Universe Cosmology. *arXiv preprint arXiv:1103.2271*, 2011.

[21] S. Perlmutter, G. Aldering, G. Goldhaber, R. A. Knop, P. Nugent, P. G. Castro, S. Deustua, S. Fabbro, A. Goobar, D. E. Groom, et al. Measurements of Ω and Λ from 42 High-Redshift Supernovae. *The Astrophysical Journal*, 517(2):565, 2009.

[22] A. G. Riess, A. V. Filippenko, P. Challis, A. Clocchiatti, A. Diercks, P. M. Garnavich, R. L. Gilliland, C. J. Hogan, S. Jha, R. P. Kirshner, et al. Observational Evidence from Supernovae for an Accelerating Universe and a Cosmological Constant. *The Astronomical Journal*, 116(3):1009, 1998.

[23] G. C. McVittie. The Mass-Particle in an Expanding Universe. *Mon. Not. R. Astron. Soc.*, 93:325, 1933.

[24] G. W. Gibbons and K. Maeda. Black Holes in an Expanding Universe. *Physical review letters*, 104(13):131101, 2010.

[25] A. Einstein and E. G. Straus. The Influence of the Expansion of Space on the Gravitation Fields Surrounding the Individual Stars. *Rev. Mod. Phys.*, 17(2-3):120–124, 1945.

[26] J. Sultana and C. C. Dyer. Cosmological Black Holes: A Black Hole in the Einstein-de Sitter Universe. *General Relativity and Gravitation*, 37(8):1347–1370, 2005.

[27] B. Carter. Black Hole Equilibrium States. *Black holes*, pages 57–214, 1973.

[28] Friedrich Kottler. Über die Physikalischen Grundlagen der Einsteinschen Gravitationstheorie. *Annalen der Physik*, 361(14):401–462, 1918.

[29] D. R. Brill and S. A. Hayward. Global Structure of a Black Hole Cosmos and its Extremes. *Classical and Quantum Gravity*, 11(2):359, 1994.

[30] R. Nandra, A. N. Lasenby, and M. P. Hobson. The Effect of an Expanding Universe on Massive Objects. *Monthly Notices of the Royal Astronomical Society*, 422(4):2945–2959, 2012.

[31] S. Peirani and J. A. de Freitas Pacheco. Dynamics of Nearby Groups of Galaxies: the Role of the Cosmological Constant. *Astronomy and Astrophysics*, 488(3):845–851, 2008.

[32] R. H. Dicke, P. J. E. Peebles, P. G. Roll, and D. T. Wilkinson. Cosmic Black-Body Radiation. *The Astrophysical Journal*, 142:414–419, 1965.

[33] A. G. Doroshkevich and I. D. Novikov. Mean Density of Radiation in the Metagalaxy and Certain Problems in Relativistic Cosmology. *Soviet Physics Doklady*, 9, 1964.

[34] W. Hu and M. White. The Cosmic Symphony. *Scientific American*, 290(2):44, 2004.

[35] D. Larson, J. Dunkley, G. Hinshaw, E. Komatsu, M. R. Nolta, C. L. Bennett, B. Gold, M. Halpern, R. S. Hill, N. Jarosik, et al. Seven-Year Wilkinson Microwave Anisotropy Probe (WMAP) Observations: Power Spectra and WMAP-Derived Parameters. *The Astrophysical Journal Supplement Series*, 192(2):16, 2011.

[36] P. A. R. Ade, N. Aghanim, D. Alina, M. I. R. Alves, C. Armitage-Caplan, M. Arnaud, D. Arzoumanian, M. Ashdown, F. Atrio-Barandela, J. Aumont, et al. Planck Intermediate Results. XIX. An Overview of the Polarized Thermal Emission from Galactic Dust. *Astronomy & Astrophysics*, 576:A104, 2015.

[37] P. A. R. Ade, N. Aghanim, M. Arnaud, M. Ashdown, J. Aumont, C. Baccigalupi, A. J. Banday, R. B. Barreiro, N. Bartolo, E. Battaner, et al. Planck 2015 Results. XIV. Dark Energy and Modified Gravity. *arXiv preprint arXiv:1502.01590*, 2015.

[38] A. H Guth. Inflationary Universe: A Possible Solution to the Horizon and Flatness Problems. *Physical Review D*, 23(2):347, 1981.

[39] P. A. R. Ade, R. W. Aikin, D. Barkats, S. J. Benton, C. A. Bischoff, J. J. Bock, J. A. Brevik, I. Buder, E. Bullock, C. D. Dowell, et al. Detection of B-Mode Polarization at Degree Angular Scales by BICEP2. *Physical Review Letters*, 112(24):241101, 2014.

[40] C. Moskowitz. Gravitational Waves from Big Bang Detected. *Scientific American*, http://www.scientificamerican.com/article/gravity-waves-cmb-b-mode-polarization/, 2014.

[41] A. Cho. Evidence for Cosmic Inflation Wanes. *Science*, 345(6204):1547–1547, 2014.

[42] R. Brandenberger. Alternatives to Cosmological Inflation. *Physics Today*, 61(3):44, 2008.

[43] C. M. Klinger. *Process Physics: Bootstrapping Reality From the Limitations of Logic*. Flinders University of South Australia, School of Chemistry, Physics and Earth Sciences, 2005.

[44] Ernest Nagel, James Roy Newman, and Douglas R Hofstadter. *Gödel's proof*. New York University Press, New York, 2001.

[45] Gregory J Chaitin. *Information, randomness & incompleteness: papers on algorithmic information theory*, volume 8. World Scientific, Singapore, 1990.

[46] Gregory J Chaitin. *Exploring randomness*. Springer Science & Business Media, London, UK, 2012.

[47] R. T. Cahill. *Process Physics: From Information Theory to Quantum Space and Matter*. Nova Science Publishers, New York, 2005.

[48] R. T. Cahill. Dynamical 3-Space: Emergent Gravity. In H. A. Múnera, editor, *Should the Laws of Gravitation be Reconsidered? The Scientific Legacy of Maurice Allias*, pages 359–372. Apeiron, Montreal, Canada, 2011.

[49] R. T. Cahill. Unravelling the Dark Matter-Dark Energy Paradigm. *Aperion*, 16:323–375, 2009.

[50] R. T. Cahill. Novel gravity probe b frame-dragging effect and gravitational wave detection. In V. Dvoeglazov, editor, *Relativity, Gravitation, Cosmology: New Developments*, pages 133 – 151. Nova Publishers, New York, United States of America, 2004.

[51] R. T. Cahill. Dynamical Fractal 3-Space and the Generalised Schrodinger Equation: Equivalence Principle and Vorticity Effects. *Progress in Physics*, 1:27–34, 2006.

[52] R. T. Cahill and D. Kerrigan. Dynamical Space: Supermassive Galactic Black Holes and Cosmic Filaments. *Progress in Physics*, 4:79–82, 2011.

[53] R. T. Cahill. 3-Space In-Flow Theory of Gravity: Boreholes, Blackholes and the Fine Structure Constant. *Progress in Physics*, 2:9–16, 2005.

[54] R. T. Cahill. Black Holes and Quantum Theory: the Fine Structure Constant Connection. *Progress in Physics*, 4:44–50, 2006.

[55] D. Brewster. *Memoirs of the Life, Writings, and Discoveries of Sir Isaac Newton*, volume 2. Edmonston and Douglas, 1860.

[56] R. T. Cahill and K. Kitto. Michelson-Morley Experiments Revisited and the Cosmic Background Radiation Preferred Frame. *Apeiron*, 10(2):104–117, 2003.

[57] D. C. Miller. The Ether-Drift Experiment and the Determination of the Absolute Motion of the Earth. *Reviews of Modern Physics*, 5(3):203, 1933.

[58] R. J. Kennedy and E. M. Thorndike. Experimental Establishment of the Relativity of Time. *Physical Review*, 42(3):400, 1932.

[59] A. Brillet and J. L. Hall. Improved Laser Test of the Isotropy of Space. *Physical Review Letters*, 42(9):549, 1979.

[60] S. Herrmann, A. Senger, K. Möhle, M. Nagel, E. V. Kovalchuk, and A. Peters. Rotating Optical Cavity Experiment Testing Lorentz Invariance at the 10^{-17} Level. *Physical Review D*, 80(10):105011, 2009.

[61] R. T. Cahill. The Michelson and Morley 1887 Experiment and the Discovery of Absolute Motion. *Progress in Physics*, 3:25–29, 2005.

[62] K. K. Illingworth. A Repetition of the Michelson-Morley Experiment using Kennedy's Refinement. *Physical Review*, 30(5):692, 1927.

[63] H. A. Múnera. Michelson-Morley Experiments Revisited: Systematic Errors, Consistency among Different Experiments, and Compatibility with Absolute Space. *Apeiron*, 5(1-2):371–376, 1998.

[64] R. T. Cahill. Quantum Foam, Gravity and Gravitational Waves. *Relativity, Gravitation, Cosmology*, pages 168–226, 2004.

[65] J. Shamir and R. Fox. A New Experimental Test of Special Relativity. *Il Nuovo Cimento B Series 10*, 62(2):258–264, 1969.

[66] R. T. Cahill and F. Stokes. Correlated Detection of Sub-mHz Gravitational Waves by Two Optical-Fiber Interferometers. *Progress in Physics*, 2:103–110, 2008.

[67] L. S. Swenson Jr. *The Ethereal Aether: a History of the Michelson-Morley-Miller Aether-Drift Experiments, 1880-1930.* University of Texas Press, 2013.

[68] R. S. Shankland, S. W. McCuskey, F. C. Leone, and G. Kuerti. New Analysis of the Interferometer Observations of Dayton C. Miller. *Reviews of Modern Physics*, 27(2):167, 1955.

[69] J. DeMeo. Dayton Miller's Ether-Drift Experiments: A Fresh Look. *Infinite Energy*, 7(38):72–82, 2001.

[70] R. T. Cahill. Optical-Fiber Gravitational Wave Detector: Dynamical 3-Space Turbulence Detected. *Progress in Physics*, 4:63–68, 2007.

[71] R. T. Cahill. The Roland De Witte 1991 Experiment (to the Memory of Roland De Witte). *Progress in Physics*, page 60, 2006.

[72] D. G. Torr and P. Kolen. Precision Measurements and Fundamental Constants, ed. by Taylor BN and Phillips WD Nat. *Bur. Stand.(US), Spec. Pub*, 617:675, 1984.

[73] T. P. Krisher, L. Maleki, G. F. Lutes, L. E. Primas, R. T. Logan, J. D. Anderson, and C. M. Will. Test of the Isotropy of the One-Way Speed of Light using Hydrogen-Maser Frequency Standards. *Physical Review D*, 42(2):731, 1990.

[74] R. T. Cahill. Characterisation of Low Frequency Gravitational Waves from Dual RF Coaxial-Cable Detector: Fractal Textured Dynamical 3-Space. *Progress in Physics*, 3:3–10, 2012.

[75] J. D. Anderson, J. K. Campbell, J. E. Ekelund, J. Ellis, and J. F. Jordan. Anomalous Orbital-Energy Changes Observed During Spacecraft Flybys of Earth. *Physical Review Letters*, 100(9):091102, 2008.

[76] R. T. Cahill. Combining NASA/JPL One-Way Optical-Fiber Light-Speed Data with Spacecraft Earth-Flyby Doppler-Shift Data to Characterise 3-Space Flow. *Progress in Physics*, 5:50–64, 2009.

[77] R. T. Cahill. Nanotechnology Quantum Detectors for Gravitational Waves: Adelaide to London Correlations Observed. *Progress in Physics*, 4:57–62, 2013.

[78] J. Dai. Macroscopic Anisotropic Brownian Motion is Related to the Directional Movement of a "Universe Field". *Natural Science*, 6(2), 2014.

[79] R. T. Cahill. Dynamical 3-Space: Anisotropic Brownian Motion Experiment. *Progress in Physics*, 11, 2015.

[80] J. K. Webb, J. A. King, M. T. Murphy, V. V. Flambaum, R. F Carswell, and M. B. Bainbridge. Indications of a Spatial Variation of the Fine Structure Constant. *Physical Review Letters*, 107(19):191101, 2011.

[81] R. D. A. Martins. Searching for the Ether: Leopold Courvoiser's Attempts to Measure the Absolute Velocity of the Solar System. *The International Journal of Scientific History*, 17:1–33, 2011.

[82] R. T. Cahill. One-Way Speed of Light Measurements Without Clock Synchronisation. *Progress in Physics*, 3:43–45, 2012.

[83] R. Nelson. Correlation of Global Events with REG Data: An Internet-Based, Nonlocal Anomalies Experiment. *The Journal of Parapsychology*, 65(3):247, 2001.

[84] R. T. Cahill. Gravitational Wave Experiments with Zener Diode Quantum Detectors: Fractal Dynamical Space and Universe Expansion with Inflation Epoch. *Progress in Physics*, 10(3):131–138, 2014.

[85] R. T. Cahill. Observed Gravitational Wave Effects: Amaldi 1980 Frascati-Rome Classical Bar Detectors, 2013 Perth-London Zener-Diode Quantum Detectors, Earth Oscillation Mode Frequencies. *Progress in Physics*, 10:21–24, 2014.

[86] R. T. Cahill. Solar Flare Five-Day Predictions from Quantum Detectors of Dynamical Space Fractal Flow Turbulence: Gravitational Wave Diminution and Earth Climate Cooling. *Progress in Physics*, 10(4):236, 2014.

[87] F. Scholkmann. Indications for a Diurnal and Annual Variation in the Anisotropy of Diffusion Patterns—A Reanalysis of Data Presented by J. Dai (2014, Nat. Sci.). *Progress in Physics*, 10(4):232–235, 2014.

[88] S. E. Shnoll. *Cosmophysical factors in stochastic processes.* American Research Press, Rehoboth, New Mexico, USA, 2012.

[89] V. A. Panchelyuga, V. A. Kolombet, M. S. Panchelyuga, and S. E. Shnoll. Local-time effect on small space-time scale. In D. G. Pavlov, Gh. Atanasiu, and V. Balan, editors, *Space-Time Structure. Algebra and Geometry*, pages 531 – 537. Lilia-Print, Moscow, Russia, 2007.

[90] S. E. Shnoll, V. A. Kolombet, E. V. Pozharskii, T. A. Zenchenko, I. M. Zvereva, and A. A. Konradov. Realization of Discrete States during Fluctuations in Macroscopic Processes. *Physics-Uspekhi*, 41(10):1025–1035, 1998.

[91] S. E. Shnoll, E. V. Pozharski, T. A. Zenchenko, V. A. Kolombet, I. M. Zvereva, and A. A. Konradov. Fine Structure of Distributions in Measurements of Different Processes as Affected by Geophysical and Cosmophysical Factors. *Physics and Chemistry of the Earth, Part A: Solid Earth and Geodesy*, 24(8):711–714, 1999.

[92] S. E. Shnoll, K. I. Zenchenko, I. I. Berulis, N. V. Udaltsova, and I. A. Rubinstein. Fine Structure of Histograms of Alpha-Activity Measurements depends on Direction of Alpha Particles Flow and the Earth Rotation: Experiments with Collimators. *arXiv preprint physics/0412007*, 2004.

[93] R. T. Cahill. Unravelling Lorentz Covariance and the Spacetime Formalism. *Progress in Physics*, 4:19–24, 2009.

[94] R. T. Cahill. Quantum-foam in-flow theory of gravity and the global positioning system (gps). *arXiv:physics/0309016v2*, 2004.

[95] H. Hertz. On the Fundamental Equations of Electro-Magnetics for Bodies in Motion. *Wiedemann's Ann*, 41:369, 1890.

[96] R. T. Cahill. Gravitation, the 'Dark Matter' Effect and the Fine Structure Constant. *Apeiron*, 12(2):144, 2005.

[97] R. T. Cahill. Dynamical 3-Space: Cosmic Filaments, Sheets and Voids. *Progress in Physics*, 2:44–51, 2011.

[98] D. O. Cooney, S. Kim, and E. J. Davis. Analyses of Mass Transfer in Hemodialyzers for Laminar Blood Flow and Homogeneous Dialysate. *Chemical Engineering Science*, 29(8):1731–1738, 1974.

[99] A. C. Fabian. Clusters and Superclusters of Galaxies. In *NATO Advanced Science Institutes (ASI) Series C*, volume 366, 1992.

[100] G. B. Airy. Account of Pendulum Experiments Undertaken in the Harton Colliery, for the Purpose of Determining the Mean Density of the Earth. *Philosophical Transactions of the Royal Society of London*, 146:297–355, 1856.

[101] M. E. Ander, M. A. Zumberge, T. Lautzenhiser, R. L. Parker, C. L. V. Aiken, M. R. Gorman, M. M. Nieto, A. P. R. Cooper, J. F. Ferguson, E. Fisher, et al. Test of Newton's Inverse-Square Law in the Greenland Ice Cap. *Physical Review Letters*, 62(9):985, 1989.

[102] J. Thomas and P. Vogel. Testing the Inverse-Square Law of Gravity in Boreholes at the Nevada Test Site. *Physical review letters*, 65(10):1173, 1990.

[103] R. T. Cahill and S. T. Deane. Dynamical 3-Space Gravitational Waves: Reverberation Effect. *Progress in Physics*, 2:9–11, 2013.

[104] M. V. Fedorov, L. V. Belousov, V. L. Voeikov, T. A. Zenchenko, K. I. Zenchenko, E. V. Pozharski, A. A. Konradov, and S. E. Shnoll. Synchronous Changes in Dark Current Fluctuations in Two Separate Photomultipliers in Relation to Earth Rotation. *Astrophysics and Space Science*, 283(1):3–10, 2003.

[105] S. E. Shnoll. Changes in the Fine Structure of Stochastic Distributions as a Consequence of Space-Time Fluctuations. *Progress in Physics*, 2:39, 2006.

[106] D. P. Rothall and R. T. Cahill. Dynamical 3-Space: Gravitational Wave Detection and the Shnoll Effect. *Progress in Physics*, 4:44–47, 2013.

[107] D. P. Rothall and R. T. Cahill. Dynamical 3-Space: Observing Gravitational Wave Fluctuations and the Shnoll Effect using a Zener Diode Quantum Detector. *Progress in Physics*, 10(1):16–18, 2014.

[108] R. T. Cahill and D. Brotherton. Experimental Investigation of the Fresnel Drag Effect in RF Coaxial Cables. *Progress in Physics*, 1:43–48, 2011.

[109] R. T. Cahill. Resolving Spacecraft Earth-Flyby Anomalies with Measured Light Speed Anisotropy. *Progress in Physics*, 3:9–15, 2008.

[110] G. Gamow. Zur Quantentheorie des Atomkernes. *Zeitschrift für Physik*, 51(3-4):204–212, 1928.

[111] R. T. Cahill. 3-Space In-Flow Theory of Gravity: Boreholes, Blackholes and the Fine Structure Constant. *Progress in Physics*, 4:9–16, 2006.

[112] M. Persic, P. Salucci, and F. Stel. The Universal Rotation Curve of Spiral Galaxies - I. The Dark Matter Connection. *Monthly Notices of the Royal Astronomical Society*, 281(1):27–47, 1996.

[113] T. S. van Albada, J. N. Bahcall, K. Begeman, and R. Sanscisi. Distribution of Dark Matter in the Spiral Galaxy NGC 3198. *The Astrophysical Journal*, 295:305–313, 1985.

[114] R. T. Cahill. Black Holes in Elliptical and Spiral Galaxies and in Globular Clusters. *Progress in Physics*, 3:51–56, 2005.

[115] S. Gillessen, F. Eisenhauer, S. Trippe, T. Alexander, R. Genzel, F. Martins, and T. Ott. Monitoring Stellar Orbits Around the Massive Black Hole in the Galactic Center. *The Astrophysical Journal*, 692(2):1075, 2009.

[116] A. M. Beloborodov, Y. Levin, F. Eisenhauer, R. Genzel, T. Paumard, S. Gillessen, and T. Ott. Clockwise Stellar Disk and the Dark Mass in the Galactic Center. *The Astrophysical Journal*, 648(1):405, 2006.

[117] R. Genzel, N. Thatte, A. Krabbe, H. Kroker, and L. E. Tacconi-Garman. The Dark Mass Concentration in the Central Parsec of the Milky Way. *The Astrophysical Journal*, 472(1):153, 1996.

[118] M. T. McGinn, K. Sellgren, E. E. Becklin, and D. N. B. Hall. Stellar Kinematics in the Galactic Center. *The Astrophysical Journal*, 338:824–840, 1989.

[119] E. Serabyn, R. Güsten, J. E. Walmsley, J. E. Wink, and R. Zylka. CO 1-0 and CS 2-1 Observations of the Neutral Disk around the Galactic Center. *Astronomy and Astrophysics*, 169:85–94, 1986.

[120] E. Serabyn and J. H. Lacy. Forbidden NE II Observations of the Galactic Center-Evidence for a Massive Black Hole. *The Astrophysical Journal*, 293:445–458, 1985.

[121] R. T. Cahill and D. Rothall. Discovery of Uniformly Expanding Universe. *Progress in Physics*, 1:65–68, 2012.

[122] W. M. Wood-Vasey, G. Miknaitis, C. W. Stubbs, S. Jha, A. G. Riess, P. M. Garnavich, R. P. Kirshner, C. Aguilera, A. C. Becker, J. W. Blackman, and others (see table 9 of http://arxiv.org/pdf/astro ph/0701041). Observational Constraints on the Nature of Dark Energy: First Cosmological Results from the ESSENCE Supernova Survey. *The Astrophysical Journal*, 666(2):694, 2007.

[123] A. G. Riess, L. Strolger, S. Casertano, H. C. Ferguson, B. Mobasher, B. Gold, P. J. Challis, A. V. Filippenko, S. Jha, W. Li, et al. New Hubble Space Telescope Discoveries of Type Ia Supernovae at $z \geq 1$: Narrowing Constraints on the Early Behavior of Dark Energy. Based on observations with the NASA/ESA Hubble Space Telescope, obtained at the Space Telescope Science Institute (STScI), which is operated by the Association of Universities for Research in Astronomy (AURA), Inc., under NASA contract NAS5-26555. *The Astrophysical Journal*, 659(1):98, 2007.

[124] National Aeronautics and Space Administration website. http://lambda.gsfc.nasa.gov/data/map/dr4/dcp/spectra/wmap_binned_tt_spectrum_7yr_v4p1.txt. 2010.

[125] R. T. Cahill. Dynamical 3-Space: Supernovae and the Hubble Expansion-the Older Universe without Dark Energy. *Progress in Physics*, 4:9–12, 2007.

[126] Class for Physics of the Royal Swedish Academy of Sciences. https://www.nobelprize.org/nobel_prizes/physics/laureates/2011/advanced-physicsprize2011.pdf. 2011.

[127] B. E. Schaefer. The Hubble Diagram to Redshift > 6 from 69 Gamma-Ray Bursts. *The Astrophysical Journal*, 660(1):16, 2007.

[128] I. D. Karachentsev, A. E. Dolphin, D. Geisler, E. K. Grebel, P. Guhathakurta, P. W. Hodge, V. E. Karachentseva, A. Sarajedini, P. Seitzer, and M. E. Sharina. The M 81 Group of Galaxies: New Distances, Kinematics and Structure. *Astronomy & Astrophysics*, 383(1):125–136, 2002.

[129] I. D. Karachentsev, M. E. Sharina, A. E. Dolphin, E. K. Grebel, D. Geisler, P. Guhathakurta, P. W. Hodge, V. E. Karachentseva, A. Sarajedini, and P. Seitzer. New Distances to Galaxies in the Centaurus A Group. *Astronomy & Astrophysics*, 385(1):21–31, 2002.

[130] P. Fontanelli. The Coma/A 1367 Filament of Galaxies. *Astronomy and Astrophysics*, 138:85–92, 1984.

[131] R. Giovanelli and M. P. Haynes. The Lynx-Ursa Major Supercluster. *The Astronomical Journal*, 87:1355–1363, 1982.